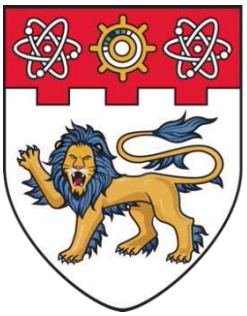

NANYANG TECHNOLOGICAL UNIVERSITY
SINGAPORE

Air balancing technology in HVAC applications

CUI CAN

SCHOOL OF ELECTRICAL & ELECTRONIC ENGINEERING

2019

Air balancing technology in HVAC applications

CUI CAN

School of Electrical & Electronic Engineering

A thesis submitted to the Nanyang Technological University
in partial fulfillment of the requirement for the degree of
Doctor of Philosophy

2019

Statement of Originality

I hereby certify that the work embodied in this thesis is the result of original research, is free of plagiarised materials, and has not been submitted for a higher degree to any other University or Institution.

18/01/2019

Cui Can

. . . . . .

Date

. . . . . .

Cui Can

Supervisor Declaration Statement

I have reviewed the content and presentation style of this thesis and declare it is free of plagiarism and of sufficient grammatical clarity to be examined. To the best of my knowledge, the research and writing are those of the candidate except as acknowledged in the Author Attribution Statement. I confirm that the investigations were conducted in accord with the ethics policies and integrity standards of Nanyang Technological University and that the research data are presented honestly and without prejudice.

18/01/2019

. . . . . .
Date

. . . . . .
Cai Wenjian

Authorship Attribution Statement

This thesis contains material from 3 papers published in the following peer-reviewed journals where I was the first author.

Chapter 3 is published as C. Cui, W. Cai, H. Chen, Airflow measurements using averaging Pitot tube under restricted conditions, Building and Environment. 139 (2018) 17-26.

The contributions of the co-authors are as follows:

- A/Prof Cai provided the initial project direction and edited the manuscript drafts.
- I performed all the laboratory work, processed and analyzed the data, and drafted the manuscript.
- Dr. Chen assisted in the collection and provided guidance in the interpretation of the measurement data.

Chapter 4 is published as C. Cui, X. Zhang, W. Cai, G. Jing, A novel online air balancing method for the ventilation duct system via distributed cooperative control, Building and Environment. 146 (2018) 177-189.

The contributions of the co-authors are as follows:

- A/Prof Cai provided the initial project direction and edited the manuscript drafts.
- Asst/Prof Zhang determined the topic of this paper.
- I proposed the model, processed and analyzed the data, and drafted the manuscript.
- A/Prof Jing assisted in building up the experimental setup.

Chapter 5 is published as C. Cui, X. Zhang, W. Cai, G. Jing, A gradient-based adaptive balancing method for dedicated outdoor air system, Building and Environment. 151 (2019) 15-29.

The contributions of the co-authors are as follows:

- A/Prof Cai provided the initial project direction and edited the manuscript drafts.
- Asst/Prof Zhang determined the topic of this paper.
- I proposed the model, processed and analyzed the data, and drafted the

manuscript.

- A/Prof Jing assisted in collecting the experimental data.

18/01/2019

Cui Can

. . . . . .

Date

. . . . . .

Cui Can

Acknowledgments

I want to express my profound thanks to my supervisor, Prof. Cai Wenjian for his patient supervision, tremendous support and invaluable guidance throughout the course of my research work. I would like to offer the same gratitude to Prof. Zhang Xin, who brought me to the research area of control theory and gave me consistent insightful guidance during my research work.

I must also give a mention to my senior Dr. Chen Haoran, who developed this research topic and built up both the simulation and experimental platform. I appreciate all the helpful discussions and guidance from him, as well as all the encouragement for hard times.

I also like to thank all staffs and lab technicians in the Process Instrumentation Lab for their professional training and maintenance of the equipment. In addition, much gratitude is to my friends Dr. Li Xiang, Dr. Chen Xuebing, Dr. Wu Bingjie etc. Their generous help have enabled me to fit in with regards to my research, coursework, as well as daily life.

At last, I would like to express my deep appreciation to my family for their company and continuous support throughout my PhD life.

Table of Contents

Summary

This thesis presents a detailed investigation into the air balancing process in HVAC systems. Improvements have been made in both the flow measurement and air balancing methods to optimize the balancing performance in terms of efficiency, accuracy and cost. The main contributions of the thesis are summarized as follows:

The accuracy of flow measurement in the air flow control stations (AFCS) is improved to achieve better control performance of the air balancing methods. A revised airflow rate calculation formula for the averaging Pitot tube is proposed taking into consideration of downstream disturbances. The revised formula significantly reduces the systematic error caused by the flow control damper and improves the accuracy of flow measurement to a large extent. Besides, the AFCS is equipped with wireless technology to achieve wireless communication.

Two online air balancing methods are proposed, which are distributed cooperative control-based air balancing (DCC-AB) method and gradient-based online adaptive balancing (GOAB) method. Both methods can be performed during system operation without interrupting the normal service of ventilation, which avoids inconvenience to the occupants and financial losses caused by maintenance shutdown. The balancing-in-service characteristic provides possibility to achieve accurate air supply under dynamic loads, which indicates a large energy saving potential.

The DCC-AB method is based on the distributed cooperative control strategy. It guarantees an asymptotic convergence towards the balanced state. the balancing process starts from the given imbalanced state and converges asymptotically to the balanced state. The drastic change of damper positions such as short cycling on and off is circumvented, which avoids overshooting and oscillations of the flow rate value. An incremental improvement in the imbalance of flow is guaranteed at each adjustment during the whole process. The DCC-AB method circumvents the centralized supervisory control and requires only a sparse communication architecture to cooperatively achieve the objective. The method also incorporates an additional adjustable term that reflects the total power consumption to optimize the energy efficiency. Besides, this method is a model-free method that requires little prior knowledge on the system topology and duct parameters.

The GOAB method is based on the gradient descent algorithm. In this method, an objective function is defined to quantify the discrepancy between the normalized flow rate and the set point, and the increment of damper angle is calculated using stochastic gradient descent. An online adaptive mechanism for the Jacobian estimation is applied to capture the change of Jacobian matrix during the balancing process. In this method, the critical damper is explicitly identified based on the null space of the gradient vector. At least one damper is guaranteed fully open, which minimizes the overall flow resistance of dampers and total energy consumption. The GOAB method incorporates a coefficient to control the speed of convergence rate and stability of the algorithm. A rapid and stable convergence is guaranteed within several steps.

List of Figures

List of Tables

Chapter 1. Introduction

1.1 Background

Heating, ventilation and air-conditioning (HVAC) system is designed to provide a comfortable indoor environment in terms of temperature, humidity and other environmental parameters for the occupants [1, 2]. It is widely used in residential, commercial and industrial buildings and has become an indispensable part of people's daily lives, especially for urban citizens who spend over 80% of their time indoors [3, 4]. However, HVAC is also known as the major energy consumer in buildings [5-7]. According to [8, 9], about 50% of the energy is consumed by HVAC in the building sector in USA. The proportion can be even higher for tropical countries like Singapore, where air-conditioning is required throughout the year [10]. Hence, a major concern in modern HVAC systems is to reduce energy consumption without compromising thermal comfort or indoor air quality (IAQ).

The mechanical ventilation system, also called the air distribution system or air duct system, is an important part of the HVAC system and accounts for a significant portion of the energy consumption in buildings. It is reported that the space heating, cooling and ventilation together comprises up to 41.4% of the total energy in the building sector in U.S. [10]. A trade-off exists between the energy efficiency of the ventilation system and the indoor environment. Decreasing the ventilation rate may reduce unnecessary energy dissipation [11] and excessive duct noise [12]. However, insufficient ventilation can lead to degraded air quality, accumulated contaminants, and can even cause occupants' sick building syndrome (SBS) [13]. Studies have shown that children's performance of schoolwork [14, 15] and occupant productivity in office [16] are also strongly affected by the ventilation rate. Therefore, precisely supplying the required air flow quantities to each conditioned space becomes critically important.

Air balancing is an important means of guaranteeing the air flow distribution in the duct system as design, which is also the main objective of the testing, adjusting, and balancing (TAB) process [17]. The system is called balanced if it delivers the required air for occupant comfort and space thermal loads [17]. Although balancing is partly taken into consideration at the early stage of duct design, the system may not operate as expected due to unpredictable modelling error and inevitable adjustments during

installation. Hence, before the system is put into use, the TAB must be performed to ensure that the system is working in conformity with the design requirement [18]. Currently, the TAB is performed in the commissioning stage since it requires a complete shutdown of the system. However, due to possible duct retrofitting and change of occupancy, the system may fall back imbalanced. For this reason, the TAB must be performed on the air distribution system regularly to ensure accurate air supply and optimum working conditions.

The main challenges faced by air balancing is the accuracy of flow measurement and lack of more systematic balancing approaches. Almost all air balancing methods rely heavily on the flow measurement. The currently most widely used flow sensor in air balancing application is the Pitot tube, which is susceptible to various disturbances. This can degrade the actual performance of the TAB process. As for the balancing methods, the commonly adopted one in industry is an iterative approach based on rule of thumb, which is time-consuming and inefficient. Hence, future trend in air balancing focuses on more accurate measurement and more intelligent control scheme. For the former, applying correction coefficient for the flow sensor or placing filter to obtain a more uniform flow are possible approaches to reduce the error caused by flow disturbances. Besides, alternative flow measuring techniques of higher accuracy can be considered within reasonable cost. For the latter, a foreseeable future is the automation of the air balancing to eliminate the dependency on human and save manpower cost.

1.2 Overview of HVAC systems

Constant air volume (CAV) is a classic type of HVAC systems that has been used since the invention of air conditioning [19]. In CAV, the volume of supply air remains constant whereas the temperature varies to satisfy the space heating/cooling load. There are typically two types of CAV systems, namely, the terminal reheat system and the mixed air system [20]. The terminal reheat system operates at a fixed volume flow rate and supply fan outlet temperature. The central air handling unit (AHU) cools the air to a temperature low enough (usually 13°C) to meet the cooling load required by the highest heat gain area within the building. The reheat coils then heats the air entering each zone to regulate the supply air temperature depending on individual requirements. The mixed air system has two separate air streams, which are set to the coldest and hottest possible required temperature respectively. The two air streams eventually meet

at the zone mixing box and being mixed to offset the space load by adjusting the proportions of warm and cool air. The mixed air system is effective in controlling the temperature, but not as proficient at controlling the humidity.

Despite the specific subtype, the CAV system, by nature of its design, share common some limitations. The supply air flow volume is fixed regardless of actual heating or cooling load, which results in unnecessary energy waste when peak load is not required. Another limitation is the energy inefficiency caused by the heating and cooling coils operating at the same time during part-load conditions [21]. The CAV system may still be an effective option for applications with a rather constant ventilation load such as concert halls, theatres, gymnasiums, department stores, warehouses etc. Nonetheless, when variable control of pressure or ventilation rate is required, adopting a CAV system will most likely result in higher energy consumption and less effective temperature, humidity and ventilation regulation.

The variable air volume (VAV) system came into view in 1960s and became prevalent across Europe after 1980s [22]. Unlike CAV system that varies the supply air temperature, the VAV varies the quantity of supply air to control the indoor climate [23]. A key component of a VAV duct system is the VAV terminal unit, also called VAV box. A typical VAV box is a sheet metal box consisting of temperature sensor, air flow sensor, controller, actuator and damper. The VAV box can be either pressure-dependent or pressure-independent. In a pressure-dependent VAV system, the damper actuator is controlled directly by the room thermostat. The actuator modulates the damper in response to the room temperature only. The actual air flow supplied to the space is dependent on the duct static pressure. The pressure-dependent control strategy can cause severe flow fluctuations in large systems [24]. By comparison, the pressure-independent VAV system adopts two cascading control loops. The outer loop controls the room temperature and the inner loop controls the supply air flow rate. When the room thermostat senses the change of temperature, the outer loop sends signal to the inner loop to reset the flow set point that satisfies the current indoor thermal load [25]. The set point can be restricted within a minimum and maximum air flow rate regardless of the duct static pressure, which assures proper distribution of air and acceptable IAQ. The pressure-independent units are regarded as a preferable option for large complex VAV systems. There are other subtypes of VAV systems developed for particular needs,

such as single duct and dual duct, cooling only and cooling with reheat, bypass and fan powered and etc. [26].

In general, the VAV systems offer superior performance over CAV systems in multi-zone buildings subject to consequently variable ventilation loads [27]. According to [28], the annual energy saving is over 17% in 6 test cities using VAV systems. Besides, the VAV provides more precise temperature control, less fan noise and additional passive dehumidification.

The dedicated outdoor air system (DOAS) is being considered as an alternative to traditional all-air VAV system in recent decades [29, 30]. The concept of DOAS is decoupling the space latent and sensible loads [30]. The DOAS supplies the required ventilation air to meet the overall space latent load and a part of sensible load. A parallel cooling system such as radiant ceiling panel works in conjunction to handle the remaining sensible load [31].

The DOAS offers substantial benefits over traditional VAV systems in the following aspects. In a multiple-zone VAV system, the central air handling unit supplies a homogenous mixture of outdoor air and recirculated air to each zone. The outdoor air fraction is determined by the critical zone that requires the highest, resulting in over-ventilation in non-critical zones [32]. In comparison, the DOAS delivers the exact amount of required air to individual zones, which significantly reduces the energy consumption [33]. The decoupling of space latent and sensible loads allows effective control of the indoor relative humidity level [34]. The main disadvantage of DOAS is the high first cost, which can be balanced by operational advantages. Overall, by choosing proper system configurations, the DOAS could provide more precise air delivery, better humidity control, reduced energy usage and enhanced indoor environmental quality.

A critical factor that affects the overall performance of HVAC systems is the ductwork design. Improperly designed or installed duct systems can cause potential air leakage, excessive noise, high energy cost and poor air quality. An important step is choosing a duct configuration that best suits the space requirements and installation conditions. There are several basic types of supply and return duct systems, as shown in Figure 1.1.

A typical radial duct system consists of a central supply plenum, connected directly to individual air outlets. This ductwork design is rather simple and requires less technical expertise, making it easy and quick to install. The radial duct systems are found exclusively in small buildings and single-story homes [35]. Another popular configuration is the trunk-and-branch ductwork, which resembles a tree trunk with multiple branches. This design uses a primary supply trunk to deliver the air, with several branches extending out from the main duct. There are a few variations of the trunk-and-branch ductwork, such as extended plenum and reducing trunk. In the extended plenum systems, the trunk duct remains the same size for the entire length of its run, which essentially serves as an extension to the supply plenum [36]. The length of the trunk duct should not exceed 24 ft (7.32 m) on either side of the supply unit to maintain the air velocity. For applications that calls for greater distances, the reducing trunk system is employed. In this design, the trunk size (cross-sectional area) is reduced after each branch take-off point to regain the air velocity. The reducing trunk system provides a relatively constant air flow throughout the duct system while also indicating a lager cost for fabricating duct transitions [37]. In the perimeter loop system, a continuous loop duct is laid out around the perimeter of the conditioned space. The loop is fed by several supply ducts radiating out from the central unit. The perimeter loop system provides enhanced comfort in cold climate with proper installation of insulated slabs. However, it is also one of the most costly duct systems to install [38].

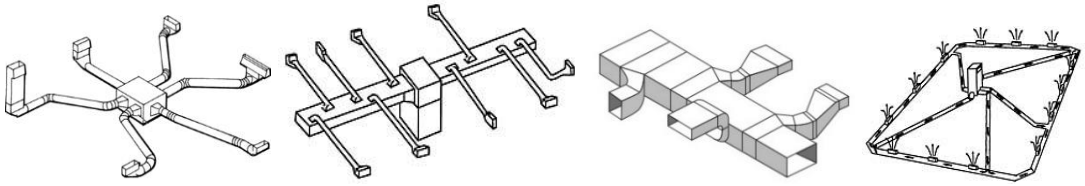

(a) *(b)* *(c)* *(d)*

Figure 1.1: Ductwork configurations
(a) Radial system; (b) Extended plenum system; (c) Reducing trunk system; (d) Perimeter loop system

The next step in duct design is to select proper components and accessories that facilitate the ductwork fabrication. A typical air duct system mainly consists of ducts, fans, fittings and terminal units. Ducts are passages used in supply, exhaust or return systems to deliver and remove air. Commonly used materials for ducts are galvanized steel, stainless steel, aluminium, fiberglass and etc. The ducts can be fabricated in rectangular, round, flat oval and flexible, as shown in Figure 1.2. Round ducts are

versatile, easy to build and connect. They are cost-effective for less material use with the same duct cross-sectional area. Round ducts provide lower frictional loss, better acoustic performance and easier insulation installation. For tight space where round ducts cannot fit, the rectangular ducts can be an alternative option. Rectangular ducts are easy to assemble and adapt to various space constraints. However, the installation cost is higher, and the joints are more difficult to seal. As a compromise, the flat oval ducts retain most advantages of the round ducts and have less space limitations. When the installation of rigid ducts is extremely difficult or impossible, the flexible ducts can be applied. Typical flexible ducts are crinkly, flexible tubes of metal wire coil covered by bendable, reinforced plastic and a layer of insulation and protective coating. They are extensively used for the connection of non-flexible ductwork and air supply outlets.

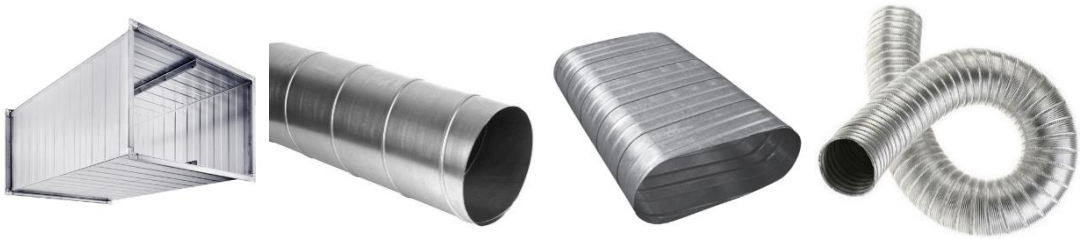

(a) *(b)* *(c)* *(d)*

Figure 1.2: Duct conduits
(a) Rectangular; (b) Round; (c) Flat oval; (d) Flexible

Fans are used to supply air to or exhaust air from the conditioned space. Two primary types of fans used in the duct system are centrifugal and axial, shown in Figure 1.3. Axial fans are so named because of the direction of air flow into and out. The fan blades rotate around the axis, producing a pressure difference that moves air in a direction parallel to the axis. Axial fans generate high volume of air flow at low pressure and therefore consume less power. The centrifugal fan, also referred to as blower, is another design that operates a bit differently. The centrifugal fan consists of a series of blades mounted on a circular hub, which accelerates air radially and outwards. The direction of the incoming flow is changed by 90° at the outlet. Centrifugal fans are used in applications that require higher pressure or steadier flow [39].

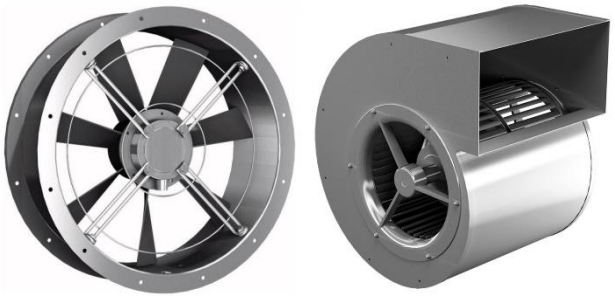

(a) (b)

Figure 1.3: Fans
(a) Axial; (b) Centrifugal

Duct fittings are duct accessories used for construction of a ductwork. There are a variety of fittings such as elbows, junctions, transitions, connectors, dampers and etc. Selected ones are shown in Figure 1.4. Elbows are used to change the direction of air flow in a ductwork. They can be classified by angle (30°, 45°, 60°, and 90°) or throat/heel (square or radius) [40]. For sharp edged elbows, it is common to insert turning vanes to reduce pressure losses. Junctions are used to split flow into multiple branches or merge flows into a main branch, which are of various shapes like T-shaped (tee), Y-shaped (wye) and cross. Numerous empirical formulas can be found to estimate pressure losses for these fittings [41-46]. Dampers are used to regulate the volume of air passing through a duct. Motorized dampers can provide precise positioning and are widely used in air duct systems. Common types of dampers include butterfly, opposite, parallel, and iris, as shown in Figure 1.5.

(a) (b) (c) (d)

Figure 1.4: Common duct fittings
(a) Elbow; (b) Tee; (c) Wye; (d) Reducer

(a) *(b)* *(c)* *(d)*

Figure 1.5: Common types of dampers
(a) Butterfly; (b) Parallel; (c) Opposite; (d) Iris

Testing, adjusting, and balancing (TAB) is a commissioning service of checking and adjusting HVAC systems to achieve design requirements [17]. Prior to the acceptance by building owners, the TAB must be conducted to ensure the system performs as anticipated. During the operation of building, the indoor environment keeps changing with time and use [47]. The HVAC system running based on a fixed work schedule can lead to unnecessary energy use during periods of low occupancy [48, 49]. Besides, the performance of HVAC systems may fail to satisfy design expectations due to improper equipment installation, poor maintenance, and sensor failures [50]. Hence, the TAB should be carried out regularly throughout the whole building lifecycle from early design, construction, and operation to accommodate for such changes [51].

A main objective of TAB is to balance the air distribution system, where the term ‘balance’ refers to proportioning flows in the system according to specified design values [17]. Studies have shown that inaccurate air supply can cause degraded IAQ [18, 52], unnecessary energy dissipation and large duct noise. Balancing the duct system to provide a precise delivery of air is therefore essential to maintain thermal comfort and optimize energy efficiency, which is required by various types of HVAC systems like CAV, VAV, DOAS and etc.

Although for CAV systems, balancing is partly taken into consideration at the early stage of duct design, they may not operate as expected due to unpredictable modelling errors and inevitable adjustments during installation. For this reason, air balancing should be conducted to make sure all terminal flow satisfies the design values. Since CAV systems are usually not equipped with motor dampers, the balancing process should be performed manually and the attainable accuracy is rather low. For VAV systems, balancing is mainly required in the configuration of CFM settings. In pressure-dependent systems, the actual minimum flow rates are not controlled and may under or

over ventilate the spaces served in minimum mode [53]. After the min/max CFM is specified, the outlets on each terminal unit should be balanced to deliver the correct minimum/maximum air flow. As for the DOAS, the outdoor air occupies 100% of the air supply [54], making air balancing a more critical issue compared with other types of HVAC systems.

Balancing air duct systems can be achieved in various ways. The approaches may differ from each other in the implementing procedures, but the objective remains the same. The commonly accepted criteria for TAB process, in accordance with the standards of ASHRAE, NEBB, CIBSE, SMACNA and etc., are listed below:

1.) All measured air flow quantities should be controlled within ±10% of the design values.
2.) At least one damper/path should be left fully open in order to minimize the overall energy consumption.

To understand the rationale behind the second one, suppose all dampers in the duct system are partially closed, and the damper that should remain fully open throughout the balancing process is named 'critical damper' in this thesis. Then the same state of the system, considering the flow rate values only, can be achieved by fully opening the critical damper while lowering down the fan static pressure, which clearly reduces the total fan power.

1.3 Challenges and motivations

Air balancing is typically a process of regulating dampers and adjusting fan speed to achieve design flow values. The current standard air balancing method in industrial practice is essentially a trial-and-error procedure based on the rule of thumb. It needs iterative attempts to balance all terminal air flow due to the coupling effect in ducts [55]. Besides, the method requires a scheduled shutdown period of the ventilation system since the dynamic state deviates largely from the normal working conditions during the balancing process. These pose stiff challenges in practical applications of air balancing considering the cost and performance.

First, the balancing process is costly in time and effort. It is a cooperative work fulfilled by a team of skilled technicians. Owing to its iterative nature, technicians need to move sensors back and forth during balancing, which is tedious and time-consuming.

The duration of the process highly depends on technicians' experience, the complexity of the duct system and required tolerance, and is thus previously unpredicted. Second, the balancing process disturbs the normal service of the ventilation system and requires a scheduled shutdown. This is only applicable during the early stage of commissioning. However, when the whole or a critical zone of a running system requires re-balancing to meet the changing demand, blocking the basic service of ventilation can cause big inconvenience to the occupants and massive financial losses. Hence, one of the challenges is to propose new air balancing methods that can work during system operation with the duration controlled in minutes.

Another challenge lies in improving the air balancing performance. For steady-state performance, the criterion is the accuracy of final balancing results. Apart from using more scientific approaches instead of rules of thumb, accurate flow measurement, which serves as the foundation for all control algorithms, is also a vital factor. However, current prevalent Pitot tube has limitations under low flow conditions and is susceptible to upstream and downstream duct geometries, which can deteriorate the actual balancing results. As for the dynamic performance, the transient response is long with current PID algorithm and the system may keep changing, which makes the system unstable. Therefore, future improvement in the performance of air balancing calls for smooth and accurate control of the air flow.

Considering the necessity of air balancing and corresponding limitations, the objective of this thesis is to optimize the balancing process in both the control algorithm and measuring devices so that it can be:

- **cost-effective**: The procedures of air balancing should be converted into clear and logical code that can be executed without human involvement. Automation of the air balancing process is imperative to reduce dependency on technicians and, as a result, save labor costs.
- **low-maintenance**: The implementation of air balancing should not disturb the normal operation of building ventilation to reduce shutdown maintenance costs. This requires development of online air balancing methods that support balancing-in-service.
- **accurate in flow measurement**: The accuracy of flow measurement should be improved, taking into consideration of low flow conditions and

installation limitations for sensors, to better serve the proposed control algorithm.

- **intelligent controlled**: The terminal devices should be able to communicate with each other using Internet of things (IoT) techniques to achieve intelligent control, monitoring and visualization of the system.

1.4 Major contributions

This thesis aims to optimize the performance of air balancing in duct systems in terms of efficiency, accuracy and cost. Improvements have been made in both the hardware and software design. The main contributions of the thesis are summarized as follows:

First, the accuracy of flow measurement for the key measuring and controlling device in DOAS and VAV systems, the air flow control station (AFCS), is improved. Based on the ANOVA test, this thesis reveals that the control damper in the AFCS has significant effect on the amplification of the averaging Pitot tube (APT), which confirms the previous findings in the literature. Then a revised flow estimation formula is proposed for the APT inside the AFCS to compensate for the error caused by the downstream damper. The revised formula incorporates the damper angle into the calculation of flow rate, which improves the estimation of air flow in the AFCS. The formula demonstrates a good generality over a large range of Reynolds numbers. By applying the proposed formula, the measuring error by APT can be controlled within 0.6% for all tested cases. The highest accuracy (0.02%) is achieved when $Re = 9.57\times10^3$, which is exponentially higher compared with the traditional formula (3.1%). Besides, the hardware design of the AFCS is improved by integrating the wireless techniques. This enables communication among individual terminal devices and provides possibility to achieve more intelligent control, easier monitoring and better visualization. The more precise measuring of air flow serves as the foundation for later proposed air balancing methods.

As for the control algorithm, two online air balancing methods are proposed, which are DCC-AB method and GOAB method. The proposed methods are in clear and logical structure that can be executed without human involvement. The automation of the balancing process significantly reduces the manpower costs. Both methods can be performed during system operation without interrupting the normal service of

ventilation, which avoids inconvenience to the occupants and financial losses caused by maintenance shutdown. The balancing-in-service characteristic provides possibility to achieve accurate air supply under dynamic loads, which indicates a large energy saving potential. The two methods are based on different principles.

The DCC-AB method is based on the distributed cooperative control strategy. The consensus algorithm that has been well developed in the field of network communication is first extended to HVAC applications to solve the air balancing problems. In the proposed DCC-AB method, the balancing process starts from the given imbalanced state and converges asymptotically to the balanced state. The drastic change of damper positions such as short cycling on and off is circumvented, which avoids overshooting and oscillations of the flow rate value. An incremental improvement in the imbalance of flow is guaranteed at each adjustment during the whole process. Besides, the energy efficiency is taken into consideration by ensuring at least one damper to be fully open, which significantly reduces the fan power consumption in damper. The DCC-AB method demonstrates a good generality over a large range of design flow requirements and is insusceptible to small sensor noise. A rapid and stable convergence is guaranteed within several steps, which significantly saves time and labour cost. Moreover, the DCC-AB method circumvents the centralized supervisory control and requires only a sparse communication architecture to achieve the balanced state. The DCC-AB method is a model-free method and requires no prior knowledge on the system topology and duct parameters, making it easy to apply in practice.

The GOAB method is based on the gradient descent algorithm. In this method, an objective function is defined to quantify the discrepancy between the normalized flow rate and the set point, and the increment of damper angle is calculated using stochastic gradient descent. To start with, the GOAB method first tests the response of terminal flow rates with respect to damper angles to obtain an initial Jacobian matrix. Based on this primary information, the algorithm starts to adjust terminal flows towards the desired air distribution, during which the Jacobian is adaptively updated according to newly obtained flow measurement data. The online adaptive mechanism for the Jacobian estimation captures the change of Jacobian matrix during the balancing process. The GOAB method stops until all measured flow rates meet the design values. In this method, the critical damper is explicitly identified based on the null space of the gradient vector. At least one damper is guaranteed fully open, which minimizes the overall flow

resistance of dampers and total energy consumption. The GOAB method also incorporates a coefficient to control the speed of convergence rate and stability of the algorithm. A rapid and stable convergence is guaranteed within several steps. Besides, this method requires little prior knowledge of the system topology and duct parameters, endowing it great potential in industrial applications.

1.5 Organization

The rest of the thesis is organized as follows:

Chapter 2 presents a comprehensive review on the studies of air balancing, including the state-of-the-art air balancing methods and common techniques for flow measurement in air duct systems. This chapter first reviews 7 commonly used methods for determining the air flow and air flow distributions, which are Pitot tube traverse, thermal anemometry, vane anemometry, vortex flowmeters, ultrasonic flowmeters, tracer gas and particle imaging velocimetry. These methods are compared in range, accuracy, resolution, costs, application and constrains. Given that the Pitot tube is currently the most widely used flow sensor in air balancing applications and is probably the bottleneck of AFCS, related studies are presented in the following section. Then this chapter reviews the existing air balancing methods available and divides them into two categories, namely, the iterative methods and non-iterative methods. The first category includes: 1.) proportional method [17] and 2.) target method [96]. The second category includes: 1.) progressive flow method [97]; 2.) fan pressure-based method [98]; 3.) Small's method [99]; 4.) Chen's method [100] and 5.) Jing's method [102]. These methods are introduced in historical context to show the development of this field. For each method, the theory is explained in detail, and the strengths and weaknesses are evaluated.

Chapter 3 proposes a revised flow estimation formula for the APT inside the AFCS to improve the accuracy of measurement. To begin with, the effect of the downstream damper on the flow measurement is studied. The statistical significance of the correlation between the damper angle and the APT flow characteristic is quantified by ANOVA analysis. Then an empirical formula for the APT is proposed to compensate for the systematic error caused by the damper, and the corresponding uncertainty analysis is given. Lastly, the proposed formula is validated under different Reynolds numbers and the accuracy is evaluated.

Chapter 4 proposes an online air balancing method, named as the DCC-AB method. First, the theory of distributed cooperative control is introduced and expanded to air balancing applications. Then the DCC-AB method is proposed based on the distributed consensus algorithm. To explore the effect of individual model parameters on the performance of the method, a detailed parameter analysis is conducted in MATLAB. 5 cases are compared and discussed in terms of the selection of model parameters and design flow requirements. Based on the simulation results, guidance is given on the parameter design to optimize the performance of the method. At the end of this chapter, laboratory experiments are conducted to validate the proposed method, and comparisons are made with the simulation studies.

Chapter 5 proposes another online air balancing method, named GOAB method. This chapter first presents the mathematical derivation, including the gradient descent algorithm, estimation of Jacobian matrix and online adaptation mechanism. Then a series of simulations are conducted in MATLAB to investigate the effect of several key model parameters and initial conditions. Following the simulation studies, laboratory experiments are conducted under different design flow requirements to test the generality of the proposed method.

Chapter 6 summarizes the major works, attained results and main contributions of the thesis. Based on the current knowledge and existing challenges in air balancing, an outlook on future directions is given.

Chapter 2. Literature review

2.1 Introduction

Accurate air balancing calls for intelligent control techniques and precise flow measurement. For this reason, this chapter reviews previous research on both the air balancing methods and common techniques for flow measurement in air duct systems. The main purpose of this chapter is to summarize the current knowledge on exposure, identify limitations and deficiencies in the balancing process and establish a theoretical framework for the research topic. To begin with, Section 2.2 introduces several flow measurement techniques including Pitot tube traverse, thermal anemometry, vane anemometry, vortex flowmeters, ultrasonic flowmeters, tracer gas and particle imaging velocimetry. Considering that Pitot tube is the most widely used flow sensor in air balancing applications, related studies are presented in Section 2.3. Sections 2.4 and 2.5 introduce conventional (iterative) air balancing methods and non-iterative air balancing methods respectively. These methods are reviewed in historical context to show the development of this field. The conventional methods include proportional method [17] and target method [96]. The non-iterative methods include progressive flow method [97], fan pressure-based method [98], Small's method [99], Chen's method [100] and Jing's method [102]. For each method, the theory is introduced and the strengths and weaknesses are evaluated.

2.2 Common approaches for flow measurements

Air balancing relies heavily on the measurement of air flow. Inaccurate or inefficient flow measurements can degrade the performance of TAB process. There are quite a few methods available to determine the air flow rate in duct systems. These methods are based on different principles and have different advantages and disadvantages in range, accuracy, resolution, costs and applications. The selection of flow measurement methods should be in accordance with manufacturer's recommendation and accuracy requirements.

The most widely used method for flow measurement in air duct systems is the Pitot tube traverse [56, 57], which also serves as a standard reference for calibrating other devices. In this method, a Pitot tube is used to measure the local flow velocity at the test point based on Bernoulli's equation. The Pitot tube contains two tubes in

different directions: one is parallel to the flow facing upstream and the other is perpendicular to the flow. By measuring the pressure difference between two tubes, the dynamic pressure is obtained and the corresponding velocity of flow can be calculated. The Pitot tube traverse is simple, straightforward and cost-effective. However, due to the long initial and response time, it is limited in measuring quasi-steady state flows. Besides, the Pitot tube is not applicable to low Reynolds numbers since viscosity imposes a stronger effect on the flow pattern at low flow and the assumption of inviscid flow in Bernoulli's equation fails [58]. Moreover, Pitot tube traverse method requires long enough upstream and downstream clear straight duct, usually 10 times of the duct diameter, to make sure the measured point locates at the fully developed region of the flow, which is rarely met in practice. Aside from Pitot tube, other flowmeters like orifice [59, 60], and Venturi tube [61] adopt the similar principle.

Thermal anemometry [62] mainly includes hot-wire [63] and hot-film [64], which consists of electrical heaters and temperature sensors. By heating a wire suspended in air and measuring the heat dissipation rate, the velocity of air flow can be calculated based on forced convection equations. The accuracy of thermal anemometry is decided by the accuracy of the temperature sensor and voltage/current meter. Thermal anemometers are of relatively low cost since the hot-wire or hot-film can be extremely small and thin. The response of thermal anemometers is significantly faster than Pitot tube, which can be up to 105 Hz. However, it requires regular calibration since the heat convection efficiency of the probe can be affected by adhered matters during usage [65, 66]. The use of thermal anemometry in extreme low air velocities needs special care and extra calibration as the natural convection becomes prevalent and the heat convection rate is no longer solely dominated by forced convection [67].

Vane anemometry [68, 69] captures the kinematic energy of flow and converts it into rotary energy. When the vane angle is given constant, the rotary speed will be proportional to the velocity of flow [70]. The simplicity of vane anemometer allows manufacturing of portable handheld devices, which can be quite convenient. Vane anemometers have a minimum detecting velocity: the air flow must be strong enough to overcome the initial friction of the rotor. On the other hand, the timer counting the interval between pauses can be overflowed when the rotary speed is too slow. Considering the accuracy of the flow measurement using vane anemometry is relatively low, it is suitable for basic applications requiring only qualitative analysis.

Vortex flowmeters work on the vortex shedding principle, which is referred to as the Karman vortex effect [71]. In the recent past, many literatures have been reported on the performance of vortex flowmeters [72, 73]. Vortex flowmeters operate within a small range of Reynolds number. The typical accuracy can reach as high as 0.5% to 1% of reading after careful calibration, which is significantly higher than Pitot tube or thermal anemometers. Besides, vortex flowmeters have relatively low cost and maintenance, and faster response time. Since the measuring range of vortex flowmeters is rather small, they are more suitable for monitoring process during normal operating conditions.

Ultrasonic flowmeters are one of the fastest-growing technologies in the field of measurement, instrumentation and control [74, 75]. Transit time ultrasonic method uses two transducers to alternately transmit and receive the ultrasonic pulses. By measuring the difference in the travel time of pulses transmitted in the direction of and against the flow, the velocity of the medium can be obtained. The advantages of ultrasonic flowmeters over competing flow technologies include: convenience of clamp-on, high accuracy, fast response (less than 1ms), wide range of measurement, high sensitivity at extreme low velocity and free of direct touch with tested flow. The accuracy of ultrasonic flowmeters can be as high as 0.5% of reading or better after calibration. By adopting multiple paths in the flowmeter, the 3-dimensional velocity component of the flow can be obtained precisely, which is desirable for indoor flow measurement. However, current ultrasonic flowmeters are all at high price, which restricts its application as testing devices in HVAC system.

Tracer gas is a volumetric approach for measuring flow in small ducts or pipes. A specific tracer gas with a known quantity is released at the upstream of the flow, and a portion of the gas eventually leaves the system and disperses into the ambient. The concentration difference between the release point and detection point will dictate the amount of infiltration. The tracer gas method is widely used in HVAC duct systems for quantifying air tightness and air exchange rate [76, 77]. Applications of this method can be flexible with different strategies of gas injection. The accuracy is mainly determined by the sensitivity of the gas concentration sensor, which is hardly below 5% in practical applications [78]. Active tracer gas method needs a tracer gas source, which causes inconveniences in many applications. Besides, the tracer gas method is currently of high

cost compared with other flow measurement techniques of similar accuracy. However, the tracer gas method is still preferable in measuring air tightness of the building.

Particle imaging velocimetry (PIV) is a technique for indoor air flow field measurements. It uses high resolution video recorder to identify the suspended particle in the flow and calculate the velocity vector field by comparing multiple frames of images [79]. The PIV provides instantaneous velocity vector measurements and quantitative information of indoor air distribution [80]. The PIV is significantly more efficient than point-wise measurements of air velocity in the space using traditional anemometry. The PIV uses the motion of tracer particles to indicate the air flow, and the size of the tracer particle should be neither too small to scatter insufficient light signal for image recording devices, nor too big to loss the tracking behaviour of turbulence. The accuracy of PIV is directly determined by the displacement error and the uncertainty in the time delay between pulses. The relative error of PIV is estimated to be around 2% in a 2-dimensional PIV system [81]. Unlike tracer gas method, the PIV requires an unobstructed view of the domain being measured, which may reduce the applicability in buildings occupied by furniture. Currently, PIV is only applied to some complex flow systems due to the relatively high cost.

Currently, Pitot tube is still the most prevalent flow measurement technique in HVAC duct systems for its simplicity and low cost. The Pitot tube is typically used as an insertion-type flow meter to measure the air flow rate in field test applications, which can be quickly and easily installed. It is also commonly found in air flow control stations (like VAV box) as an embedded sensor. Considering that measurements of air flow in TAB are mainly fulfilled by the Pitot tube, related studies are reviewed in the following section.

2.3 Studies on Pitot tube

Pitot tube comes in many varieties, where the averaging Pitot tube (APT) is more commonly used in HVAC applications. The APT is a type of multiport self-averaging flow meter that has two isolated plenum chambers with multiple sensing ports. These ports are precisely drilled along the chamber in a certain pattern to obtain multiple samples across the section of the pipe. The APT offers a more precise reading over the plain Pitot tube since the measurement reflects the average velocity of the flow across the entire pipe diameter instead of only a single point in the flow stream.

The readout device measures the differential pressure between two plenum chambers and converts it to the volumetric flow rate (or flow velocity) based on Bernoulli's equation. The flow rate is proportional to the product of flow coefficient and the square root of the differential pressure. For a given probe, the flow coefficient varies with the operating conditions including fluid velocity, density and viscosity [82] and is usually given empirically by the manufacture. Apart from these external factors, the cross-sectional shape and relative positions of the openings can also dramatically change the characteristics of the Pitot tube, which has been extensively studied in [83-87].

[83] formulated a mathematical model for the flow coefficient of APT, taking into consideration of factors like probe shape, selected constructional features and flow conditions. [83] pointed out that the obtained pressure difference and the change of flow coefficient with Reynolds number are strongly dependent on the probe shape. The effect of averaging chamber size on the uniformity of the pressure distribution in the chambers was also investigated. The sensor characteristic shows little difference on the number and location of holes, indicating possible simplification of sensor manufacturing. [84] examined 8 designs of APT cross-sections to find the optimal shape that maximizes the differential pressure. The distribution of the static pressure upstream and downstream of the APT were studied using computational fluid dynamics (CFD). It was found that the circular APT has the minimum differential pressure, and the diamond-shaped design has the maximum. [85] conducted a series of numerical simulations to investigate the characteristics of 15 different probe cross-sections. By solving the formulated mathematical equations under assumed boundary conditions, the distribution of velocity and pressure in the surroundings of APT can be obtained. To find the probe design with best metrological properties, comparisons were made between the value of flow coefficient and its dependency on Reynolds number. The probe with relatively low and constant flow coefficient value was selected and further optimized in [86]. The characteristics of the flow coefficient was then studied under different Reynolds number, and empirical formulas were given for estimation. Analysis shows that the uncertainty in the determination of the flow coefficient is around ±0.7%. Experiments were repeated under various pipe diameters (104-296 mm) in a wind tunnel. The observed characteristics are consistent over a large range of flow under all cases, making it possible to use a constant flow coefficient value in practice. [87] conducted numerical studies to investigate the effect of APT probe shape on the permanent pressure loss. 4

types of APT were tested to find the optimum shape that maximizes the differential pressure while minimizing the permanent pressure loss.

Pitot tube is sensitive to the deformation of the velocity profile. Accurate flow measurement requires fully-developed and symmetrical pipe flow. According to the industry standards [88-90], a minimum of 7 duct diameters upstream and 3 duct diameters downstream clear duct should be guaranteed for the installation of Pitot tube to ensure the flow is fully-developed at the measuring point. However, this is rarely met in practice due to space limitations, and the accuracy of measurement can be drastically affected by upstream and downstream duct geometries. Extensive studies can be found in the open literature investigating the performance of Pitot tube subjected to upstream and downstream disturbances.

According to a review by [91], the log-linear method proposed by Winternitz and Fischl exhibits superior accuracy (0.5%) for non-fully developed flow conditions in Pitot tube measurement, which offers a solution for measuring irregular flow that is commonly encountered in non-ideal duct configurations. Applying the log-linear method (10-point), [89] studied the velocity contour with respect to varying distances from 1D to 50D downstream of plain duct and obstructions including 30º junction, single 90º elbow, offset elbows and C-shape elbows. The results demonstrate that the velocity profile will be highly skewed when obstructions exist close upstream, associated with a large error in the obtained mean velocity. By comparing the measure data with the ideal case (50D plain duct), the author concluded that at least 7D length of plain duct prior to the measuring point should be guaranteed to achieve 5% accuracy using a single traverse. [92] also investigated the velocity profile at various distances downstream of an obstacle (3×30º segmented elbow). Experiments were repeated at different mean velocities (10m/s, 18m/s, 26m/s) using two designs of APT respectively. A large deformation of velocity profile can be observed at even 9D from the obstacle. [93] examined the flow coefficient of an APT installed behind an elbow bend and indicated that the measuring uncertainty resulting from the asymmetric velocity profile can be eliminated, providing sufficient upstream and downstream distances from the meter.

There are a number of studies reporting in VAV applications since the Pitot tube (mainly APT) is commonly adopted as an embedded sensor in VAV boxes. [94]

investigated the major factors that cause inaccuracy and instability issues in VAV air distribution systems. It was found that the inlet conditions, low VAV damper positions and low airflow rates have significant influence upon the air flow measurement by Pitot tube. To further examine the effect of inlet conditions (the upstream duct geometry) on the Pitot tube amplification and precision, a series of designed laboratory and field tests were conducted. Among all test conditions, the kinked inlet condition induces the largest reading error, which can be up to 45% of the reference value. The subsequent research [95] demonstrates that the error caused by non-ideal inlet conditions in Pitot tube flow measurement can be reduced by a flow conditioner. With the flow conditioner installed immediately upstream of the VAV box, the reading errors were controlled within ± 5% for all tested inlet conditions. The results of experiments again indicate that the upstream duct geometry can dramatically affect the accuracy of Pitot tube measurement. [88] compared the response of VAV air flow sensor (Pitot tube) between non-ideal duct configurations commonly found in buildings and a baseline case for two types of VAV terminals in three different sizes. In the baseline case, 40 diameters of straight unobstructed duct was constructed prior to the VAV box. In the test cases, the upstream disturbances including 90° short radius elbows, concentric reducers, expanders, S-shape geometries and their combinations were investigated. Significant loss of both sensor amplification and accuracy could be observed in almost every non-ideal inlet case. In particular, placing a 90º elbow immediately prior to a transition shows no apparent difference in the sensor response compared with the transition only, which implies that the joint effect of multiple fittings may be dominated by the nearest one to the VAV box. On the other hand, the supporting flow visualization experiments demonstrate that the position of the embedded damper strongly interferes with Pitot tube. The author also mentioned that increasing the distance between the damper and Pitot tube in a VAV box is expected to mitigate the non-uniform velocity profile.

Most efforts to date have focused on the studies of upstream duct geometry. There is a lack of research addressing the effect of downstream duct geometry on Pitot tube measurement. The flow visualization experiments conducted by [88] provide strong evidence that the downstream damper in the VAV box can significantly reduce the amplification of Pitot tube. The current configuration of VAV box that the damper is placed immediately downstream of the Pitot tube is obviously contrary to the generally accepted industry standards specifying a minimum of 7D upstream and 3D

downstream clear duct for its installation, and this is likely to cause noticeable errors in flow measurement. However, this problem has been widely ignored by industry and the effect remains unquantified.

2.4 Conventional air balancing methods

Conventional air balancing methods are essentially trial-and-error methods that require iterative attempts to balance all terminal air flow to design values. Due to the coupling effect, the previously balanced branches can be re-imbalanced when air flow in neighbouring ducts changes, which makes the balancing process rather difficult to implement. Consequently, conventional air balancing methods are laborious and costly, and the duration highly depends on technicians' experience, system complexity and required tolerance. Although conventional methods have some deficiencies, they are extensively used in engineering for fairly straightforward operation and low expertise requirements.

Proportional method [17] is the most commonly used method for balancing supply, return and exhaust systems. According to ASHRAE, the procedures for proportional method are:

a) Measure the total system air flow at the fan outlet and calculate the flow ratio r_{tol} (actual air flow to design air flow).
b) Measure each terminal air flow and calculate the corresponding flow ratio r_i.
c) Arrange r_i in ascending order and keep the damper with the lowest ratio (r_{min}) fully open throughout the process.
d) Starting from the second lowest ratio, sequentially adjust r_i to r_{min} by regulating the corresponding damper.
e) Repeat procedure (a) to (d) until all terminals have been balanced within ±10% of the design values.
f) Adjust the fan speed so that the total air flow is controlled within ±10% of the design value.
g) Re-measure all terminal air flow and make final adjustments.

[96] proposed a revised method, named target method, to speed up the convergence of balancing process. An empirical formula for the calculation of target flow is established to partially compensate for the secondary effect in ducts. In

proportional method, the branch air flow and static pressure will gradually rise at the beginning due to the increase of duct resistance. The previously well-adjusted terminals will be no longer correct as the balancing process proceeds. In particular, the first adjusted terminal will receive the largest excess of flow over its design value, and the subsequent adjusted terminals will receive descending ones. This implies that directly adjusting towards the target could be problematic. Therefore, the target method includes a margin in the calculation of target flow, which varies with the sequence of damper adjustment to compensate for later increase of flow rate. An empirical law is established based on extensive simulation experiments. The deduction factor is given by $\%k = (n/N)^{0.0445} \times 100\%$, where n is the sequence of the damper being adjusted, N is the total number of dampers, and $\%k$ is the deduction factor in percent form. Although the method improves the efficiency of balancing process to a certain extent, it remains iterative with the duration unpredicted.

2.5 Non-iterative air balancing methods

A few researches on the development of non-iterative air balancing methods have been reported recently. [97] proposed progressive flow method (PFM) where the balancing process starts from the furthest terminal and progressively proceeds backward. The most downstream damper is set as the critical damper, and a control loop is established between the measured flow and fan speed to achieve and maintain the design value. Then the upstream dampers are adjusted sequentially. The control loop guarantees the invariance of air flow through the whole downstream during balancing. In this method, each damper is only adjusted once, thereby theoretically saving 2n+b−1 measurements for a system with n terminals and b branches compared with the conventional method. However, this method requires additional devices for the control loop and branch dampers, which increases the operating complexity and equipment costs.

Following this backward-adjusting approach, [98] proposed another non-iterative method, named fan pressure-based method (FPM) that dispenses with direct measurements at terminals. In this method, fan pressure is controlled to be constant during the balancing process and fan flow rate is estimated by the QP curve. At each step, the damper is regulated until the estimated fan air flow satisfies the desired total. The method is validated by experimental tests and demonstrates nearly the same

performance as progressive flow method while requiring only a fan pressure sensor. This method eliminates the need for flow measurement at terminals, which saves labour work and costs of TAB process. However, this method only applies to small-scale ventilation systems with short common pipes, and the accuracy of estimation relies on manufacturer's data and precision of the control system.

Although progressive flow method and fan pressure-based method improve the efficiency of TAB process to some extent, they actually circumvent the problem caused by secondary effect and the nature of the duct system remains unclear. [99] first established a mathematical model explicitly calculating the damper positions satisfying the design flow requirements. This model relates nodal pressures to branch flows by mass conservation law and pressure loss equations. The system parameters including fan characteristics and the minimum friction loss coefficient of each branch are determined by two sets of measurements on terminal air flow. The first set is taken with all dampers fully open and the second set is taken with one of the dampers closed. The number of equations established is exactly equal to the number of unknowns introduced, and the static system parameters can be obtained solving the nonlinear equations. Then the desired damper positions are determined in a similar way by substituting the design flow values into the model. The flow rate at each step of the balancing process can be predicted from the identified model. Hence, by adjusting the terminal dampers singly and sequentially while aligning the measured flow rates with the predicted values, the system can finally achieve balance. However, this method only applies to simple duct systems without junctions and may fail to provide reliable predictions for a complex case.

[100] made further improvements to Small's method in the efficiency of data acquisition and the accuracy of parameter identification. The model is validated both numerically and experimentally. Unlike traditional methods that take one measurement at each terminal, Chen's method collects multiple measurement data at a time to avoid moving the sensor back and forth, which improves the efficiency of measuring process. To fully utilize the acquired data, the maximum-a-posterior (MAP) estimation and trust-region method are applied to achieve better accuracy in identifying system parameters. In this method, dampers are closed in turns during the measuring process instead of selecting a specific damper to regulate. In this way, the established equations for identifying unknown parameters could be less ill-conditioned and easier to solve.

Another work by [101] reduces the requirement on the fan model and generalizes the application of the method to any subset of a duct system. However, Chen's method relies heavily on optimization algorithms and requires high computational power, which is currently unavailable on most mobile devices. Besides, acquiring model structure from either manual input or building information model (BIM) is not yet a common and easy expertise that has been widely obtained by technicians.

[102] proposed a revised method where the identification of the inherent system parameters is separated from that of the damper resistance coefficients. In this method, the least squares regression is applied to identify the underdetermined parameters. A variation of this method [103] adopts support vector machine to establish the pressure prediction model and calculate unknown variables. The two methods circumvent the difficulties encountered in solving non-linear equations by using supervised machine learning. However, these methods only focus on the balancing accuracy and neglect the TAB standards that at least one damper should be fully open. Besides, collecting enough training data can be time-consuming and costly and may sometimes be unavailable due to the lack of proper automatic devices.

Chapter 3. Air flow control station (AFCS) with improved APT flow estimation formula

3.1 Introduction

The basic device for measuring and controlling the air flow quantities in VAV and DOAS systems is the air flow control station (AFCS). For VAV systems, the AFCS is also known as the VAV box. The AFCS mainly consists of an air flow sensor, controller, actuator and damper. The controller modulates the damper to different positions based on the set point as well as the measured air flow rate. The AFCS intends to deliver the required amount of air to the zone such that 1) the cooling/heating capacity satisfies the cooling/heating load, 2) the room temperature matches the set point, and 3) the ventilation rate meets the IAQ requirement. However, the actual performance of AFCS is often affected by the accuracy of the embedded air flow sensor [95]. The commonly adopted flow sensor in AFCS (such as VAV box) is the Pitot tube, which is sensitive to various disturbances like ambient temperature, velocity profile and protuberances and may fail to provide accurate readings in certain circumstances. Even though some AFCS adopts cascade control architecture on the ambient temperature or IAQ probes, inaccurate measurement of air flow rate in the inner loop could still deteriorate the system's control performance. Moreover, if the design minimum air flow rate is below the minimum detectable value by the sensor, the AFCS will cycle on and off to maintain the space temperature, which could result in an uneven air flow and reduced life expectancy of the AFCS [94].

This chapter proposes a revised formula for the APT to estimate the air flow rate inside the AFCS. The proposed formula takes into consideration of the effect exerted by both the Reynolds number and the downstream disturbances on the APT flow coefficient. The incorporation of damper position into the calculation of flow rate compensates for the error caused by the downstream damper, and thereby improves the accuracy of measurement. Besides, the AFCS is equipped with wireless techniques to achieve commutation among terminal devices. The remainder of this chapter is organized as follows: Section 3.2 introduces the experimental setup and designed AFCS. Section 3.3 describes the experimental procedures. Prior to the experiments, necessary sensor calibration is performed to reduce possible systematic errors and the bubble test is conducted to avoid air leakage. Section 3.4 first applies the analysis of variance

(ANOVA) to assess the statistical significance of the correlation between the measured data and damper position. Then an empirical formula for the APT is proposed and the corresponding uncertainty analysis is given. Section 3.5 validates the proposed formula under different Reynolds number conditions and evaluates the accuracy. In the end, Section 3.6 gives a summary.

3.2 Designed AFCS and experimental setup

The AFCS in our platform is designed imitating the common industrial ones, as shown in Figure 3.1. It mainly comprises an APT, differential pressure transmitter, damper actuator and controller. The geometry of the APT is shown in Figure 3.2. It has similar metrological properties to the two-plate APT investigated in [85] based on a preliminary study. The imbedded differential pressure sensor in the AFCS is Omron D6F-PH0505AD3, of which the measuring range is ±50 Pa with ±3% reading accuracy. The single-plate damper is driven by a servo motor to rotate around the shaft within a range of -90° to 90° originally. After calibrating the damper angle and installing position limiter, the damper works in a range from the neutral 0° position (fully open) to 90° (fully closed). The damper position is controlled linearly by a 20ms-period pulse signal with modulated width. A 1ms pulse will turn the damper to 0°, and 2ms pulse will turn the damper to 90°. The motor provides an angular resolution of ±0.18°. The controller regulates the damper until the measured flow rate satisfies the reference value. The AFCS is equipped with a Wi-Fi communication module so that the data can be bidirectional transferred by the supervisory computer wirelessly. Detailed specifications are listed in Table 3.1.

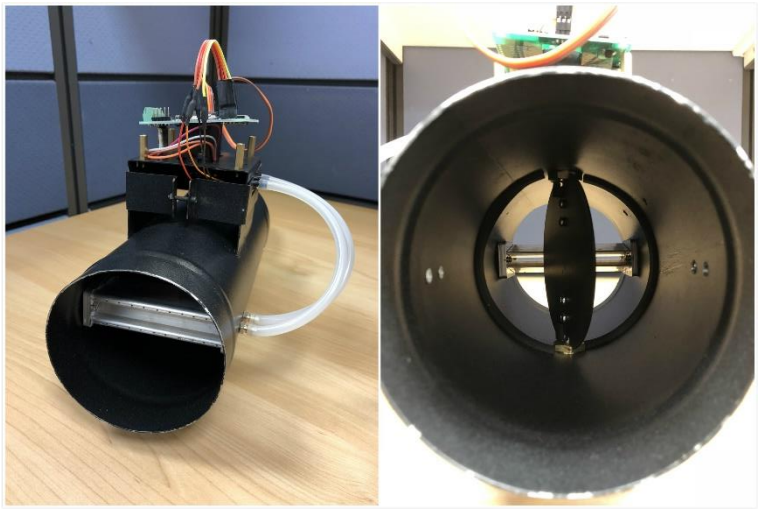

Figure 3.1: The designed AFCS

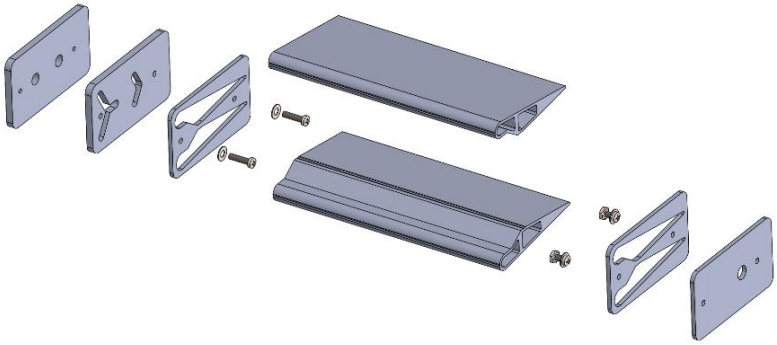

Figure 3.2: Exploded view of the APT geometry

Table 3.1: Specifications of the AFCS

Diameter	100mm
Length	260mm
Power Supply	5VDC
Measuring Range	15-150 m^3/h
Accuracy	0.6%
Damper Position	0-90°
Angular Resolution	+/-0.18°
Wireless Communication	802.11n

The experimental platform for flow calibration is shown in Figure 3.3. The main duct, located in the first row, contains a centrifugal fan to provide air supply. The manifold distributes the flow from the main duct into four branches. Each branch is installed with a control damper to switch between different air supply paths. All testing was conducted in the second row (from top), which is independent to the rest of the branches. Hence, the schematic diagram of the experimental setup is simplified as Figure 3.4. The simplified one consists of several essential components including ducting, fan, AFCS and reference sensors.

Figure 3.3: Flow calibration platform

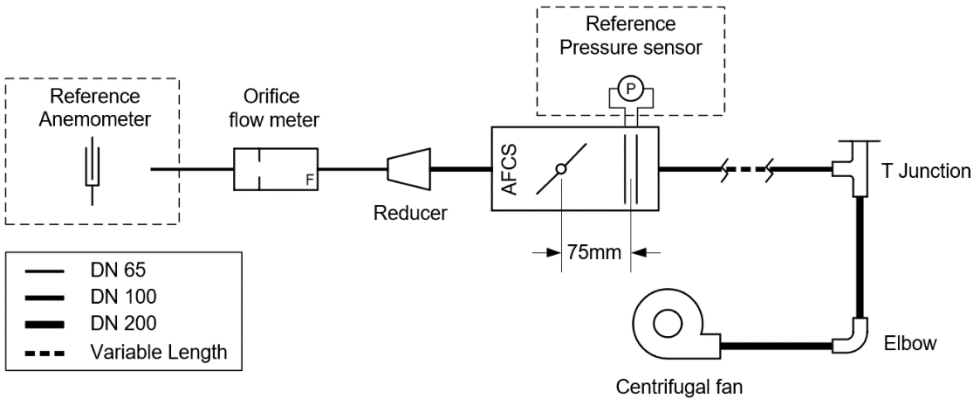

Figure 3.4: Schematic diagram of the flow calibration platform

The system is made of 0.6mm Z22 SGCC galvanized steel spiral duct. The diameter of the main duct is 200mm, and the branch under investigation is 100mm. The elbow used in this platform is a 90° welded gored segmented elbow without internal vent. And a 90° T-junction with 45° entry branch is adopted to reduce the air resistance. As denoted in Figure 3.4, the duct between the T-junction and AFCS is of variable length. The ducting is separated into several segments of straight duct with flanged connection. The upstream and downstream clear straight duct of the AFCS can reach up to 16 times of the pipe diameter. A reducer is installed behind the AFCS to change the diameter into 65mm to satisfy the accuracy requirements for the orifice flow meter. And the distance from reducer to the orifice is sufficiently long to ensure the accuracy of the measurement.

The LTI FSE 355-EC centrifugal fan is installed in this platform. A maximum of 1800 m^3/h (0.5 m^3/s) of air flow rate can be supplied when the fan operates at 1900 rpm and the discharge pressure reaches 1600 Pa. The fan is controlled by 0-10VDC

signal to vary the fan speed, which is generated by an NI voltage output module (NI 9264) through a computer control system.

The range of the velocity under investigation is selected as 1m/s to 3m/s according to the requirements of DOAS. Then the corresponding air volume flow rate will be 28.3-84.8 m^3/h (7.85×10^{-3}-2.36×10^{-4} m^3/s) for the DN100 pipe. To accurately measure the flow within this range, the YPLGK-65 orifice flow meter is selected following the standards GB/T2624-2006, and the corresponding properties are given in Table 3.2. The overall relative uncertainty level is below 0.8%. The orifice flow meter offers a 4-20mA output signal, which is connected to an NI current input module (NI 9208) for data acquisition.

Table 3.2: Parameters of the orifice flow meter

Model	Diameter Nominal (mm)	Maximum Flow (m^3/h)	Orifice Plate Bore Diameter (mm)	Beta Ratio	Discharge Coefficient	Measuring Uncertainty
YPLGK-65	65	191	40.144	0.590288	0.613037	0.78%

As shown in Figure 3.5, the TSI 8455-150-1 air velocity transducer is applied to measure the discharge velocity from the outlet. The TSI 8455-150-1 provides selectable measuring ranges from 0.127m/s to 50.8m/s with the accuracy of ±2.5%.

Figure 3.5: The TSI 8455-150-1 air velocity transducer

The Dwyer MS-121-LCD Magnesense differential pressure transmitter is used to measure the pressure differential between the Pitot tube and the static tube, as a

reference for the imbedded differential pressure transmitter. The Dwyer MS-121-LCD offers an accuracy of ±1% for 50 Pa bi-directional ranges.

3.3 Sensor calibration

All physical measurements are inevitably subjected to uncertainties. When exposed to certain conditions, the readings of the sensor can drift slightly over time. It is necessary to perform sensor calibration for reliable, accurate and repeatable measurements. Considering that the accuracy of the measured air flow quantities is the critical factor that determines the success of this project, an additional reference anemometer, the TSI 8455-150-1 air velocity transducer was applied to calibrate the orifice flow meter YPLGK-65. Up to 49 points are measured by the anemometer over the outlet cross-section (>3D downstream of YPLGK-65). The results are plotted in cylindrical coordinate, as shown in Figure 3.6. The red dots demonstrate the measure data and the z-axis represents the value of velocity. A surface fitting was performed on the experimental data to obtain the velocity profile $V(r,\theta)$. Then the volumetric flow can be estimated by the surface integral of the velocity:

$$\hat{Q} = \int_{-\pi}^{\pi} \int_{0}^{D/2} V r dr d\theta \tag{3.1}$$

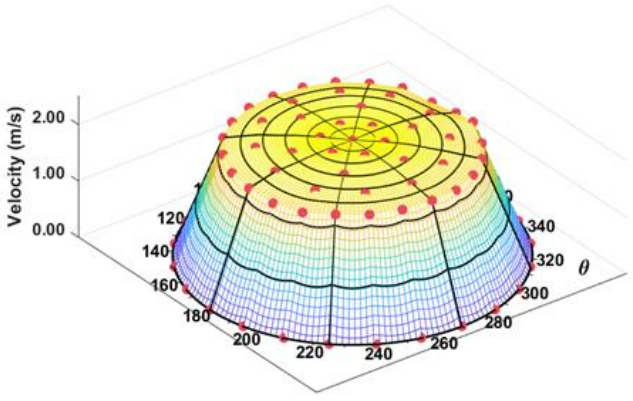

Figure 3.6: Velocity distribution over the outlet cross-section

Table 3.3 compares the estimations with the direct measurements under 5 different flow rates, where the percent difference ε is defined as the absolute difference between the two values divided by their average:

$$\varepsilon = 2 * \left| V_1 - V_2 \right| / (V_1 + V_2) \tag{3.2}$$

As can be seen, the flow rates obtained by two sensors show good consistency among all tests. The largest difference (1.35%) occurs in the fifth test when flow rate approaches the lower bound, and the results appear to be rather small (within 0.5%) when flow rate is greater than 50 m^3/h. Hence, the orifice flow meter is considered to be accurate within its measuring range.

Table 3.3: Comparisons of theoretical and directly measured air flow rates

Test	$\widehat{Q}$ (m^3/h)	Q (m^3/h)	ε (%)
1	84.5	84.1	0.48
2	66.2	66.0	0.30
3	48.9	49.1	0.41
4	32.6	32.3	0.93
5	14.7	14.9	1.35

Similarly, the imbedded pressure sensor (Omron) was calibrated by the external reference sensor (Dwyer), and comparisons were made between the two sensors. A total of 200 pairs of data were collected at different flow rates and the results are shown in Figure 3.7. The x-axis and y-axis denote the measured values by two sensors. In this thesis, a relative residual sum of squares (RelRSS) is defined in Eq. (3.3) to quantify the discrepancy between the two sets of samples. The RelRSS is defined as the ratio of the residual sum of squares (RSS) to the sum of squares. The straight line in Figure 3.7 represents the linear equation y = x, and the shaded band represents the 95% confidence interval for x when RelRSS = 0.006. It can be found that most points fall within the bounds of the interval, and the experimental RelRSS achieves 0.0058. Hence, we assume that the differential pressure sensor is sufficiently accurate.

$$RelRSS = \frac{\sum_{i=1}^{N} \left(y_i - x_i \right)^2}{\sum_{i=1}^{N} x_i^{\,2}} \tag{3.3}$$

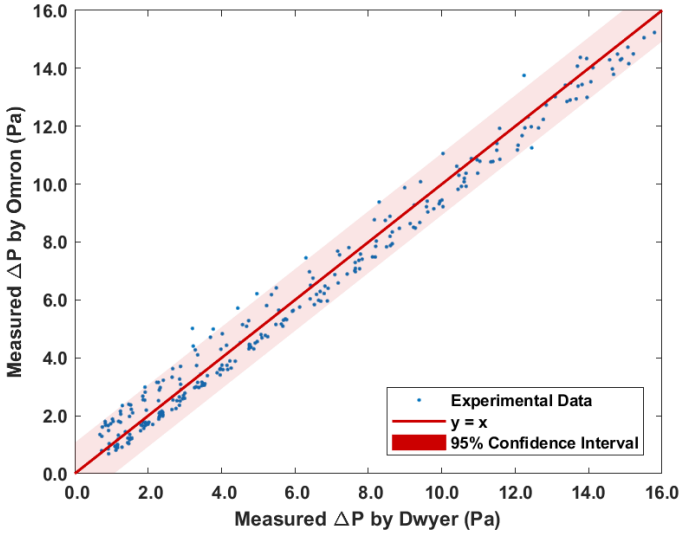

Figure 3.7: Comparisons of measured differential pressure by Dwyer and Omron

The installation of the damper plate is calibrated visually as shown in Figure 3.8, where the left-hand side is the photo of AFCS from the front view before calibration and the right-hand side is the schematic diagram from the top view. The diameter of the damper axes is 2mm. A plumb line of 0.75mm diameter is adhered at the forefront of AFCS, which aligns with the damper axes with an uncertainty of 0.5mm. The neutral position (0°) is calibrated until the plumb line, damper axis and the tip of damper plate are all aligned. After calibration, the accuracy of damper angle is achieved ±0.34°.

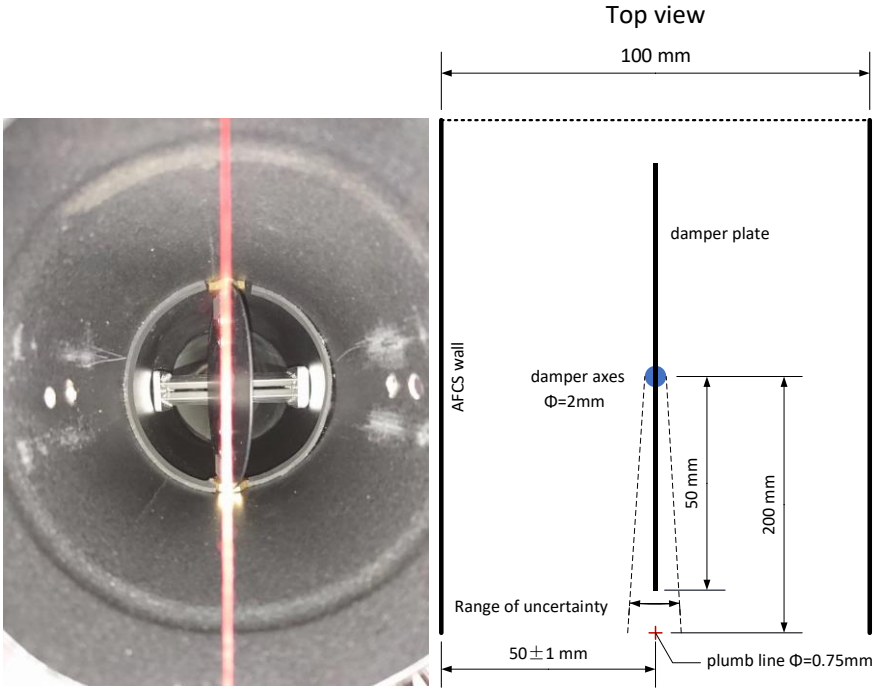

Figure 3.8: Calibration of the damper angle

Prior to the experiments, the bubble test was conducted to ensure there was no detectable air leaks in the duct system. The ductwork was pressurized to approximately 1600 Pa with all vents blocked off, and the soapy water was sprayed on the joints along the ductwork. If bubble appears, then there is a leak in the joint and the aluminium foil tapes will be applied onto the surface.

After all these preparation works, experiments were conducted to find the relationship between ΔP and θ under different Reynolds numbers, where ΔP is the differential pressure between the Pitot tube and static tube, θ is the damper angle. The clear straight ducts for both upstream and downstream of the AFCS is sufficiently long (16D) to allow the attainment of fully developed flow. The control signals as well as the sensor output signals were connected to the NI DAQ devices that could be accessed by the supervisory computer. To begin with, the control signal was sent by the computer to start the fan and sufficiently long time was spent waiting for the stabilization of the system. For the base case ($Re = 1.28\times10^4$), the flow rate target was set to 56 m^3/h, and a control loop was established to approach and maintain this target by varying the fan speed. Then ΔP was measured at different damper positions following a specific sequence. The damper is gradually closed ($\theta \in \{0°, 5°, 10°, \ldots, 85°\}$) and the test stops until the maximum fan power cannot satisfy the flow rate target. The sampling rate was 10Hz and the duration lasted for 2s. A total of 20 data were sampled at each θ to reduce the measurement noise and the average was recorded. The entire process was repeated 40 times to ensure the measurement was representative. In particular, the sequence of damper angle was altered in each run to eliminate possible systematic errors. The whole process was repeated under different Reynolds numbers ($Re \in \{6.38\times10^3, 9.57\times10^3, 1.28\times10^4, 1.59\times10^4, 1.91\times10^4\}$) by switching the target flow rate Q to another value ($Q \in \{28, 42, 56, 70, 84\}$ (m^3/h)). The flow chart of experimental procedures is shown in Figure 3.9.

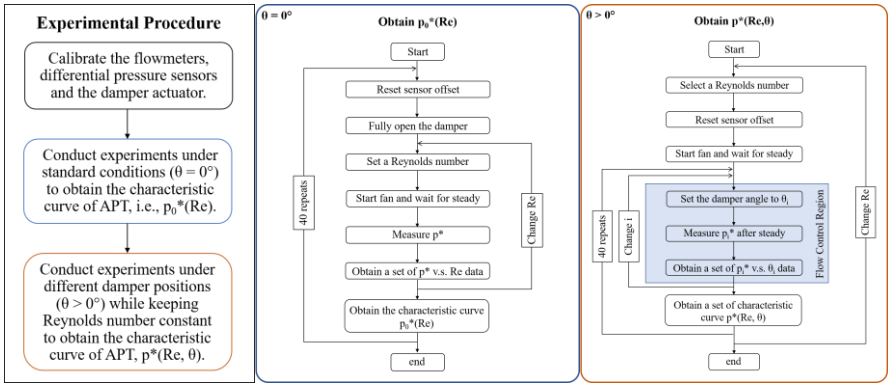

Figure 3.9: Flow chart of experimental procedures

3.4 Improved flow estimation formula for the APT

The Pitot tube and/or APT operates on the principle of the Bernoulli's equation that the kinetic energy of the fluid is converted into potential energy at the stagnation point, located at the Pitot tube entrance. The pressure differential measured by an ideal Pitot tube should be equal or proportional to the local dynamic pressure, irrespective of Reynolds number, flow condition and etc. In order to reduce the number and complexity of the variables that govern the problem, the dimensional analysis is applied and a normalized variable, p*, is introduced in this thesis. p* is defined as the ratio of the differential pressure to the dynamic pressure, as shown in Eq. (3.4).

$$p^* = \frac{\Delta P}{\frac{1}{2}\rho v^2} \tag{3.4}$$

where, v = Q/A. In engineering applications, the commonly adopted calculation formula for APT flowmeters is given by Eq. (3.5).

$$v = K\sqrt{\frac{2\Delta P}{\rho}} \tag{3.5}$$

where K is the flow coefficient of the APT provided by the manufacturer and is usually a constant under a certain Reynolds number. Equating Eqs. (3.4) and (3.5) gives $p^* = 1/K^2$, which implies that p* is also supposed to be a constant. However, a noticeable variation in p* was observed in the experiments. The results for the base case ($Re = 1.28\times10^4$) are shown in Figure 3.10, where the error bars indicate the standard deviation of the 40 repeated measurements.

As depicted in Figure 3.10, p* appears to vary with θ when Reynolds number remains constant. When damper is almost fully open (θ = 0°), p* is relatively high. As the damper is gradually closed, a distinct decrease in p* can be observed. In order to

determine whether the change in p* is correlated with the change in θ or just attributed to a random effect, the ANOVA test is conducted. The ANOVA is a statistical technique that assesses potential differences among two or more group means. In this chapter, it is applied to determine whether introducing a θ-dependent model will significantly reduce the residuals than the θ-independent model by comparing the variances of residuals of the two regression models. Without additional information, a simple linear function with respect to θ is assumed as follows:

$$p^* = \beta_0 + \beta_1 \theta \tag{3.6}$$

The hypothesis test is formulated as:

$$\begin{aligned} H_0 &: \beta_1 = 0 \\ H_1 &: \beta_1 \neq 0 \end{aligned} \tag{3.7}$$

where the null hypothesis states that there is no significant relationship between p* and θ, and the alternative hypothesis states the opposite. The results of the ANOVA test are shown in Table 3.4, where DF denotes the degrees of freedom, SS denotes the sum of squares and MS denotes the mean square terms. F-critical follows an F-distribution with numerator degrees of freedom 1 and denominator degrees of freedom 12. The obtained p-value is 4.42×10^{-5}, which is significantly lower than the alpha level ($\alpha = 0.025$), and the F-ratio (38.7494) is greater than the F-critical (6.5538). Hence, the null hypothesis is rejected at 2.5% significance level. The Q-Q (quantile-quantile) plot, shown in Figure 3.11, also provides a visual indication of univariate normality of the dataset. The quantile values of the standard normal distribution are plotted on the x-axis, and the corresponding quantile values of the experimental data are plotted on the y-axis. The points deviate largely from the reference line, which indicates that p* is not normally distributed. Therefore, we conclude that the damper position has a significant effect on p*.

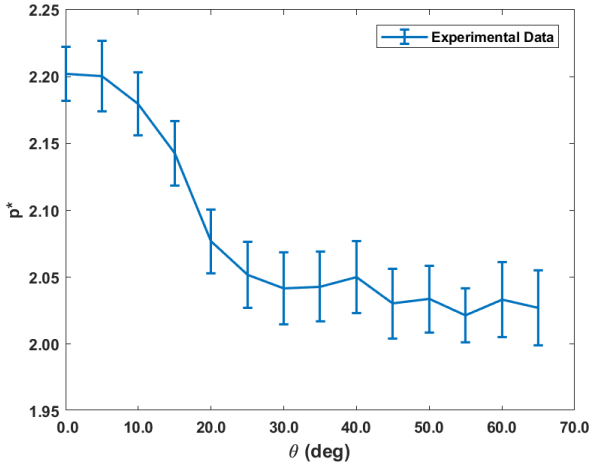

Figure 3.10: Normalized differential pressure vs damper angle ($Re = 1.28\times10^4$)

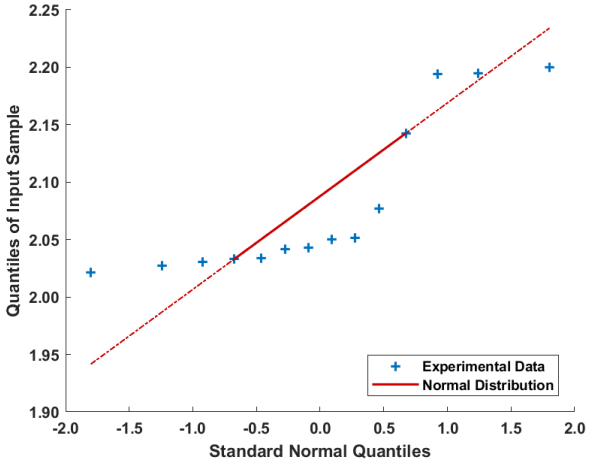

Figure 3.11: Q-Q plot of sample data vs. standard normal

Table 3.4: The ANOVA table

Source	DF	SS	MS	F-critical	F-ratio	p-value
Factor	1	0.0475	0.0475	6.5538	38.7494	4.42×10^{-5}
Error	12	0.0147	0.0012			
Total	13	0.0622	0.0048			

The variation in p* implies that the damper could introduce a systematic error in the measurement of air flow when simply assuming p* (or K) to be a constant. It can be seen from Figure 3.10 that this error becomes larger as the damper angle increases. This might be explained as follows: when the damper is about closed, the flow will accumulate on the edge of the blade. The relatively large values of the velocity measured at these points will increase the systematic measurement error.

To compensate for this error, the relationship between p* and θ is investigated and an empirical formula is proposed based on Figure 3.10:

$$\begin{aligned} p^* &= f(\theta) + p_0^*(\mathrm{Re}) \\ &= -\frac{c}{1+e^{-a(\theta-b)}} + p_0^*(\mathrm{Re}) \end{aligned} \tag{3.8}$$

where $p_0^*(\mathrm{Re})$ is the normalized differential pressure versus Reynolds number when $\theta = 0°$; $f(\theta)$ is a negated sigmoid function representing the deviation from the fully open state; a, b together with c are unknown model parameters. The Reynolds number is calculated by the duct parameters and the air properties at 300K ($\nu = 1.568\times10^{-5}$ m^2/s). $p_0^*(\mathrm{Re})$ is the Pitot tube characteristics provided by the manufacturer. It is often given as an empirical function [83, 86] or interpolation table. In this thesis, the curve of $p_0^*(\mathrm{Re})$ is given in Figure 3.14.

The unknown parameters are identified by the least squares method using the data shown in Figure 3.10. The final formula is given in Eq. (3.9):

$$\frac{\Delta P}{\frac{1}{2}\rho(Q/A)^2} = -\frac{0.1656}{1+e^{-0.2988\times(\theta-16.88)}} + p_0^*(\mathrm{Re}) \tag{3.9}$$

Compared with the traditional formula that considers only the change of Re, the incorporation of θ into the calculation can compensate for the error caused by the damper.

To validate the proposed formula, experiments were repeated at another set of damper angles ($\theta \in \{2.5°, 7.5°, 12.5°, \ldots, 67.5°\}$) and the results are compared with the predications given by Eq. (3.9). As shown in Figure 3.12, all experimental data falls within the 95% confidence interval, and the root mean squared error (RMSE) of the predications is less than 0.01 (RMSE = 0.0095). The proposed calculation formula corrects the deviation of the pressure coefficient from p_0^* when damper disturbance occurs, which makes the estimated Q approach closer to the true value.

Figure 3.13 compares the computation of Q with and without correction. The measured ΔP is denoted by the blue line with vertical error bars representing the standard deviation. The corresponding axis is located on the left-hand side of the plot. The computed Q without correction is denoted by triangle makers and its estimated uncertainty level is rendered pink. The uncertainty of Q can be attributed to two sources,

i.e., sensor uncertainty and model uncertainty, and the value can be estimated by the propagation law. Then the computed Q with correction is denoted by circle makers. And the true value of Q is represented by the dashed line. The scale of Q is shown on the right axis. As can be seen from this figure, the 95% confidence interval deviates significantly from the true value before correction. A non-negligible systematic error will be introduced when damper angle is greater than 30°. By applying the correction, this systematic error in Q is reduced from 3% to 0.2% on average. It should also be noted that the confidence interval becomes wider after correction, which means the uncertainty level is increased since extra model uncertainty is introduced when calculating p*. Overall, the proposed model reduces the disturbance caused by the damper and improves the accuracy of the APT flow measurement to a large extent.

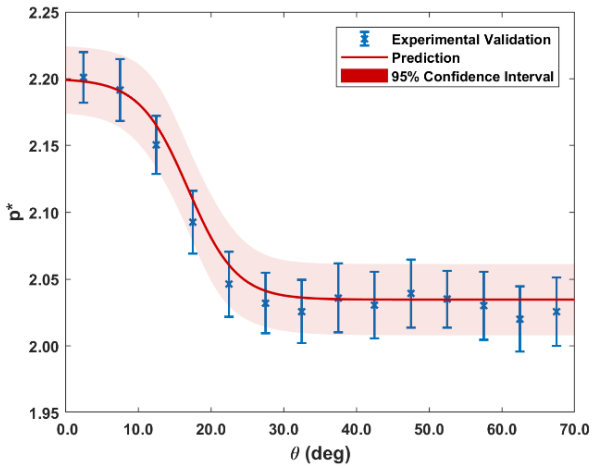

Figure 3.12: Experimental validation of the proposed formula for the normalized differential pressure (Re = 1.28×10⁴)

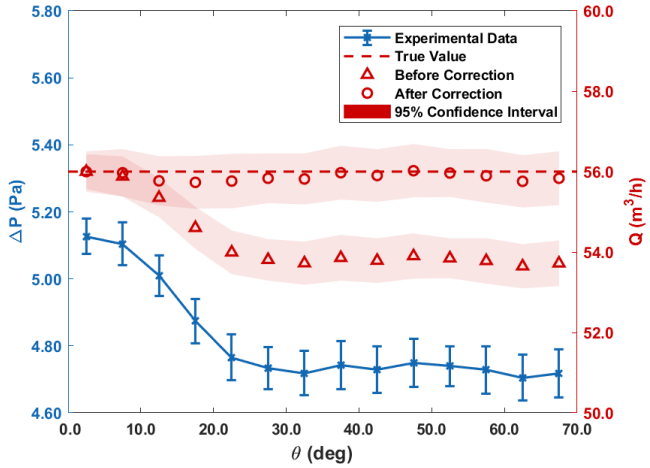

Figure 3.13: Comparisons of APT flowmeter readings before and after correction (Re = 1.28×10⁴)

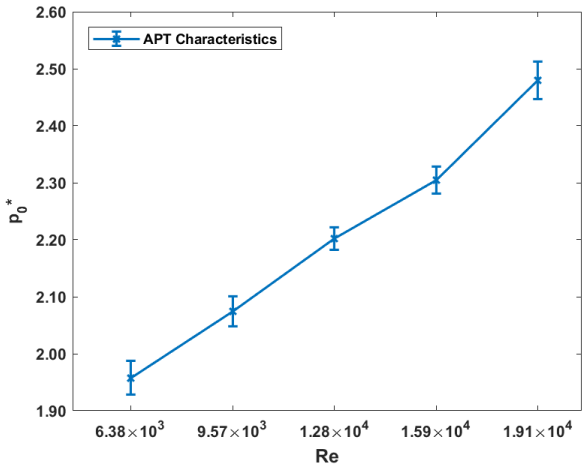

Figure 3.14: The characteristic curve of APT with respect to Reynolds number

The two sensors are assumed to be independent and the repeated measurements are assumed uncorrelated. The uncertainty of the model can be estimated using the Kline-McClintock method [85]. For the differential pressure ΔP, the uncertainty is given by Eq. (3.10):

$$\left(\frac{\delta\Delta P}{\Delta P}\right)^2 = \frac{1}{N}\left(\varepsilon^2{}_{OMR} + \varepsilon^2{}_{DWY} + \frac{Var(\Delta P)}{\Delta P^2}\right) \tag{3.10}$$

where the term ε_{OMR} and ε_{DWY} are sensor accuracy given previously, and the $Var(\Delta P)$ can be obtained from the 40 sets of experimental data.

Similarly, the uncertainty of the flow measurement is given by Eq. (3.11):

$$\left(\frac{\delta Q}{Q}\right)^2 = \frac{1}{N}\left(\varepsilon^2{}_{YPL} + \varepsilon^2{}_{TSI} + \frac{Var(Q)}{Q^2}\right) \tag{3.11}$$

Based on the definition in Eq. (3.4), the uncertainty level of pressure coefficient p* is given by:

$$\left(\frac{\delta p*}{p*}\right)^2 = \left(\frac{\delta\Delta P}{\Delta P}\right)^2 + 2\left(\frac{\delta Q}{Q}\right)^2 \tag{3.12}$$

Then the uncertainty of model parameters s (s = a, b, c, ...) can be determined by:

$$(\delta s)^2 = \left(\frac{\partial s}{\partial \theta}\delta\theta\right)^2 + \left(\frac{\partial s}{\partial p*}\delta p*\right)^2 \tag{3.13}$$

And the uncertainty of model prediction can be estimated by:

$$\left(\frac{\delta\Delta P}{\Delta P}\right)^2 = \frac{1}{\Delta P^2}\left(\sum_s\left(\frac{\partial\Delta P}{\partial s}\delta s\right)^2 + \left(\frac{\partial\Delta P}{\partial\theta}\delta\theta\right)^2\right) + 2\left(\frac{\delta Q}{Q}\right)^2 \qquad (3.14)$$

3.5 Further validation of the proposed formula under different Reynolds numbers

The previous results demonstrate that the damper has a dramatic effect on p*, and this effect is quantified by f(θ) in Eq. (3.9). The estimated flow rate by the proposed formula shows good agreement with the experiments when Re = 1.28×10^4. To further explore the generality of the formula, experiments are conducted under different Reynolds numbers and the results are shown in Figure 3.15.

Figure 3.15 shows the plots of f(θ) under different Reynolds numbers. It can be found that the trends of f(θ) are quite similar under all cases. A notable drop can be witnessed when θ is increased to about 30°. After that, f(θ) becomes nearly stable with some small fluctuations. The formula exhibits generality over a large range of Re when θ is relatively small. The maximum RMSE is less than 0.02 (RMSE = 0.0184) among all tested cases. However, for the latter part of the graph, the curves are less consistent with model predictions and the uncertainties become larger as well. One possible reason is that when damper is nearly closed (θ > 60°), severe turbulence occurs around the blade and the asymmetric velocity profiles causes inaccuracy in the APT measurement. It should also be noted that the experimental data points are not aligned. For large θ under high Reynolds number cases, the data are missing since the maximum fan power still cannot reach the target flow rate, which is also impractical in real applications.

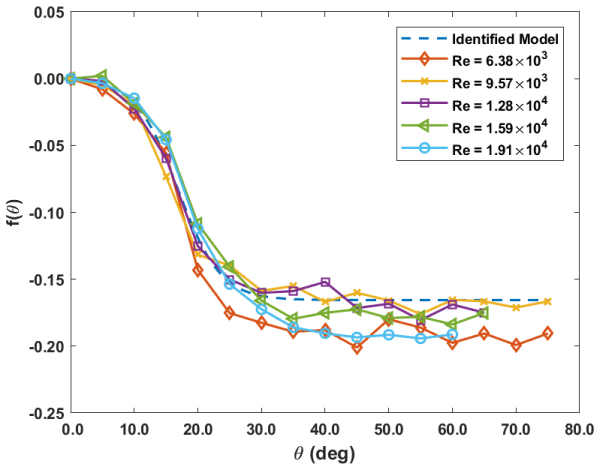

Figure 3.15: Comparison of f(θ) under different Reynolds numbers

Figure 3.16 compares the errors in the estimated flow rate values before and after correction under different Re. As can be clearly seen from these figures, the flow rate inferred from the measured ΔP deviates greatly from the true value by simply assuming a constant p* (K). And the relative error can be as large as 3.78% when Re = 6.38×10^3. By applying the proposed formula, the error is significantly reduced and the confidence interval of the estimated flow rate successfully covers true value in all tested cases. The improvement of the sensor accuracy is shown in Figure 3.17. The errors induced by the damper are all controlled within 0.6%, and the highest accuracy (0.02%) is achieved when Re = 9.57×10^3. Hence, the proposed formula is validated over the working flow rate range of the specific AFCS.

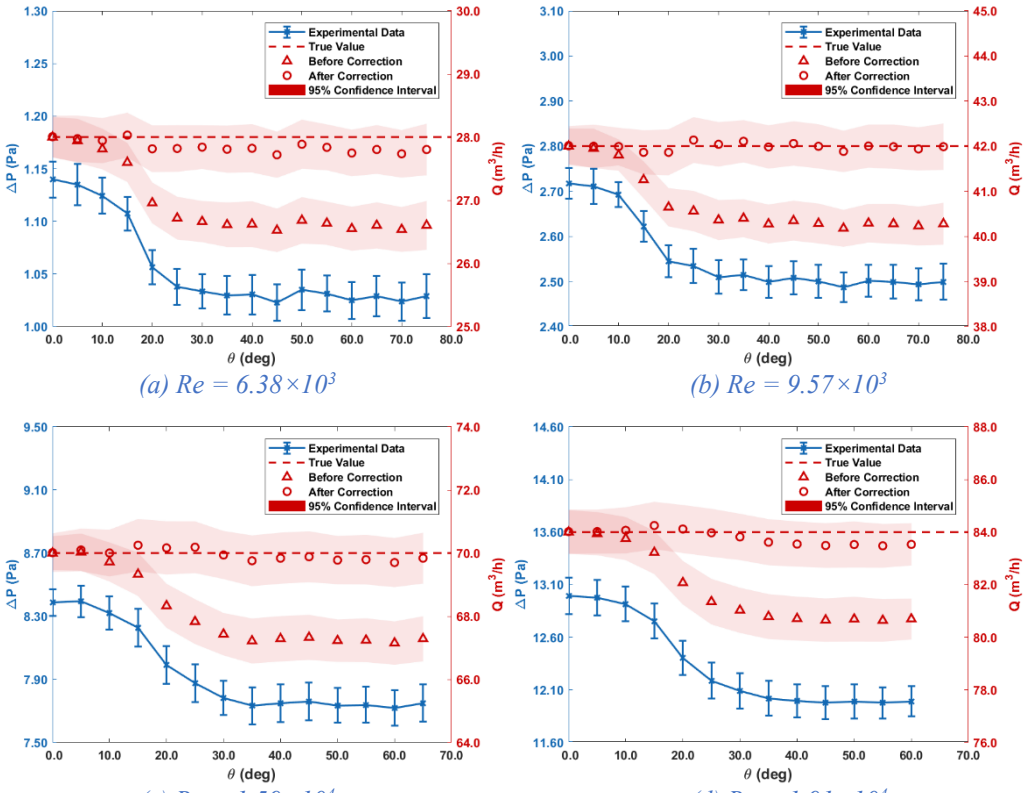

(a) Re = 6.38×10^3 *(b) Re = 9.57×10^3*

(c) Re = 1.59×10^4 *(d) Re = 1.91×10^4*

Figure 3.16: Validation of the identified formula under various Reynolds numbers

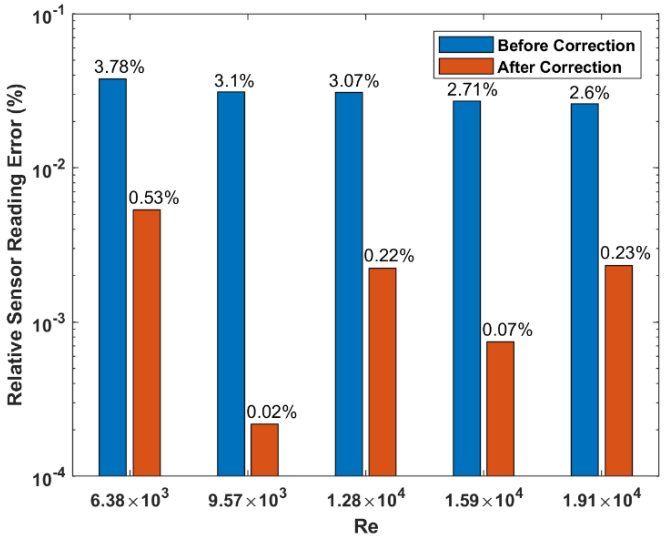

Figure 3.17: The reduction of error under different Reynolds numbers

3.6 Conclusion

This chapter proposes a revised flow estimation formula for the APT inside the AFCS to improve the accuracy of measurement. First, the effect of the embedded damper on the APT flow coefficient is investigated using ANOVA. The result reveals a statistically nontrivial correlation between p* and θ when a damper is placed immediately downstream of an APT, which is in line with the findings by Klaczek. Then, a flow estimation formula for the APT is proposed to compensate for the systematic error caused by the damper and is later validated under different Reynolds numbers. By applying the revised formula, the measuring error of APT can be controlled within 0.6% for all tested cases, and the highest accuracy (0.02%) is achieved when Re = 9.57×10^3. The proposed formula significantly reduces the systematic error caused by the flow control damper in AFCS and improves the accuracy of flow measurement to a large extent.

To put it into practical applications, a diagram of the instruction is given in Figure 3.18. For manufacturers, in addition to the characteristic curve of the APT under standard conditions, the correction function for the damper opening angle also need to be provided as another correction coefficient. For the customers, no extra inconvenience is introduced during the use of the AFCS.

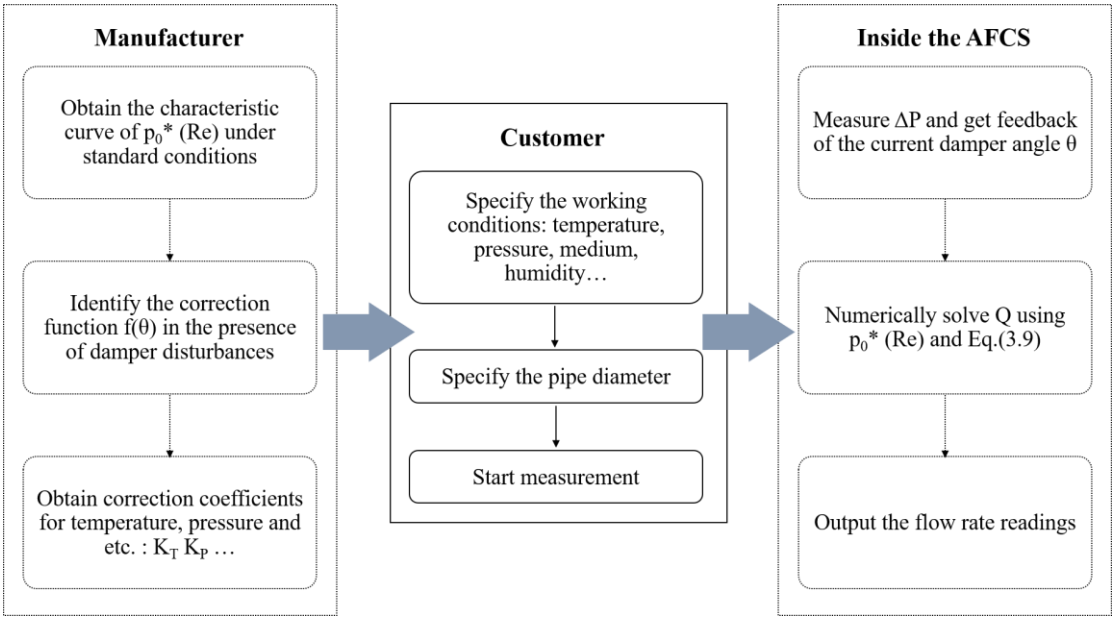

Figure 3.18: Proposed APT measurement procedure diagram

Chapter 4. Distributed cooperative control-based air balancing (DCC-AB) method

4.1 Introduction

Currently, most air balancing methods share a common drawback that these methods are 'offline' procedures that can only be performed during commissioning or maintenance when the air distribution system is not in use. As previously stated in Section 2.4, the proportional method requires multiple runs and the dynamic state of the system can deviate largely from the working conditions during this process. The progressive flow method and fan pressure-based method starts with all dampers fully closed. As for Small's method and Chen's method, measurements are taken when a subset of the dampers are fully closed. Consequently, these methods will disturb the normal operation of the air distribution system and therefore require a scheduled shutdown period, which could cause inconvenience and sometimes enormous financial losses.

Inspired by the distributed consensus algorithm that achieves synchronized behaviour of the agents in a multi-agent dynamical system, this chapter proposes a novel online air balancing method to balance the air duct system based on the distributed cooperative control. In this method, the balancing starts from the given imbalanced state and converges asymptotically to the final balanced state. The drastic change of damper positions such as short cycling on and off is circumvented, which avoids the occurrence of overshooting and oscillations of the flow rate value. And an incremental improvement of the balancing result can be guaranteed during the whole process. Hence, the method can be performed during normal operation dispensing with service interruptions. Moreover, the system reaches the balanced state through information exchange among agents without computing any objective functions, making it a model-free method.

The remainder of this chapter is organized as follows: Section 4.2 introduces the basic concept of the distributed consensus algorithm and proposes the DCC-AB method. Section 4.3 conducts a detailed parametric analysis to explore the effect of individual model parameters on the performance of the proposed method. Section 4.4 presents the experimental results in comparison with the simulation studies. In the end, Section 4.5 summarizes this chapter and draws conclusions.

4.2 Theory of the proposed DCC-AB method

The objective of distributed cooperative control is to formulate a control protocol for the multi-agent system to achieve a synchronized behaviour of all agents in some prescribed sense. This section introduces a consensus-based distributed control protocol where the multi-agent dynamical system is interconnected by a fixed communication graph topology, and each agent is allowed to depend only on the information of its own and the neighbours.

A graph is a pair $G=(V,E)$ that consists of a set of vertices V and a set of edges $E \subseteq V \times V$. The node is denoted by $v_i \in V$, or $i \in I = \{1,\cdots,n\}$, and the edge is denoted by (v_i, v_j), pointing from v_i to v_j. If $(v_i, v_j) \in E \Rightarrow (v_j, v_i) \in E, \quad \forall i, j$, then the graph G is called an undirected graph, otherwise, it is called a directed graph. The set of neighbours of node i is denoted by $N_i = \{ j \in V \mid (v_i, v_j) \in E \}$. The degree of node i is the number of its neighbours, which is denoted by $\deg(v_i)$. The degree matrix of G is defined as a diagonal $n \times n$ matrix, $\mathbf{\Delta} = diag\{\deg(v_i)\}$.

The structure of the graph is described by the adjacency matrix $\mathbf{A}$, whose elements are given by:

$$a_{ij} = \begin{cases} 1, & \text{if } (v_i, v_j) \in E \\ 0, & \text{otherwise} \end{cases} \tag{4.1}$$

An example of the communication graph is illustrated in Figure 4.1. For an undirected graph, the adjacency matrix is symmetric, $\mathbf{A} = \mathbf{A^T}$. If there exists a path between every pair of nodes, the graph is called connected. In this thesis, G is assumed to be a simple graph: no self-loops, i.e., $(v_i, v_i) \notin E$ which implies $a_{ii} = 0$, and no multiple edges.

The Laplacian matrix $\mathbf{L}$ is defined as:

$$\mathbf{L} = \mathbf{\Delta} - \mathbf{A} \tag{4.2}$$

Intuitively, the elements of $\mathbf{L}$ are given by:

$$l_{ij} = \begin{cases} -1, & j \in N_i \\ |N_i|, & j = i \end{cases} \tag{4.3}$$

where $|N_i|$ denotes the number of the neighbours of node i. One can easily show that all row sums of $\mathbf{L}$ are zero, i.e., $\sum_j l_{ij} = 0$, which leads to an important property of the Laplacian matrix that $\mathbf{v_0} = (1,\cdots,1)^{\mathrm{T}}$ is an eigenvector of $\mathbf{L}$ associated with the zero eigenvalue [104]. Moreover, since the undirected graph has a symmetric Laplacian matrix $\mathbf{L}$, all its eigenvalues are real [105].

Suppose each node is assigned with a value x_i, then $\mathbf{x} = (x_1,\cdots,x_n)^{\mathrm{T}}$ denotes the state of the graph G. The Laplacian potential [106] of the graph is defined as:

$$\psi(\mathbf{x}) = \mathbf{x}^{\mathrm{T}}\mathbf{L}\mathbf{x} \tag{4.4}$$

where

$$\mathbf{x}^{\mathrm{T}}\mathbf{L}\mathbf{x} = \frac{1}{2}\sum_{(v_i,v_j)\in E} a_{ij}\left(x_i - x_j\right)^2 \tag{4.5}$$

and the proof of Eq. (4.5) is given in [105]. The Laplacian potential of a graph quantifies the total disagreement among all nodes (agents). It can be shown that $\psi(\mathbf{x}) = 0$ if and only if the multi-agent system reaches the consensus [107], which means the system converges asymptotically to a one-dimensional agreement space characterized by:

$$x_1 = x_2 = \cdots = x_n \tag{4.6}$$

A simple linear consensus protocol for networks of continuous-time integrators without communication time-delays is given as follows [107-109]:

$$\dot{\mathbf{x}} = -\nabla\psi(\mathbf{x}) = -\mathbf{L}\mathbf{x}, \quad \mathbf{x}(0) \in \mathbb{R}^n \tag{4.7}$$

which can be expressed in a more explicit way:

$$\dot{x}_i(t) = -\sum_{j\in N_i} a_{ij}\left(x_i(t) - x_j(t)\right) \tag{4.8}$$

For the discrete-time agents, the protocol is given as follows:

$$x_i(k+1) = x_i(k) - T_s\sum_{j\in N_i} a_{ij}\left(x_i(k) - x_j(k)\right) \tag{4.9}$$

where T_s is the step-size.

The consensus algorithm guarantees the convergence to a collective decision via local communication with the neighbours. If a consensus is asymptotically achieved, the equilibrium of the system is a state where all nodes agree:

$$\mathbf{x}^* = (\alpha, \cdots, \alpha)^{\mathrm{T}} \tag{4.10}$$

Summing Eq. (4.8) over i obtains $\sum_i \dot{x}_i = 0$, which leads to $\dot{\bar{\mathbf{x}}} = 0$. This implies that $\bar{\mathbf{x}}$ is an invariant quantity, i.e., $\bar{\mathbf{x}}(\infty) = \bar{\mathbf{x}}(0)$. Hence, we obtain:

$$\alpha = \frac{1}{n}\sum_i x_i(0) \tag{4.11}$$

A consensus algorithm satisfying this specific invariance property is known as the average-consensus algorithm [110], which has broad applications in load balancing [111], sensor fusion [112], coordination of mobile autonomous agents [113] and etc.

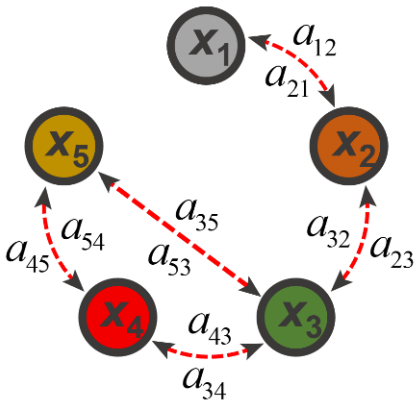

$$\mathbf{A} = \begin{bmatrix} 0 & 1 & 0 & 0 & 0 \\ 1 & 0 & 1 & 0 & 0 \\ 0 & 1 & 0 & 1 & 1 \\ 0 & 0 & 1 & 0 & 1 \\ 0 & 0 & 1 & 1 & 0 \end{bmatrix}$$

Figure 4.1: An example of the communication graph

The objective of air balancing is to ensure that air is evenly distributed throughout the duct system. By 'evenly distributed', we mean the system delivers precisely the amount of required air to each terminal. With this in mind, the duct network could be regarded as a multi-agent dynamical system interconnected by a fixed communication graph topology, where the agents (terminals) collaborate with their neighbours to achieve an agreement:

$$\frac{q_1}{q_1^*} = \cdots = \frac{q_n}{q_n^*} = \alpha \tag{4.12}$$

where q is the actual flow rate, q^* is the design flow rate, α is the final consensus value, and the subscript n denotes the terminal. Eq.(4.12) indicates that the duct system is 'proportioned' [17], i.e., the ratio of q to q^* is equal for every terminal. This equilibrium can be achieved applying the average-consensus algorithm given in Eq. (4.9) if we let x be the flow ratio, i.e., $x_i = \frac{q_i}{q_i^*}$, which leads to:

$$\frac{q_i(k+1)}{q_i^*} - \frac{q_i(k)}{q_i^*} = -T_s \sum_{j \in N_i} a_{ij} \left(\frac{q_i(k)}{q_i^*} - \frac{q_j(k)}{q_j^*} \right) \tag{4.13}$$

Then the left-hand side of Eq. (4.13) is converted to the increment of a control variable θ:

$$\frac{q_i(k+1) - q_i(k)}{q_i^*} = \frac{J_{ii}\left(\theta_i(k+1) - \theta_i(k)\right)}{q_i^*} \tag{4.14}$$

where θ is the damper opening angle and J_{ii} is the i_{th} diagonal element of the Jacobian matrix $\mathbf{J} \approx \begin{bmatrix} \frac{\partial q_1}{\partial \theta_1} & & \\ & \ddots & \\ & & \frac{\partial q_n}{\partial \theta_n} \end{bmatrix} = \begin{bmatrix} J_{11} & & \\ & \ddots & \\ & & J_{nn} \end{bmatrix}$.

Then Eq. (4.13) can be further simplified as:

$$\theta_i(k+1) - \theta_i(k) = \kappa_i \sum_{j \in N_i} a_{ij} \left(\frac{q_i(k)}{q_i^*} - \frac{q_j(k)}{q_j^*} \right) \tag{4.15}$$

where $\kappa_i = -\frac{T_s q_i^*}{J_{ii}}$.

In this thesis, $\mathbf{J}$ is simplified to a diagonal matrix, which indicates that the flow rate change associated with the variation of the damper angles from other terminals is ignored. In other words, the modulation of the flow value for a terminal only considers regulating its own damper. The Jacobian matrix can be obtained by analysing the q-θ characteristic curves of the dampers through experiments, where J_{ii} is estimated from the average derivative of $q(\theta)$.

Practical criteria for air balancing in accordance with the standards of ASHRAE, NEBB, CIBSE, SMACNA and etc. can be summarized as follows: 1.) All measured air flow quantities should be controlled within ±10% of the design values; 2.) At least one damper should be left fully open in order to minimize the overall energy consumption. To understand the rationale behind the second one, suppose all dampers in the duct system are partially closed. Then the same state of the system, considering the flow rate values only, can be achieved by fully opening the critical damper while lowering down the fan static pressure, which clearly reduces the total fan power. The principles for the selection of the critical damper follows proportional method [17] that the terminal with the lowest flow ratio should remain fully open.

Based on the above criteria, a new air balancing method, named DCC-AB method, is proposed as follows:

$$\theta_i(k+1)-\theta_i(k)=\kappa_i\sum_{j\in N_i}a_{ij}\left(\frac{q_i(k)}{q_i^*}-\frac{q_j(k)}{q_j^*}\right)+\beta\theta_c \tag{4.16}$$

where θ_c is the damper angle of the critical terminal, β is a negative gain. Together, $\beta\theta_c$ is a penalty term that discourages θ_c from reaching large values. As long as $\beta\theta_c$ is non-zero, the algorithm will continue until this term vanishes. The coefficient β governs the relative importance of the flow imbalance term and the critical damper angle deviation term. When β is too small, the algorithm will mainly focus on eliminating the flow imbalance, and θ_c may remain very large when the algorithm stops. On the other hand, if β is too large, the $\beta\theta_c$ term will dominate. The algorithm will mainly focus on reducing θ_c, and the convergence rate can be slowed down. Hence, β is a compromise between the two terms. By tuning the parameter β, the proposed algorithm could achieve air balancing with a minimum overall energy consumption. It should be noted that the value of α in Eq. (4.12) is the weighted average of the initial states in average-consensus problems. For the case under investigation in this thesis, α is determined by the final equilibrium state and cannot be predicted since the fan operating point changes with the system resistance. If α is exactly equal to 1, then the total flow in the equilibrium equals the design total, and the balancing process ends. Otherwise, a final adjustment of the fan speed is needed to proportionally bring the terminal flows to the corresponding design values.

4.3 Design principle of the proposed DCC-AB method

In this section, a detailed parameter analysis is conducted to aid the understanding of the rationale behind the proposed algorithm and provide guidance on the parameter design. A simulation model that computes the duct system dynamics is built in MATLAB, where the simulation solving package is provided by Chen et al. [100]. Then the DCC-AB method can be numerically implemented. 5 selected cases are compared and discussed in terms of the selection of model parameters and the setting of the design flow values. To isolate the independent parameter's effects on the simulation results, a 'base case' is set up in Section 4.3.2.

4.3.1. β = 0, equal q*

Prior to presenting the results of the base case, a simple case is first discussed. In this case, the time step T_s is set to 10s and the parameter β is set to zero. The initial damper angles are [5.0, 40.0, 35.0, 50.0, 10.0] (°) with the corresponding terminal flow $\mathbf{q}_{\text{int}}$ = [173.8, 48.4, 59.8, 20.5, 131.7] (m^3/h), and the design value $\mathbf{q}^*$ = [144.0, 144.0, 144.0, 144.0, 144.0] (m^3/h). The adjacency matrix $\mathbf{A}$ is given in Eq. (4.17). The results are shown in Figure 4.2.

$$\mathbf{A} = \begin{vmatrix} 0 & 1 & 1 & 0 & 0 \\ 1 & 0 & 1 & 0 & 0 \\ 1 & 1 & 0 & 1 & 1 \\ 0 & 0 & 1 & 0 & 1 \\ 0 & 0 & 1 & 1 & 0 \end{vmatrix} \tag{4.17}$$

Figure 4.2 (a) depicts the trajectories of the system state (flow ratio). The terminal flow ratio is denoted by the blue line with the corresponding axis located on the left-hand side of the plot. The degree of consensus, defined in Eq. (4.18), is denoted by the red line with its scale shown on the right axis. The degree of consensus is evaluated by the relative standard deviation (RSD) of the system state, which is defined as the ratio of the standard deviation to the mean:

$$RSD(\mathbf{x}) = \frac{std(\mathbf{x})}{mean(\mathbf{x})} = \frac{n}{\sqrt{n-1}} \frac{\sqrt{\sum_{i=1}^{n} (x_i - \bar{x})^2}}{\sum_{i=1}^{n} x_i} \tag{4.18}$$

It can be seen from Figure 4.2 (a) that the flow ratios (blue lines) gradually converge to the same point with a synchronized pacing, and the corresponding degree of consensus declines asymptotically towards zero. As previously mentioned, the value of α depends on the final state of the system since the system resistance changes during the balancing process. At the 10th time step, α converges to around 0.49 and the RSD achieves 0.0127, and the system is assumed to reach the equilibrium state. The regulation of damper angles is shown in Figure 4.2 (b). The increment of θ for a certain damper is calculated based on the proposed algorithm at each time step and it approaches zero, which means the system gradually becomes steady. Figure 4.2 (c) tracks the change of terminal flow rates. At the equilibrium state, all terminals achieve the same flow rate, which is 0.49 times of the design value. Hence, a final adjustment of the fan speed is needed. Intuitively, the total flow should be increased by a factor of 1/0.49 such that all terminal flows can be changed proportionally to meet the design values. This can be accomplished by regulating the fan input voltage U, and the adjustment process is shown in Figure 4.2 (d). It is noteworthy that the lines are getting slightly wider apart as U increases. The reason is that the terminal flow is not perfectly proportional to the total flow and can be changed marginally from the desired value as U changes. The final balancing results are shown in Table 4.1, where ε is the absolute percentage error (APE) defined in Eq. (4.19). All terminal flows fall within ±10% of the design value and the maximum APE achieves 5%.

$$\varepsilon = \frac{abs(q - q^*)}{q^*} \tag{4.19}$$

Table 4.1: The simulation results of Case 4.1

Terminal	q_{int} (m^3/h)	q^* (m^3/h)	q_f (m^3/h)	θ_f (°)	ε (%)
1	173.8	144.0	137.6	35.4	4.4
2	48.4	144.0	136.8	32.6	5.0
3	59.8	144.0	139.8	33.5	2.9
4	20.5	144.0	141.1	31.4	2.0
5	131.7	144.0	141.2	31.4	2.0

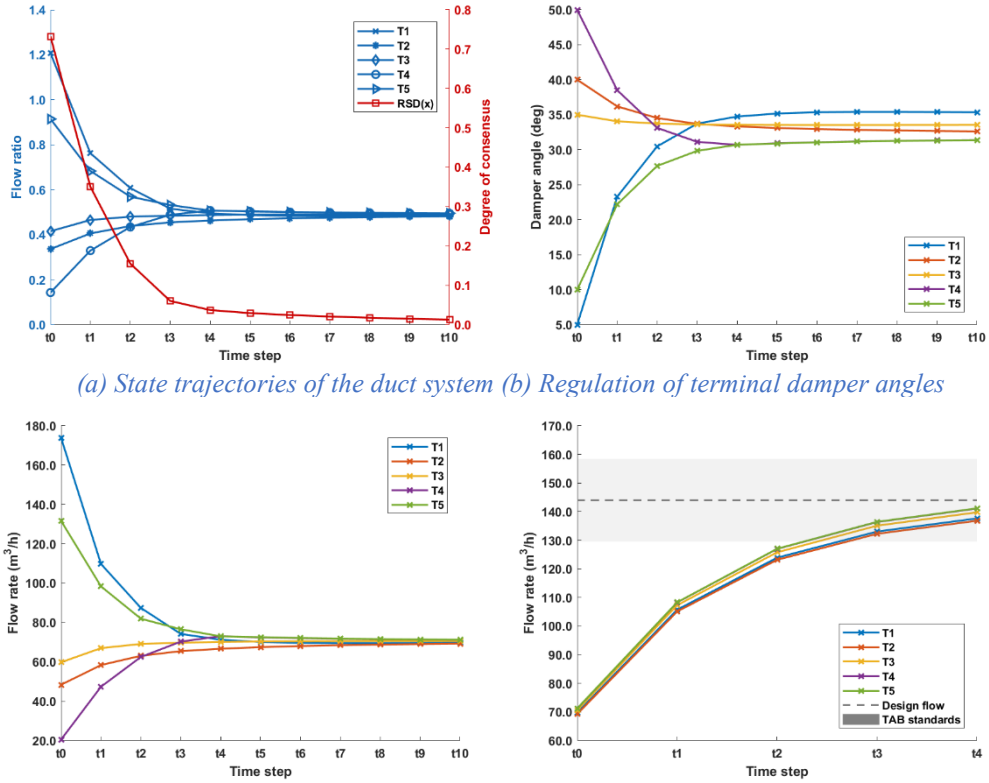

(a) State trajectories of the duct system (b) Regulation of terminal damper angles

(c) Dynamic curves of terminal flow rates (d) Final adjustment in the balancing process

Figure 4.2: The simulation results of Case 4.1

4.3.2. β ≠ 0, equal q*

In Case 4.2, the parameter β is set to a non-zero (negative) value with all other initial conditions remaining unchanged. This case will serve as the base case for later comparison, and the results are shown in Figure 4.3. It can be clearly seen from Figure 4.3 (b) that the introduction of β renders the critical damper (purple line) wide-open. The increment of θ at each time step considers not only the disparity in system state among neighbours, but also the opening angle of the critical damper. The damper angle of T4 gradually approaches zero, causing all other damper angles to decrease on the whole compared with Case 4.1. Specifically, at the equilibrium state, T5 (green line) becomes fully open as well since T4 and T5 are symmetric branches. We also notice from Figure 4.3 (b) that the time to reach steady state differs with terminals, and this in turn affects the convergence curves of flow ratio. The system reaches a higher consensus value (0.712) compared with Case 4.1 as the damper resistance in the equilibrium state is lower. The balancing results are listed in Table 4.2. The fan power consumption is also reduced due to the introduction of β, which will be discussed later in Section 4.5.

In summary, a non-zero β will force the critical damper to open gradually until the term associated with β in the protocol vanishes. This causes all the other damper angles to decrease as well and ensures that at least one damper will be fully open at the equilibrium state.

Table 4.2: The simulation results of Case 4.2 (base case)

Terminal	q_{int} (m^3/h)	q^* (m^3/h)	q_f (m^3/h)	θ_f (°)	ε (%)
1	173.8	144.0	144.3	22.5	0.2
2	48.4	144.0	141.5	8.8	1.7
3	59.8	144.0	145.7	17.1	1.2
4	20.5	144.0	143.4	0.5	0.4
5	131.7	144.0	142.0	0.6	1.4

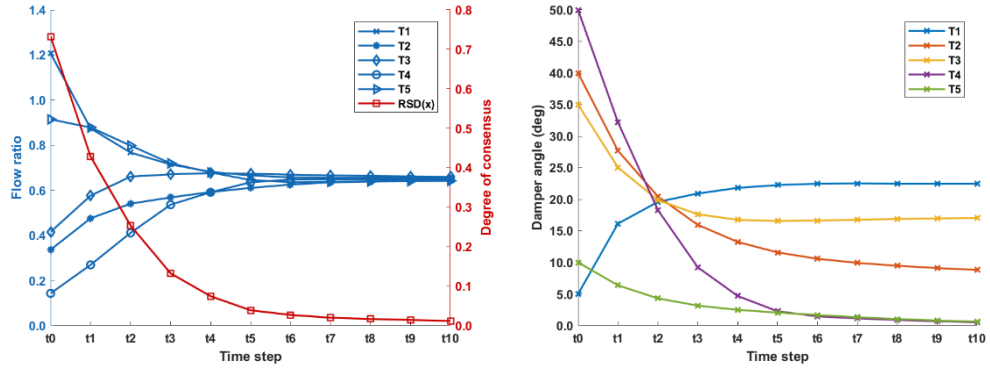

(a) State trajectories of the duct system (b) Regulation of terminal damper angles

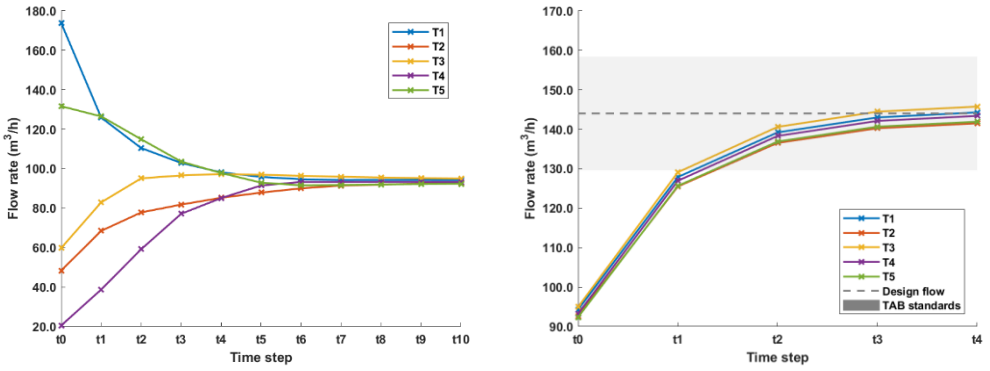

(c) Dynamic curves of terminal flow rates (d) Final adjustment in the balancing process

Figure 4.3: The simulation results of Case 4.2 (base case)

4.3.3. β ≠ 0, different q*

The settings of Case 4.3 remain unchanged, except for the specification of design flow values. In this case, each terminal is assigned with a different flow target, and the results are presented in Table 4.3 and Figure 4.4. As can be seen, the system can still

reach the balanced state under varied flow targets since the algorithm focuses on achieving consensus on the flow ratio value rather than the absolute flow rate value. After the fan adjustment, the maximum APE is controlled within 2.5%. For clarity, Figure 4.4 (d) only shows the design flow for T4 (purple line) and its corresponding ±10% interval (rendered purple).

Other sets of design flow values have also been tested, and the results demonstrate that the DCC-AB method applies over a wide range of design flow requirements.

Table 4.3: The simulation results of Case 4.3

Terminal	q_{int} (m³/h)	q^* (m³/h)	q_f (m³/h)	θ_f (°)	ε (%)
1	173.8	52.0	51.3	44.5	1.3
2	48.4	186.0	181.4	0	2.5
3	59.8	132.0	132.0	21.2	0
4	20.5	105.0	106.1	24.0	1.1
5	131.7	80.0	80.7	30.8	0.8

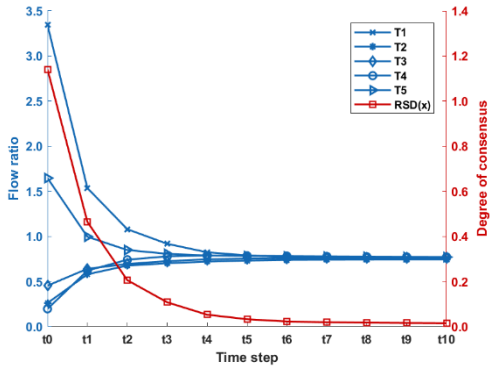

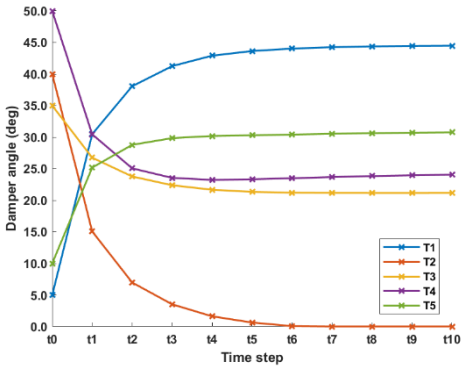

(a) State trajectories of the duct system (b) Regulation of terminal damper angles

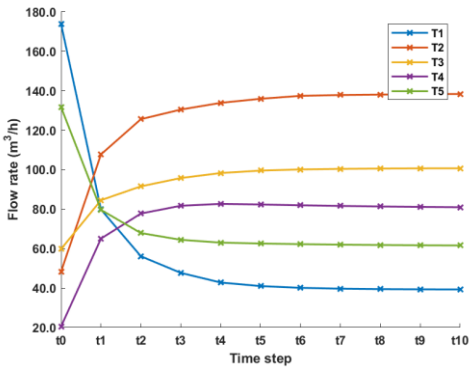

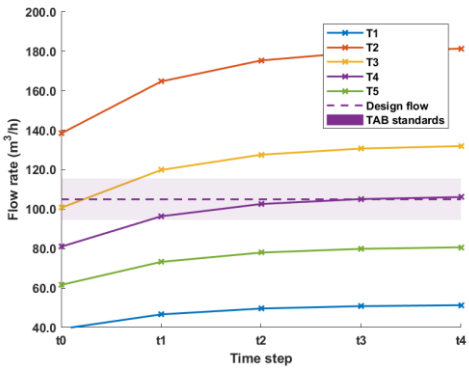

(c) Dynamic curves of terminal flow rates (d) Final adjustment in the balancing process

Figure 4.4: The simulation results of Case 4.3

4.3.4. β ≠ 0, different T_s

The time step size actually controls the rate of convergence as the gain coefficient κ is proportional to T_s. A small T_s will lead to a conservative κ while a large T_s will result in an aggressive κ. In Case 4.4, T_s is set to 5s, which is halved compared to the base case, and the results are shown in Figure 4.5. It is apparent from Figure 4.5 (a) that the convergence speed is slowed down when T_s is reduced. At the 10th step, the blue lines are still far apart from each other and the RSD is greater than 0.07. We also notice that the individual convergence rates are affected differently by T_s, as shown in Figure 4.5 (b). The steady state of T5 (green line) occurs earlier since the second term in Eq. (4.16) becomes dominant. The curves of the left terminals are still developing, either decreasing or increasing. On the other hand, if T_s is threefold, which is the case shown in Figure 4.6, oscillation occurs. Hence, a trade-off exists between the stability and convergence time, and T_s should be chosen properly to speed up the convergence while avoiding overshooting.

To summarize, a conservative T_s will cause an increase in convergence time, whereas an aggressive T_s may lead to oscillation.

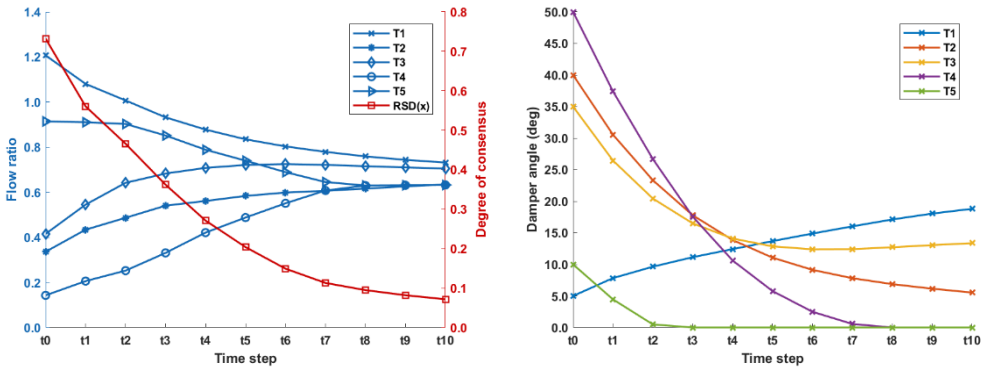

(a) State trajectories of the duct system (b) Regulation of terminal damper angles

Figure 4.5: The simulation results of Case 4.4

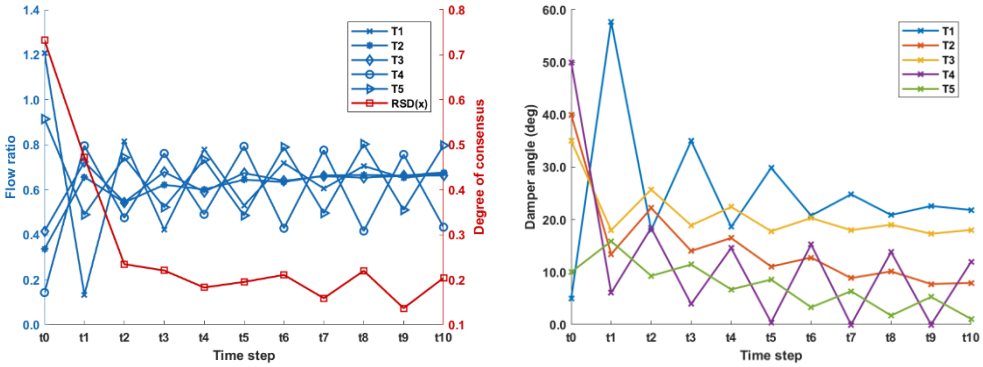

(a) State trajectories of the duct system (b) Regulation of terminal damper angles

Figure 4.6: The simulation results of Case 4.5

4.4 Experimental validation

To validate the proposed method, laboratory tests were conducted on the air distribution platform, given in Figure 4.7. The air distribution platform is a trunk-and-branch duct system of 5 terminals. The duct system mainly consists of a centrifugal fan with variable speed drive, a network of circular duct conduits, several fittings including elbows and junctions, which are introduced in Section 3.2, and five terminals equipped with controllable dampers.

Figure 4.7 Air distribution platform

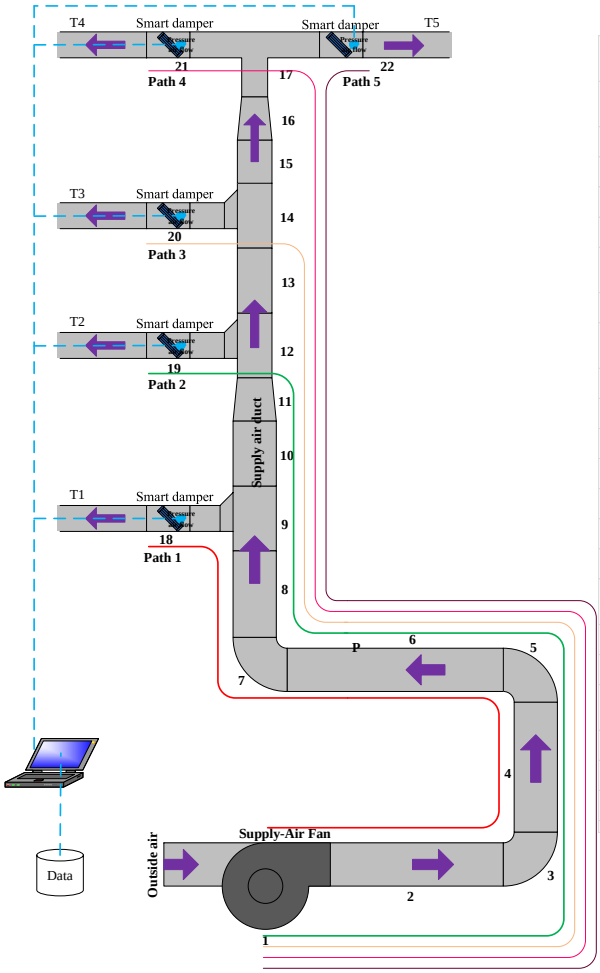

Terminal	T1, T2, T3, T4, T5		
Tee	Dc (m)	Db (m)	Ds (m)
9	0.2	0.2	0.2
12	0.2	0.2	0.1
14	0.2	0.2	0.1
17	0.1	0.1	0.1
Elbow	L (m)		r/D
3, 5, 7	0.2		1
Duct	L (m)		D (m)
2	2.5		0.2
4	1.3		0.2
6	3		0.2
8	0.8		0.2
10	0.7		0.2
13	0.6		0.15
15	0.75		0.15
Transition	D1 (m)		D2 (m)
11	0.2		0.15
16	0.15		0.1
Damper	D (m)		
18, 19	0.1		
20	0.1		
21, 22	0.1		

Figure 4.8 Schematic diagram of the air distribution platform

Prior to the experiments, the Wi-Fi module was checked to ensure a stable connection among terminals. The design flow for each terminal together with the communication structure were specified. The fan control signal was connected to the NI DAQ device which could be accessed by the supervisory computer. To begin with, the signal was sent by the computer to start the fan and sufficiently long waiting time was spent to make sure the system has been stabilized. At each time step, the terminal air flows were measured, and the corresponding flow ratios were calculated. Then the terminals communicated with their neighbours following the prescribed architecture to exchange information on the current system state (flow ratio). The actuator would then modulate the damper angle according to Eq. (4.16), as shown in Figure 4.9. The process was repeated until the system reached the equilibrium within the specified tolerance (RSD within 2% in this thesis). A closed-loop was established to monitor the measured total flow rate and compare it with the reference value. The controller modulated the fan input voltage until the measured total satisfies the design total. In the end, all flows were

re-measured to make sure the duct system was balanced. A flow chart describing the experimental procedures is given Figure 4.10.

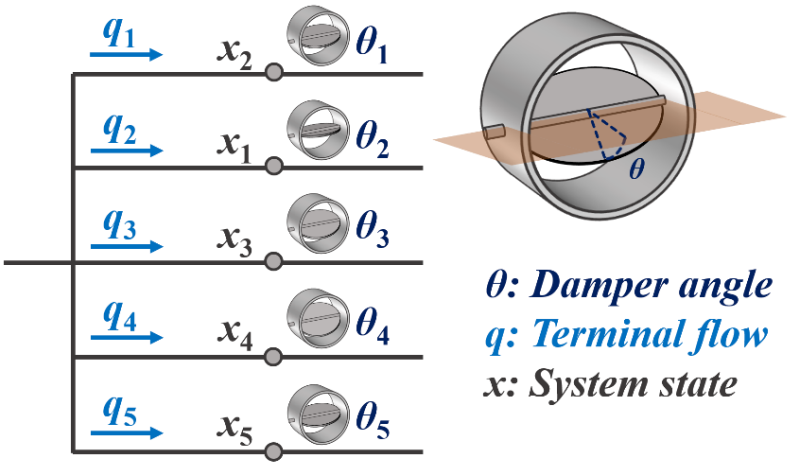

Figure 4.9: Graphic explanation of the DCC-AB method

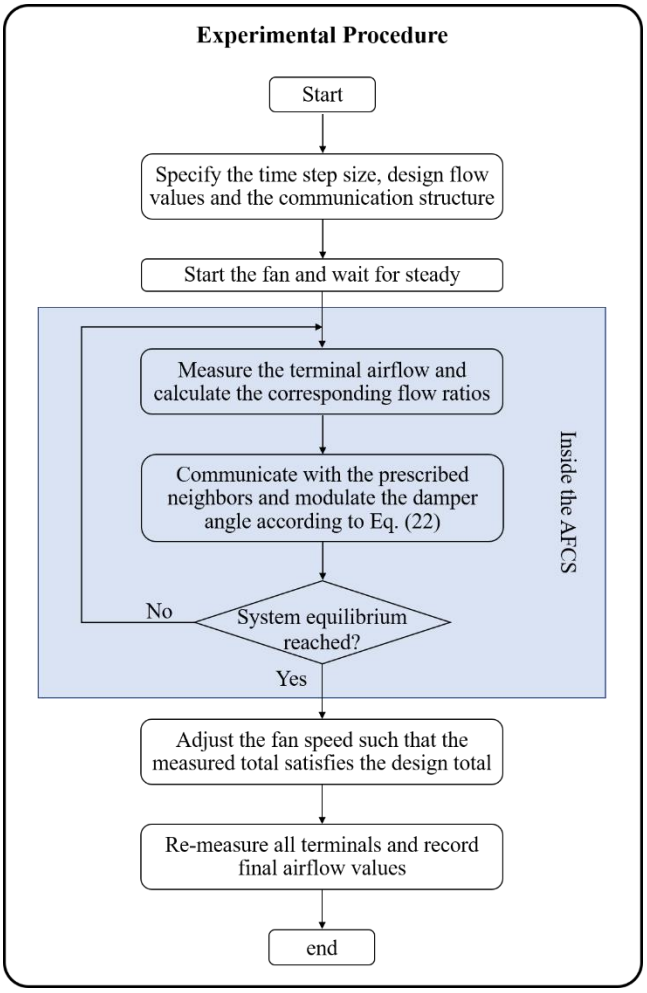

Figure 4.10: Flow chart of experimental procedures

The 5 cases in Section 4.4 were reproduced experimentally, and the results are presented in the same sequence. The experimental results of Case 4.1 are given in Table 4.4 and Figure 4.11. As can be seen, the initial terminal flows deviate far from the reference value, and the corresponding APE can be up to 58% (T4). After applying the DCC-AB method, the maximum APE can be controlled within 5%. Moreover, the system state exhibits a stable convergence with some small fluctuations, which indicates that the proposed method is insusceptible to the small sensor noise.

Table 4.4: The experimental results of Case 4.1

Terminal	q_{int} (m^3/h)	q^* (m^3/h)	q_f (m^3/h)	θ_f (°)	ε (%)
1	147.7	110.0	109.8	45.1	0.2
2	48.5	110.0	105.7	34.6	3.9
3	86.8	110.0	104.5	40.3	5.0
4	45.7	110.0	112.0	28.1	1.8
5	102.8	110.0	111.6	26.0	1.5

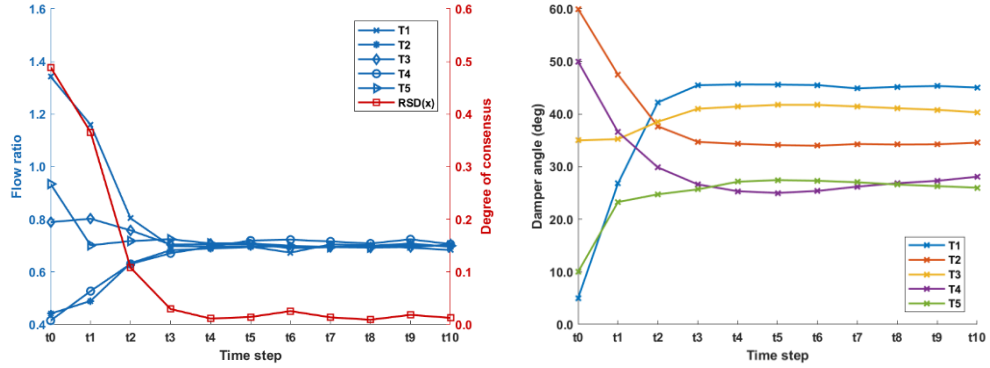

(a) State trajectories of the duct system (b) Regulation of terminal damper angles

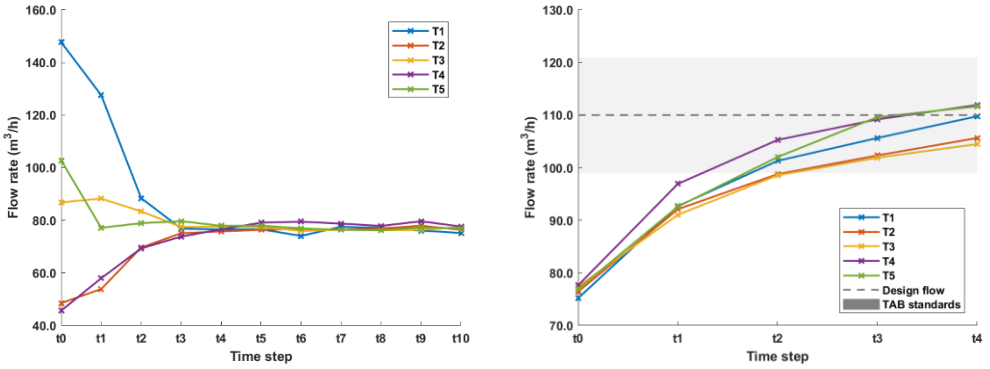

(c) Dynamic curves of terminal flow rates (d) Final adjustment in the balancing process

Figure 4.11: The experimental results of Case 4.1

Table 4.5 lists the initial conditions and the final balancing results of Case 4.2. All terminal flows reach the design value after balancing, and the maximum APE achieves 2.3%. It can be clearly seen from Figure 4.12 (b) that the damper angles are

decreased on the whole compared with Case 4.1, and T5 is fully open in the end. This leads to a smaller system resistance and a lower power consumption. The fan voltage is 4.91 V in Case 4.2, whereas it is 5.32 V in Case 4.1. According to the third fan law, the total power is proportional to the cube of the fan rotational speed. For PWM fans, the fan speed is directly proportional to the DC voltage applied, and this leads to:

$$\frac{P_1}{P_2} \approx \left(\frac{U_1}{U_2}\right)^3 \tag{4.20}$$

where P denotes the and U denotes the fan voltage.

Hence, the fan power consumption is reduced to about 78% when β is introduced.

Table 4.5: The experimental results of Case 4.2

Terminal	q_{int} (m³/h)	q^* (m³/h)	q_f (m³/h)	θ_f (°)	ε (%)
1	146.3	110.0	110.7	31.7	0.6
2	47.2	110.0	111.1	21.7	1.0
3	89.6	110.0	107.9	27.8	1.9
4	44.1	110.0	107.5	4.1	2.3
5	100.1	110.0	111.5	0	1.4

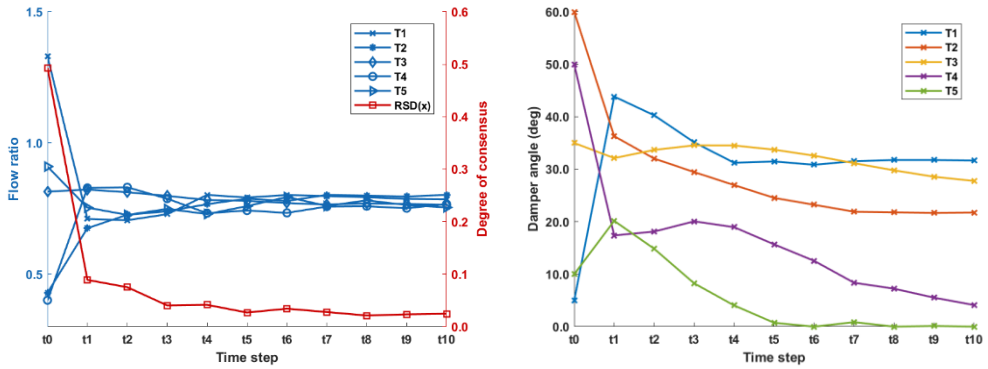

(a) State trajectories of the duct system (b) Regulation of terminal damper angles

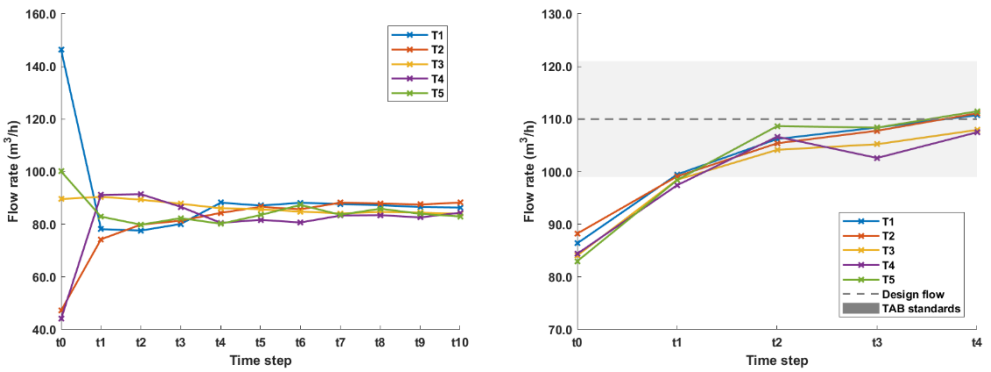

(c) Dynamic curves of terminal flow rates (d) Final adjustment in the balancing process

Figure 4.12: The experimental results of Case 4.2

The DCC-AB method is also validated in Case 4.3 where terminal design flows are different, as shown in Figure 4.13 and Table 4.6.

Table 4.6: The experimental results of Case 4.3

Terminal	q_{int} (m³/h)	q^* (m³/h)	q_f (m³/h)	θ_f (°)	ε (%)
1	150.2	80.0	78.1	41.2	2.4
2	48.6	120.0	118.0	13.8	1.7
3	72.4	140.0	148.2	13.3	5.9
4	52.2	100.0	100.5	0	0.5
5	94.4	70.0	73.3	28.6	4.7

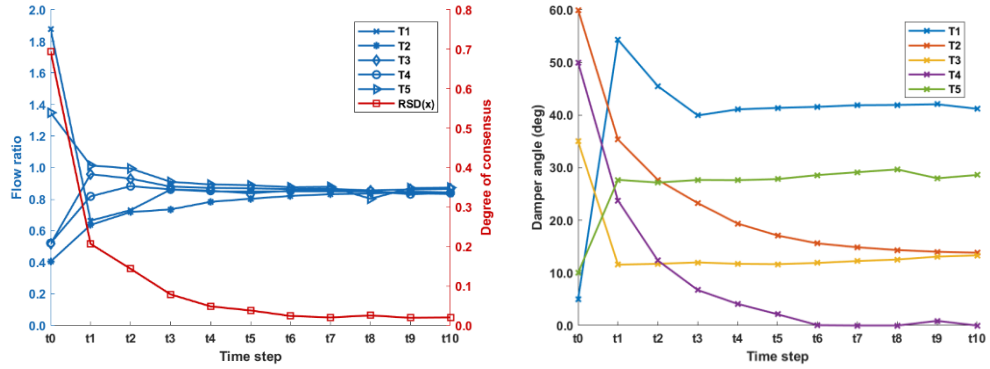

(a) State trajectories of the duct system (b) Regulation of terminal damper angles

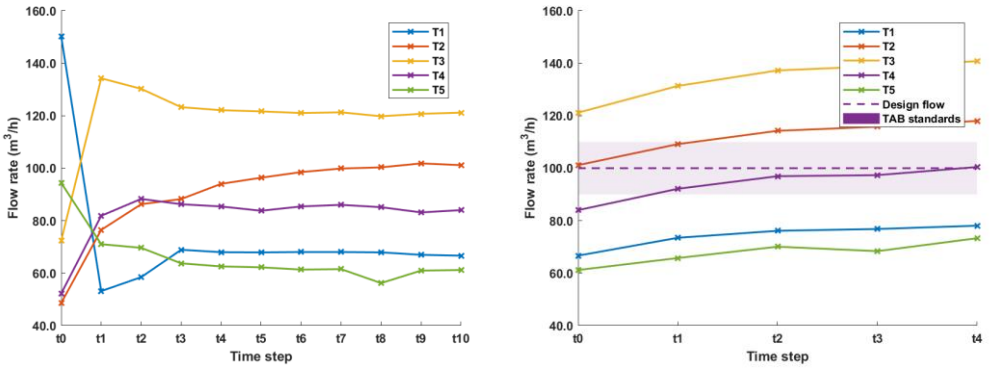

(c) Dynamic curves of terminal flow rates (d) Final adjustment in the balancing process

Figure 4.13: The experimental results of Case 4.3

For Cases 4.4 and 4.5, a similar conclusion holds for the experimental results. The system is still far from the equilibrium after 10 steps when T_s is too small. On the other hand, an apparent oscillation can be observed when T_s is too large. The selection of T_s in practical applications will depend on the parameters of the duct system and should be chosen properly to speed up the convergence while guaranteeing the stability.

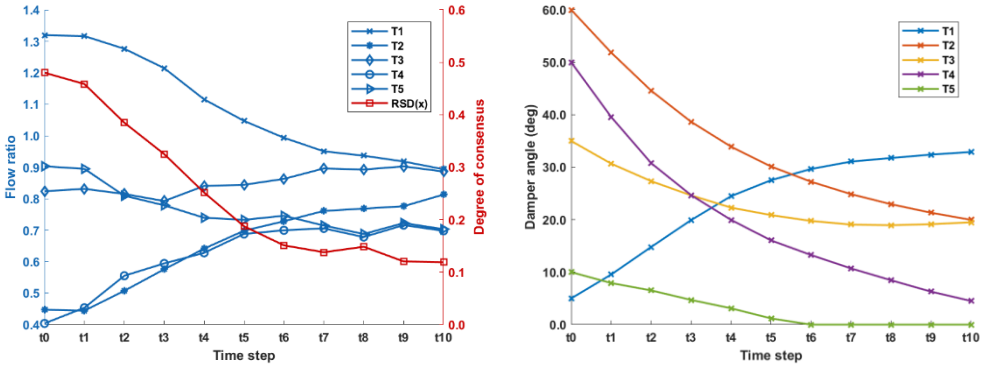

(a) State trajectories of the duct system (b) Regulation of terminal damper angles

Figure 4.14: The experimental results of Case 4.4

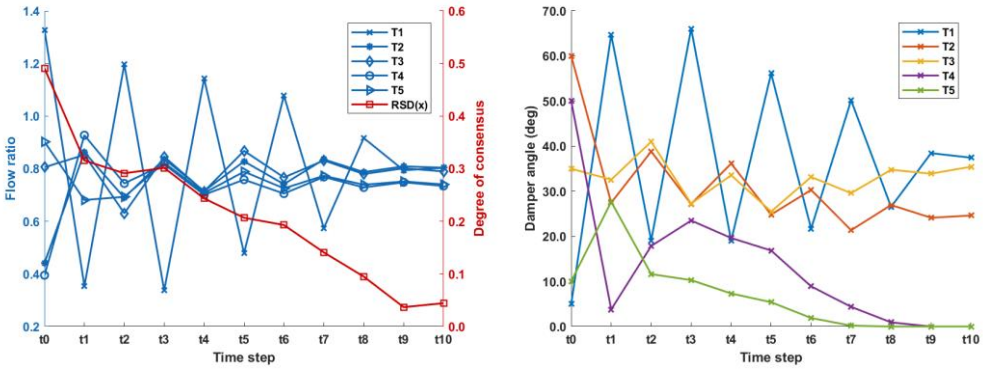

(a) State trajectories of the duct system (b) Regulation of terminal damper angles

Figure 4.15: The experimental results of Case 4.5

4.5 Conclusion

This chapter proposes a new online air balancing method, named DCC-AB method, to balance the air flow in ventilation systems. The consensus algorithm that has rich history in the field of network communication is first extended to HVAC applications to solve the air balancing problems. The DCC-AB method guarantees an asymptotic convergence towards the balanced state and can be performed during normal operation of the ventilation system without service interruptions. The energy efficiency is taken into consideration in the proposed method by ensuring at least one damper to be fully open. The DCC-AB method circumvents the centralized supervisory control and requires only a sparse communication architecture to cooperatively achieve the objective. Besides, this method is a model-free method that requires no prior knowledge on the system topology and duct parameters.

The proposed DCC-AB method is validated numerically and experimentally. A qualitative parametric analysis is conducted in MATLAB to investigate the individual model parameters on the performance of the method, followed by laboratory

experiments for further validation. Guidance is given on the parameter design based upon the simulation and experimental results. For parameter β, a non-zero value will guarantee an optimized energy efficiency, and a moderate T_s can speed up the convergence while maintaining the stability. The maximum APE is controlled within 6% among all tested cases with the best one achieving 2.3%. The fan power can be reduced by about 78% compared with ordinary consensus algorithm that considers only the flow imbalance among agents.

The experiments demonstrate that the proposed DCC-AB method applies over a large range of design flow requirements and yield a good robustness against small sensor noise. The DCC-AB method can guarantee a rapid and stable convergence within several steps, which significantly saves time and labour cost. Moreover, the DCC-AB method requires little expertise, making it easy to apply in practical use.

Chapter 5. Gradient-based online adaptive balancing (GOAB) method

5.1 Introduction

This chapter proposes another online air balancing method, named gradient-based online adaptive balancing (GOAB) method to achieve the desired air flow distribution in duct systems. The GOAB method can be performed during normal operation of the ventilation system without service interruptions. To start with, this method first tests the response of terminal flow rates with respect to damper angles to obtain an initial Jacobian matrix. Based on this primary information, the algorithm starts to adjust the terminal flows towards the desired air distribution, during which the Jacobian is adaptively updated according to newly obtained flow measurement data. The method stops until the measured flow rates meet the design values for all dampers. The key contributions of the GOAB method are summarized as follows: 1.) a recurrent form of damper adjusting rule is proposed based on gradient descent; 2.) the critical damper is explicitly identified based on the null space of the gradient vector to minimize the energy loss on dampers without compromising the balancing accuracy.

The remainder of this chapter is organized as follows: Section 5.2 presents the mathematical derivation of the GOAB method. Section 5.3 investigates the effect of several key parameters and provides guidance on the parameter design. Section 5.4 presents and discusses the experimental results. In the end, Section 5.5 summarizes this chapter and draws conclusions.

5.2 Theory of the proposed GOAB method

5.2.1. Objective function

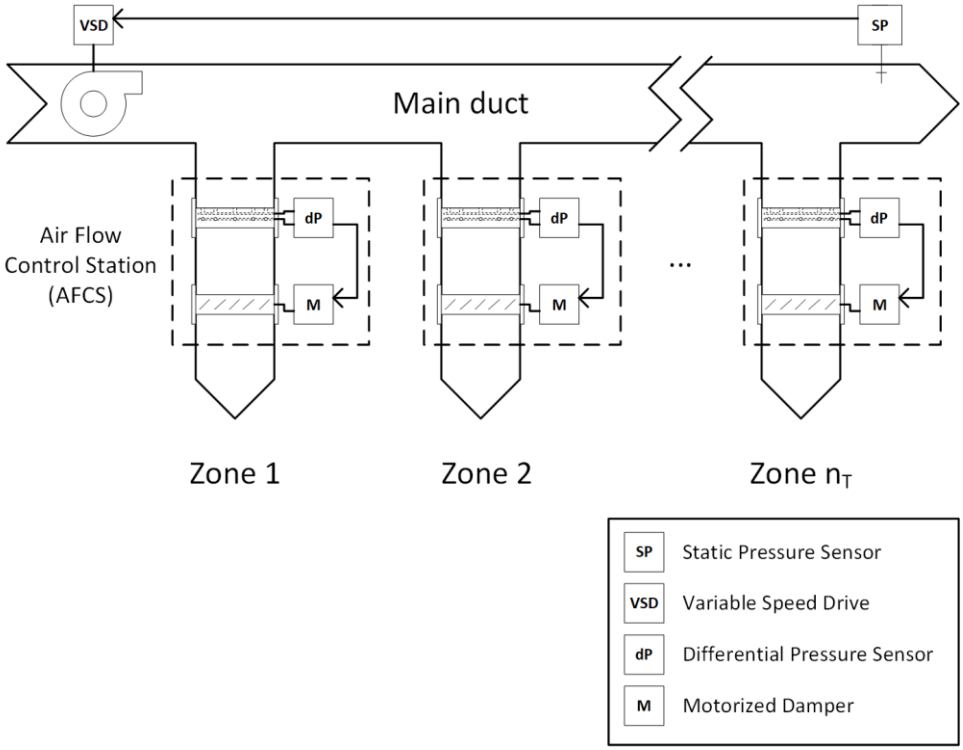

Figure 5.1: Schematic diagram of an exemplary duct system

Figure 5.1 shows a duct system with a single supply fan and n ($n \in \mathbb{N}$) number of terminals (air discharge outlets). Each terminal is equipped with a flow sensor and a damper that regulates the passing air flow rate continuously from its maximum value to absolute zero. The reference flow rates for terminals, $\mathbf{q}^*$ ($\mathbf{q}^* \in \mathbb{R}^{+n}$), are given by the indoor environment sensor, central controller, or building designer. The actual flow rates passing through the terminals, $\mathbf{q}$ ($\mathbf{q} \in \mathbb{R}^{+n}$), are assumed to be accessible by flow sensors. The damper angles are controllable by a set of control signal, $\boldsymbol{\theta}$ ($\boldsymbol{\theta} \in [\theta_{\min}, \theta_{\max}]^n$), within reasonable response time. The system dynamics is assumed as follows:

$$\dot{\mathbf{q}} = \mathbf{A}(\mathbf{q} - \mathbf{q}_{ss}) \tag{5.1}$$

where $\mathbf{A}$ is the state matrix which satisfies the exponential stability condition that $\mathbf{A}^{\mathrm{T}}\mathbf{M} + \mathbf{M}\mathbf{A}$ is negative definite for some positive definite matrix $\mathbf{M} = \mathbf{M}^{\mathrm{T}}$. The relevant Lyapunov function is:

$$V(\mathbf{z}) = \mathbf{z}^{\mathrm{T}}\mathbf{M}\mathbf{z}, \forall \mathbf{z} \in \mathbb{R}^n \tag{5.2}$$

$\mathbf{q}_{ss}$ is the steady state that dependents nonlinearly on the damper position and the fan pressure:

$$\mathbf{q}_{ss} = P_{fan} \cdot f\left(\boldsymbol{\theta}_{ss}\right) \tag{5.3}$$

The GOAB method focuses on proportioning the flow rather than the absolute quantities. Therefore, the normalization of flow rate is introduced, and the target for balancing can be expressed as an equality of two flow ratios in steady and balanced states:

$$\frac{\mathbf{q}_{ss}}{\mathbf{e}_n^T \mathbf{q}_{ss}} = \frac{\mathbf{q}^*}{\mathbf{e}_n^T \mathbf{q}^*} \tag{5.4}$$

where $\mathbf{e}_n = \begin{bmatrix} 1 & \cdots & 1 \end{bmatrix}^T$.

Then it becomes a constrained optimization problem where the objective function can be given as:

$$\min_{\boldsymbol{\theta}} \frac{1}{2} \left\| \frac{\mathbf{q}}{\mathbf{e}_n^T \mathbf{q}} - \frac{\mathbf{q}^*}{\mathbf{e}_n^T \mathbf{q}^*} \right\|^2 \tag{5.5}$$

such that

$$\theta_{\min} < \theta_i < \theta_{\max}, \forall i = 1, \cdots, n$$

The gradient of the above objective function is given by:

$$\mathbf{g}_{\boldsymbol{\theta}} = \left(\frac{\mathbf{q}}{\mathbf{e}_n^T \mathbf{q}} - \frac{\mathbf{q}^*}{\mathbf{e}_n^T \mathbf{q}^*} \right)^T \mathbf{M} \frac{\partial f}{\partial \boldsymbol{\theta}} \tag{5.6}$$

where $\mathbf{M} = \frac{1}{\mathbf{e}_n^T \mathbf{q}} \left(\mathbf{I} - \frac{\mathbf{q}\mathbf{e}_n^T}{\mathbf{e}_n^T \mathbf{q}} \right)$, and $\frac{\partial f}{\partial \boldsymbol{\theta}}$ is the Jacobian matrix that describes the local change of flow rates with respect to the change of damper angles. It is assumed that the terminal flow rates can be approximated by a first-order Taylor polynomial:

$$\mathbf{q} = \mathbf{q}_\circ + \frac{\partial f}{\partial \boldsymbol{\theta}} \left(\boldsymbol{\theta} - \boldsymbol{\theta}_\circ \right) + O\left(\left\| \boldsymbol{\theta} - \boldsymbol{\theta}_\circ \right\|^2 \right) \tag{5.7}$$

The value of Jacobian matrix will be updated during the balancing process based on newly obtained measurement data. Based upon Eq. (5.6), one can derive the stochastic gradient descent algorithm [114, 115] to approach the extrema of objective function:

$$\boldsymbol{\theta}_{t+1} = \boldsymbol{\theta}_t - \alpha \mathbf{g}_{\boldsymbol{\theta}} \tag{5.8}$$

where α is the step size.

5.2.2. Refinement of damper adjustment with consideration of energy conservation

It can be shown that multiple solutions could exist in the duct system, i.e., different combinations of the fan static pressure and damper angle set exist that satisfy the design flow requirement. The optimum is the one with the lowest fan power consumption, which is also the one with the lowest duct resistance. Therefore, as required by the TAB standards, at least one damper (critical damper) should be wide open to minimize the energy consumption. Unlike traditional methods that identify the critical damper by trial-and-error or even neglect it, the GOAB method can explicitly solve the optimal damper angle set by the following theory.

Noticed that the matrix $\mathbf{M}$ in Eq. (5.6) has an eigenvalue $\eta = 0$ and a corresponding eigenvector $\mathbf{v} = \mathbf{q}$. This guarantees the following equation for any arbitrary constant λ, named as the refinement coefficient:

$$\mathbf{g}_{\boldsymbol{\theta}} \Delta\boldsymbol{\theta} = \left(\frac{\mathbf{q}}{\mathbf{e}_n^T \mathbf{q}} - \frac{\mathbf{q}^*}{\mathbf{e}_n^T \mathbf{q}^*} \right)^T \mathbf{M} \left(\frac{\partial f}{\partial \boldsymbol{\theta}} \Delta\boldsymbol{\theta} + \lambda \mathbf{q} \right) = \mathbf{g}_{\boldsymbol{\theta}} \left(\Delta\boldsymbol{\theta} + \lambda \left(\frac{\partial f}{\partial \boldsymbol{\theta}} \right)^{-1} \mathbf{q} \right) \tag{5.9}$$

Eq. (5.9) provides the possibility to select the optimal solution among all possible ones by tuning λ. Since θ=0° denotes fully open and θ=90° denotes fully closed, the optimal refinement coefficient $\lambda^\dagger$ can be obtained by:

$$\lambda^\dagger = \arg\min_{\lambda} \sum \left(\Delta\boldsymbol{\theta} + \lambda \left(\frac{\partial f}{\partial \boldsymbol{\theta}} \right)^{-1} \mathbf{q} \right) \tag{5.10}$$

such that

$$\mathbf{0}^\circ < \boldsymbol{\theta}_t + \Delta\boldsymbol{\theta} + \lambda \left(\frac{\partial f}{\partial \boldsymbol{\theta}} \right)^{-1} \mathbf{q} < \mathbf{90}^\circ$$

which leads to the final adjustment law for damper angles:

$$\Delta\boldsymbol{\theta} = -\alpha \mathbf{g}_{\boldsymbol{\theta}} + \lambda^{\dagger} \left(\frac{\partial f}{\partial \boldsymbol{\theta}} \right)^{-1} \mathbf{q} \tag{5.11}$$

5.2.3. Estimation of Jacobian matrix and online adaptation

The GOAB method will roughly estimate the Jacobian matrix at the beginning and then adaptively modify it during the process of damper adjustment based on new measurement data.

Assume the measurement noise is independent Gaussian-distributed (white noise), then the Jacobian matrix around $\boldsymbol{\theta}_\circ$ can be approximated by least squares estimation:

$$\left. \frac{\partial f}{\partial \boldsymbol{\theta}} \right|_\circ \approx \boldsymbol{\Psi}\boldsymbol{\Sigma}^T \left(\boldsymbol{\Sigma}\boldsymbol{\Sigma}^T \right)^{-1} \tag{5.12}$$

where

$$\boldsymbol{\Sigma} = \begin{bmatrix} & | & \\ \cdots & \boldsymbol{\theta}_i - \boldsymbol{\theta}_\circ & \cdots \\ & | & \end{bmatrix}$$

$$\boldsymbol{\Psi} = \begin{bmatrix} & | & \\ \cdots & \mathbf{q}_i - \mathbf{q}_\circ & \cdots \\ & | & \end{bmatrix}$$

Noticed that Eq. (5.12) requires $\det\left(\boldsymbol{\Sigma}\boldsymbol{\Sigma}^T \right) \neq 0$, which indicates that m ($m \geq n$) different sets of $(\mathbf{q}, \boldsymbol{\theta})$ tuples are needed to establish the initial Jacobian matrix. In this thesis, m is chosen equal to n, and $\boldsymbol{\theta}_i$ is set to be pairwise-orthogonal.

The recurrent form of Jacobian adaptation is given by:

$$\left.\frac{\partial f}{\partial \boldsymbol{\theta}}\right|_t \approx \mathbf{P}_t^T \mathbf{S}_t^{-1} = \left(\mu \mathbf{P}_{t-1} + \Delta\boldsymbol{\theta}_t \Delta\mathbf{q}_t^T\right)^T \left(\mu \mathbf{S}_{t-1} + \Delta\boldsymbol{\theta}_t \Delta\boldsymbol{\theta}_t^T\right)^{-1} \tag{5.13}$$

where

$$\begin{aligned} \mathbf{P}_t &= \mu^t \boldsymbol{\Sigma}\boldsymbol{\Psi}^T + \sum_{i=1}^{t} \mu^{(t-i)} \Delta\boldsymbol{\theta}_i \Delta\mathbf{q}_i^T \\ \mathbf{S}_t &= \mu^t \boldsymbol{\Sigma}\boldsymbol{\Sigma}^T + \sum_{i=1}^{t} \mu^{(t-i)} \Delta\boldsymbol{\theta}_i \Delta\boldsymbol{\theta}_i^T \end{aligned} \tag{5.14}$$

μ is the forgetting factor, $\Delta\boldsymbol{\theta}_i$ is the adjustment of damper angles at the i_{th} step and $\Delta\mathbf{q}_i$ is the corresponding change in flow rates.

During the balancing process, the terminal flow rates in response to the damper adjustment are recorded, and the matrix $\mathbf{S}_t$ and $\mathbf{P}_t$ are updated online based on Eq. (5.14) to estimate the Jacobian matrix on demand.

5.2.4. Low-pass filter trick

In practical application, the following trick can be applied to reduce sensor noise:

$$\frac{\Delta\mathbf{q}(s)}{F(s)} = \frac{\mathbf{J}\Delta\boldsymbol{\theta}(s)}{F(s)} \tag{5.15}$$

In this thesis, F(s) is a low pass filter that replaces $\boldsymbol{\theta}_t$ and $\mathbf{q}_t$ with filtered $\boldsymbol{\theta}_t$ and $\mathbf{q}_t$:

$$\mathbf{P}_t = \mu^t \boldsymbol{\Sigma}\boldsymbol{\Psi}^T + \sum_{i=1}^{t} \mu^{(t-i)} \Delta\boldsymbol{\theta}_i \Delta\mathbf{q}_i^T \tag{5.16}$$

$$\mathbf{S}_t = \mu^t \boldsymbol{\Sigma}\boldsymbol{\Sigma}^T + \sum_{i=1}^{t} \mu^{(t-i)} \Delta\boldsymbol{\theta}_i \Delta\boldsymbol{\theta}_i^T \tag{5.17}$$

5.2.5. Final form of the GOAB method

To summarize, the proposed GOAB method can be executed as follows:

Algorithm 1 Gradient-based online air balancing (GOAB) method

Require: step size α, forgetting factor μ, target flow $\mathbf{q}^*$, initial damper angle $\boldsymbol{\theta}_\circ$, initial flow $\mathbf{q}_\circ$, balancing step limit n, convergence tolerance ε

Procedure:

for each terminal:

1: Adjust the damper angle by $\Delta\boldsymbol{\theta}_i$

2: Record the change of flow rate $\Delta\mathbf{q}_i = \mathbf{q}_i - \mathbf{q}_{i\circ}$

3: Set back the damper angle to $\boldsymbol{\theta}_\circ$

end for

4: Initialize the Jacobian by Eq. (5.12)

repeat n **times**:

5: Compute the gradient $\mathbf{g}_{\boldsymbol{\theta}}$ by Eq. (5.6)

6: Compute the refinement coefficient λ by Eq. (5.10)

7: Compute the damper adjustment by Eq. (5.11)

8: Measure the terminal flow rate $\mathbf{q}$

9: Update the Jacobian by Eq. (5.16) and (5.17)

end repeat

repeat:

10: Adjust the fan speed

11: Measure the terminal flow rate $\mathbf{q}$

until $\left|\mathbf{q}-\mathbf{q}^*\right| \Big/ \mathbf{q}^* < \varepsilon$:

12: ***return***

5.3 Design principle of the proposed GOAB method

To aid the understanding of the rationale behind the GOAB method, a detailed parameter analysis is conducted in MATLAB. Two key parameters, λ and α, are investigated to provide guidance on the parameter design. To isolate the independent parameter's effects on the performance of the algorithm, a base case is set up in Section 5.3.1 as a benchmark.

5.3.1. Base case

In the base case, the step size α is set to be $1/3$, and the forgetting factor μ is 0.8. The refinement coefficient λ is determined based on Eq. (5.10). The initial terminal flow $\mathbf{q}_\circ$ = [100.0, 94.1, 83.5, 75.4, 65.3](m^3/h), and the target flow is set as $\mathbf{q}^*$ = [100, 100, 100, 100, 100](m^3/h).

Figure 5.2 depicts the process of air balancing by using the GOAB method, and Table 5.1 summarizes the obtained results. Figure 5.2 (a) tracks the trajectories of

terminal flow rates during the process. The corresponding flow ratio, $r = \mathrm{q} / \mathrm{q}^{*}$, is shown in Figure 5.2 (b). To better illustrate the degree to which the flow ratios approach consensus, i.e., whether flows are proportioned through the system, the relative standard deviation (RSD) of the flow ratio is introduced. The $RSD(r)$ is denoted by a red line in Figure 5.2 (b) with the corresponding axis located on the left-hand side of the plot. The adjustment of damper angles is shown in Figure 5.2 (c). It can be found that T5 remains fully open throughout the balancing process, and the left dampers gradually converge to steady-state after experiencing a rapid change in the first few steps. Noticed from Figure 5.2 (b) that all flow ratios approach 0.84 at the 10^{th} step, which means the terminal flows end up being proportioned at 84% of the design values. Hence, a final adjustment of the fan speed is needed. Intuitively, the total flow should be increased by a factor of 100/84 such that all terminal flows can be proportionally changed to meet the design values. This can be accomplished by regulating the fan input voltage, and the adjustment process is shown in Figure 5.2 (d). The results are listed in Table 5.1, where $\mathbf{q}_b$ denotes the flow rate in the balanced state (in terms of flow ratio), $\mathbf{q}_f$ denotes the final flow rate, and ε is the absolute percentage error (APE). By applying the GOAB method, all terminal flows are controlled within ±0.3% of the design values.

Table 5.1: The simulation results of Case 5.1 (base case)

Terminal	$q_\circ$ (m³/h)	q_b (m³/h)	q_f (m³/h)	q^* (m³/h)	ε (%)
1	100.0	83.7	99.7	100.0	0.3%
2	94.1	83.7	99.8	100.0	0.2%
3	83.5	83.6	99.9	100.0	0.1%
4	75.4	83.6	100.2	100.0	0.2%
5	65.3	83.6	100.3	100.0	0.3%

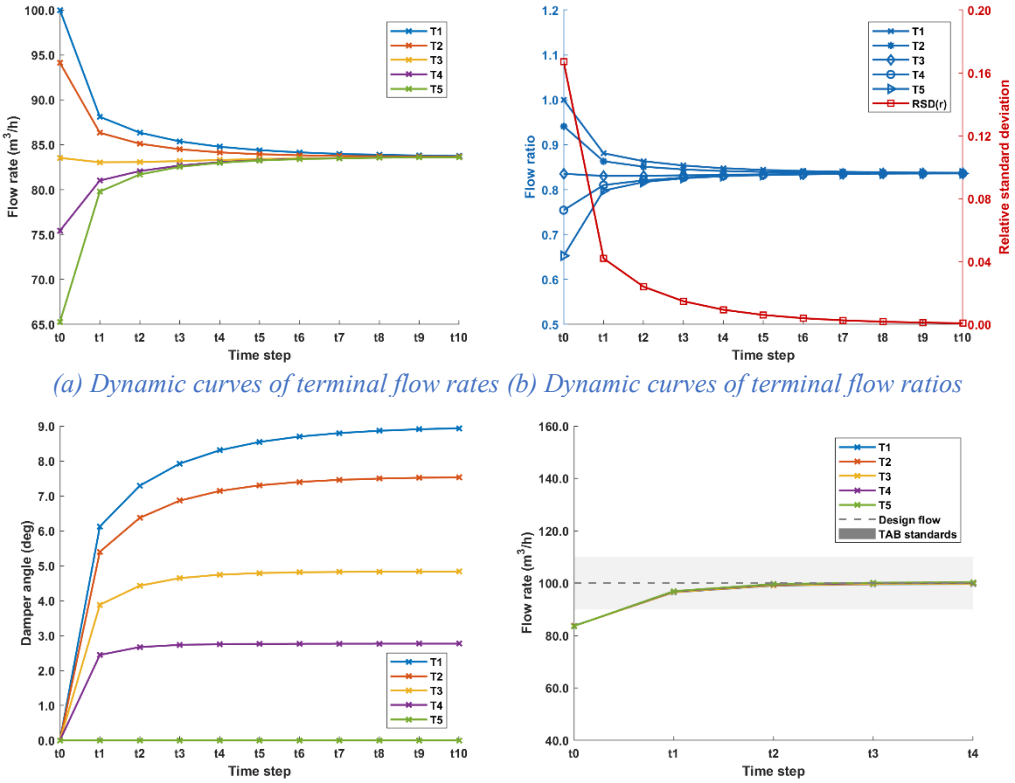

(a) Dynamic curves of terminal flow rates (b) Dynamic curves of terminal flow ratios

(c) Regulation of terminal damper angles (d) Final adjustment in the balancing process

Figure 5.2: The simulation results of Case 5.1 (base case)

5.3.2. Investigation into the initial damper angle $\boldsymbol{\theta}_{\circ}$

The GOAB algorithm is designed to work online, and it is not always the case that the balancing procedure starts with all dampers fully open. To explore whether the proposed GOAB method is independent of initial conditions, the initial damper angle is set as $\boldsymbol{\theta}_{\circ}$ = [10.0, 10.0, 10.0, 10.0, 10.0](°) in this test case. The corresponding initial flow $\mathbf{q}_{\circ}$ = [100.0, 96.9, 91.0, 86.5, 80.6](m^3/h).

The results shown in Figure 5.3 demonstrate that the GOAB algorithm is also workable under non-zero initial damper angle conditions. As can be seen from Figure 5.3 (c), the GOAB algorithm will force one of the dampers (T5) to fully open at the first step, causing all the other dampers to open as well. Then each terminal damper regulates towards the target and T5 keeps wide open during the process, which guarantees a minimum fan power consumption. Besides, the balancing accuracy is nearly unaffected by $\boldsymbol{\theta}_{\circ}$, as shown in Table 5.2.

Other settings of $\boldsymbol{\theta}_{\circ}$ have also been tested, and the results indicate that the GOAB method applies to any initial damper angle conditions.

Table 5.2: The simulation results of base case with non-zero initial damper angles

Terminal	$q_\circ$ (m^3/h)	q_b (m^3/h)	q_f (m^3/h)	q^* (m^3/h)	ε (%)
1	100.0	91.0	99.8	100.0	0.2%
2	96.9	91.0	99.9	100.0	0.1%
3	91.0	91.0	99.9	100.0	0.1%
4	86.5	91.0	100.1	100.0	0.1%
5	80.6	91.0	100.2	100.0	0.2%

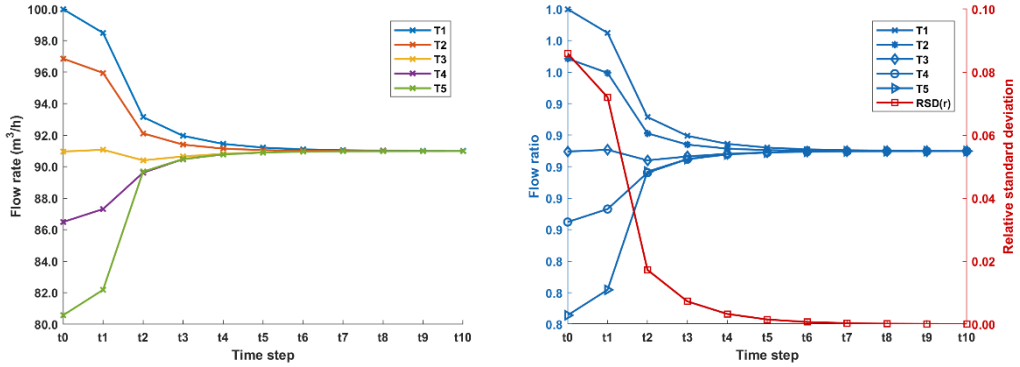

(a) Dynamic curves of terminal flow rates

(b) Dynamic curves of terminal flow ratios

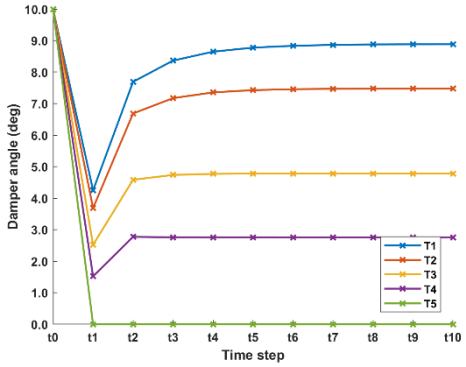

(c) Regulation of terminal damper angles

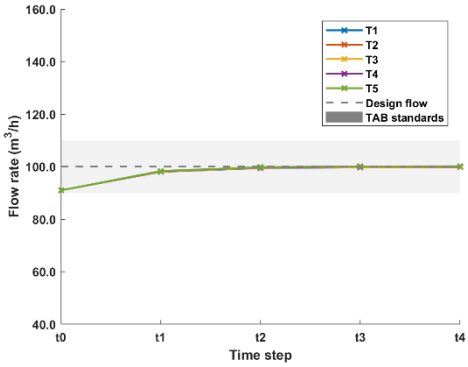

(d) Final adjustment in the balancing process

Figure 5.3: The simulation results of base case with non-zero initial damper angles

5.3.3. Investigation into the refinement coefficient λ

To investigate the effect of the refinement coefficient, λ is set to zero in Case 5.2. The initial terminal flow remains $\mathbf{q}_\circ$ = [100.0, 94.1, 83.5, 75.4, 65.3](m^3/h) as in the base case. Other conditions including the step size α and forgetting factor μ also keep unchanged.

The simulation results are shown in Figure 5.4 and Table 5.3. It can be found that the convergence speed of T5 is apparently slower than others, which leads to an overall degraded balancing result. Further investigation into Figure 5.4 (c) reveals that

the damper regulation proceeds out of step among terminals. The response of T1 and T2 starts from the beginning followed by T3, whereas T4 starts even later. We also noticed that negative values can occur in the calculation of $\boldsymbol{\theta}_{t+1}$ in this test case when damper is adjusted based solely on Eq. (5.8) and no correction is made by $\lambda^{\dagger}$. Under such circumstance, the illegal values of $\boldsymbol{\theta}_{t+1}$ given by an arbitrary λ will be chopped by the operating range constraint, which alters the desired state trajectory. Consequently, the convergence rate will be slowed down and the balancing accuracy will also be affected. The maximum APE can be as high as 4.7% in this case.

Table 5.3: The simulation results of Case 5.2 where λ=0

Terminal	$q_\circ$ (m³/h)	q_b (m³/h)	q_f (m³/h)	q^* (m³/h)	ε (%)
1	100.0	85.0	101.3	100.0	1.3%
2	94.1	84.8	101.2	100.0	1.2%
3	83.5	84.6	101.0	100.0	1.0%
4	75.4	84.3	101.1	100.0	1.1%
5	65.3	79.5	95.3	100.0	4.7%

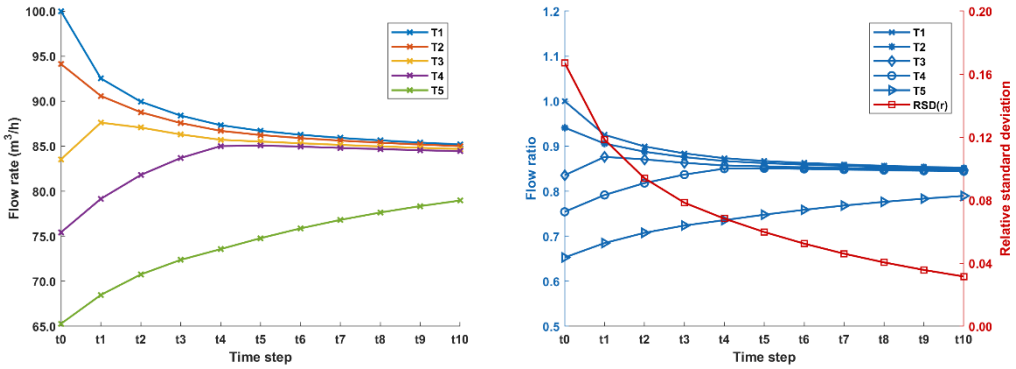

(a) Dynamic curves of terminal flow rates (b) Dynamic curves of terminal flow ratios

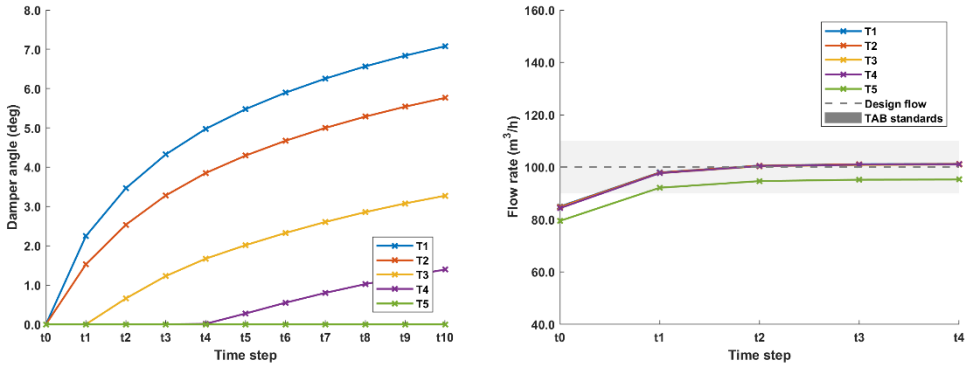

(c) Regulation of terminal damper angles (d) Final adjustment in the balancing process

Figure 5.4: The simulation results of Case 5.2 where λ=0

The parameter λ has another important effect that it controls dampers towards fully open during the balancing process, which can be better observed under non-zero initial damper angle conditions. Hence, a supplementary case (Case 5.3) is provided in this section. In Case 5.3, $\boldsymbol{\theta}_{\circ}$ = [10.0, 10.0, 10.0, 10.0, 10.0](°), $\mathbf{q}_{\circ}$ = [100.0, 96.9, 91.0, 86.5, 80.6](m^3/h) and λ =0.

By comparing Figure 5.5 (c) with Figure 5.3 (c), we found that the system will end up with all dampers partially closed if we set λ to zero. The damper T5, which is supposed to be fully open as indictaed in Figure 5.3 (c), is now partially closed. Meanwhile, all other damper angles are increased, indicating a larger duct resistance. By checking the product of pressure drop and flow rate through all terminals, it is estimated that the energy consumption in dampers can be 43% higher in Case 5.3 when λ =0.

In summary, the parameter λ provides an additional degree of freedom to choose the optimum direction of the damper angle increment. The utilization of an optimized λ (i.e., $\lambda^{\dagger}$) effectively avoids distortion in the predefined trajectory towards target and significantly reduces the energy consumption by minimizing the overall damper resistance.

Table 5.4: The simulation results of Case 5.3 (supplementary case) where λ=0

Terminal	$q_{\circ}$ (m^3/h)	q_b (m^3/h)	q_f (m^3/h)	q^* (m^3/h)	ε (%)
1	100.0	91.0	99.9	100.0	0.1%
2	96.9	91.0	99.9	100.0	0.1%
3	91.0	91.0	100.0	100.0	0.0%
4	86.5	91.0	100.1	100.0	0.1%
5	80.6	91.0	100.1	100.0	0.1%

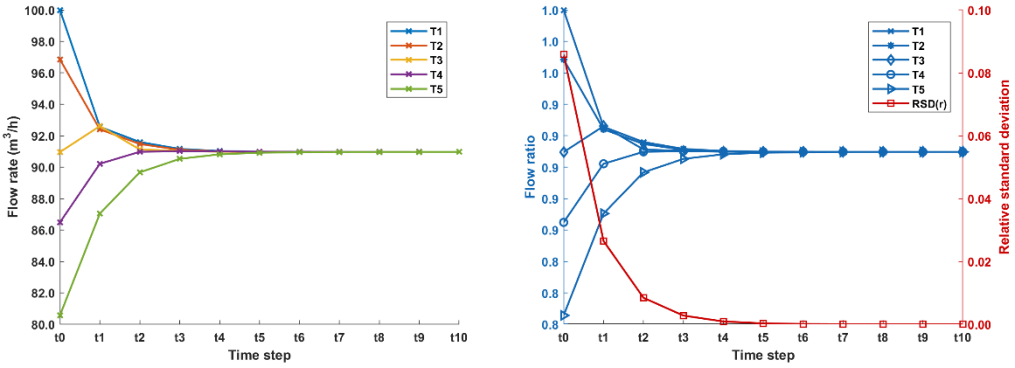

(a) Dynamic curves of terminal flow rates (b) Dynamic curves of terminal flow ratios

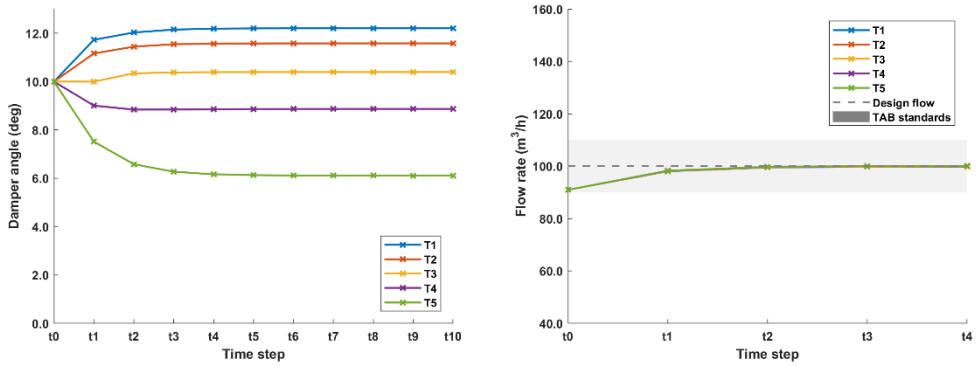

(c) Regulation of terminal damper angles (d) Final adjustment in the balancing process

Figure 5.5: The simulation results of Case 5.3 (supplementary case) where λ=0

5.3.4. Investigation into the step size α

The parameter α controls the speed of convergence rate and stability of the algorithm. In this section, two cases (α =1/15 and α =2/3) will be tested.

In Case 5.4, α is set to 1/15 and the results are given in Figure 5.6 and Table 5.5. Compared with the base case where α =1/3, the convergence speed is distinctly slowed down when α is reduced. It takes around 10 times longer to achieve the same RSD as in the base case, and the final balancing result is slightly less accurate due to slower convergence.

Table 5.5: The simulation results of Case 5.4 where α=1/15

Terminal	$q_\circ$ (m³/h)	q_b (m³/h)	q_f (m³/h)	q^* (m³/h)	ε (%)
1	100.0	86.0	102.5	100.0	2.5%
2	94.1	84.9	101.3	100.0	1.3%
3	83.5	83.2	99.4	100.0	0.6%
4	75.4	82.4	98.6	100.0	1.4%
5	65.3	81.8	98.1	100.0	1.9%

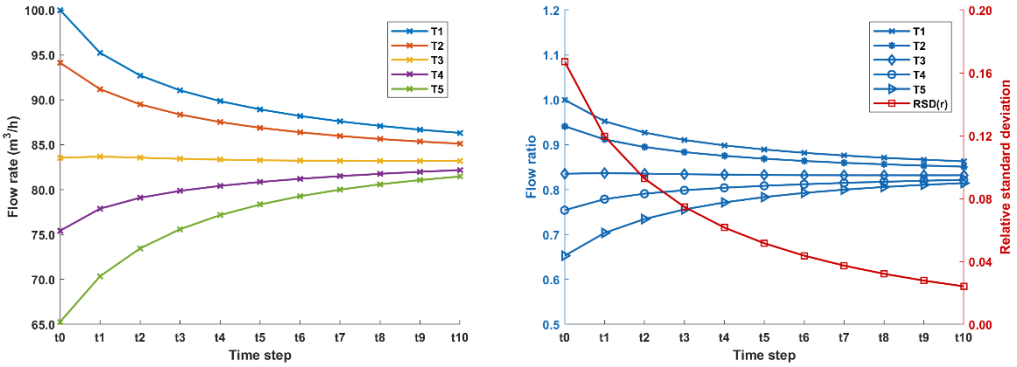

(a) Dynamic curves of terminal flow rates (b) Dynamic curves of terminal flow ratios

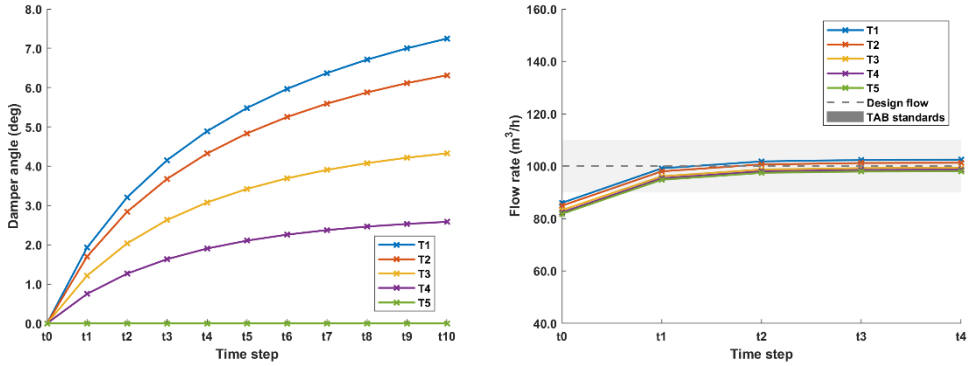

(c) Regulation of terminal damper angles (d) Final adjustment in the balancing process

Figure 5.6: The simulation results of Case 5.4 where α=1/15

Figure 5.7 and Table 5.6 show the results when α =2/3. Oscillation can be observed when the step size is twofold. In this case, the increment of damper angle is much too aggressive, and the system is over-tuned. The algorithm becomes susceptible to the sensor noise and is therefore less stable. It can be found from Table 5.6 that the balancing result is worse than the base case with a relative error of 8.6%. For certain test cases where the flow rate set point varies, the algorithm can even fail to converge.

To conclude, a conservative α will slow down the convergence, whereas an aggressive α may lead to oscillations. The selection of α in practical applications shall depend on the parameters of the duct system and should be chosen properly to speed up the convergence while guaranteeing the stability.

Table 5.6: The simulation results of Case 5.5 where α=2/3

Terminal	$q_\circ$ (m³/h)	q_b (m³/h)	q_f (m³/h)	q^* (m³/h)	ε (%)
1	100.0	84.7	100.9	100.0	0.9%
2	94.1	84.6	101.0	100.0	1.0%
3	83.5	84.8	101.2	100.0	1.2%
4	75.4	76.4	91.4	100.0	8.6%
5	65.3	87.8	105.4	100.0	5.4%

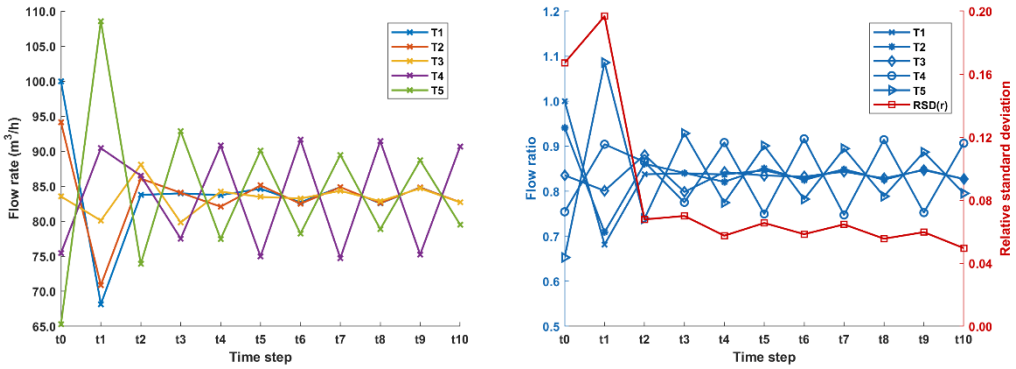

(a) Dynamic curves of terminal flow rates (b) Dynamic curves of terminal flow ratios

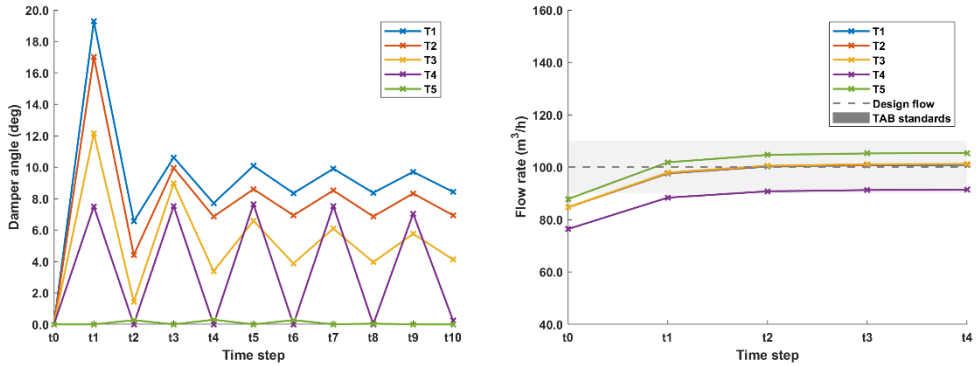

(c) Regulation of terminal damper angles (d) Final adjustment in the balancing process

Figure 5.7: The simulation results of Case 5.5 where α=2/3

5.4 Experimental validation

The procedure of the GOAB method is shown in Figure 5.8. To begin with, all dampers were set to fully open. A signal was sent by the computer to start the fan and sufficiently long waiting time was spent to make sure the system has been stabilized. The flow rate of each terminal at initial state was measured and recorded. To obtain an initial Jacobian matrix, the terminal dampers were partially closed in turn. The response of each terminal flow was tracked and the initial Jacobian matrix was calculated by Eq. (5.12). Then the algorithm comes to the adjusting and balancing stage. The regulation of damper position at each time step was calculated by Eq. (5.11), and the Jacobian matrix was updated by Eq. (5.16) and Eq. (5.17). The process was repeated until all terminal flows reach the design values within tolerance. At the end of balancing stage, the fan speed was adjusted to proportionally bring the terminal flows to the corresponding design values, which was realized by a closed-loop established between fan speed and the total flow rate. Lastly, all flows were re-measured to make sure the

duct system was balanced. A flow chart describing the experimental procedures is given in Figure 5.9.

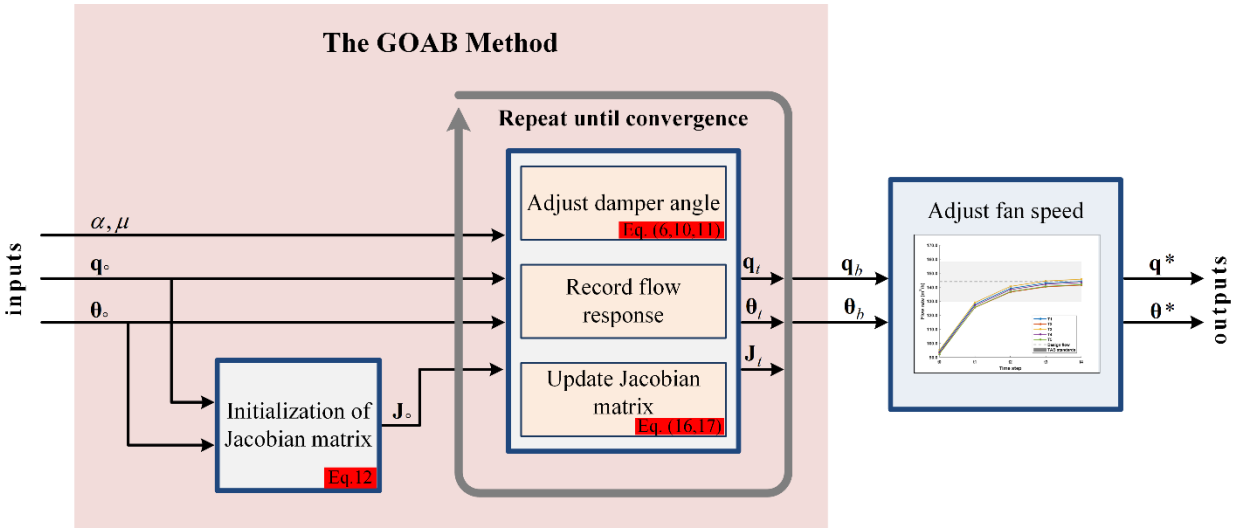

Figure 5.8: Graphic explanation of the GOAB method

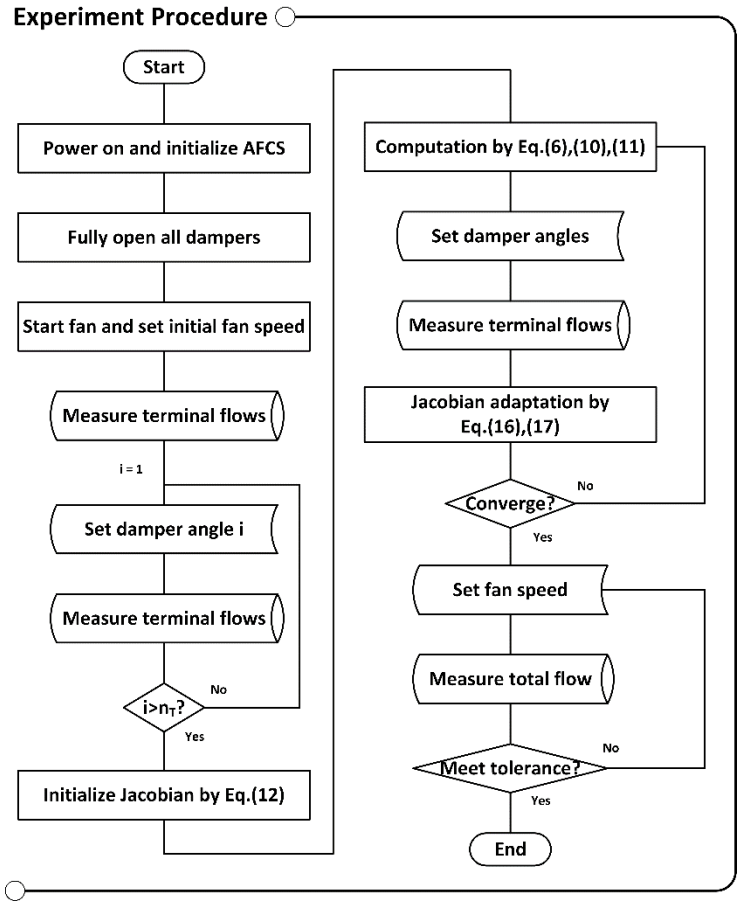

Figure 5.9: Flow chart of experimental procedures

With the air distribution platform (Section 4.4), experiments were conducted to validate the GOAB method. Following the simulation in Section 5.3.1, the design flow

is set to 100 m^3/h for every single terminal, and the regulation of damper angle at each time step is optimized by λ. The initial terminal flow varies from 74.7 m^3/h to 129.5 m^3/h. The results are shown in Figure 5.10.

At the beginning, the terminal flow deviates largely from the design value with the maximum relative error up to 30%. During the balancing process, the terminal flow rates exhibit a nearly exponential convergence with some small fluctuations, as shown in Figure 5.10 (a). The damper T4 maintains fully open throughout the whole process, indicating a minimized duct resistance. At the end, the fan speed is adjusted to reduce the error in total flow. It can be found from Table 5.7, by applying the proposed GOAB method, all terminal flows are controlled within ±2.6% of the design value.

Table 5.7: Experimental validation of the base case

Terminal	$q_\circ$ (m^3/h)	q_b (m^3/h)	q_f (m^3/h)	q^* (m^3/h)	ε (%)
1	129.5	94.8	98.8	100.0	1.2%
2	108.8	94.7	100.9	100.0	0.9%
3	120.7	94.6	98.3	100.0	1.7%
4	74.7	97.7	98.7	100.0	1.3%
5	79.0	96.1	97.4	100.0	2.6%

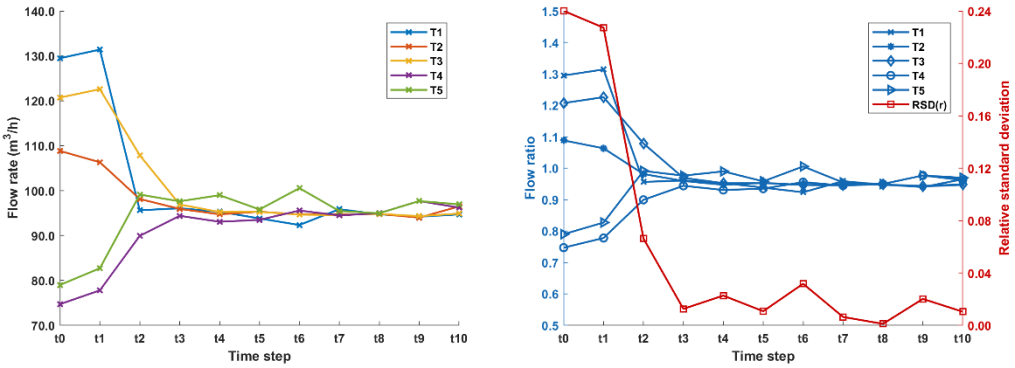

(a) Dynamic curves of terminal flow rates (b) Dynamic curves of terminal flow ratios

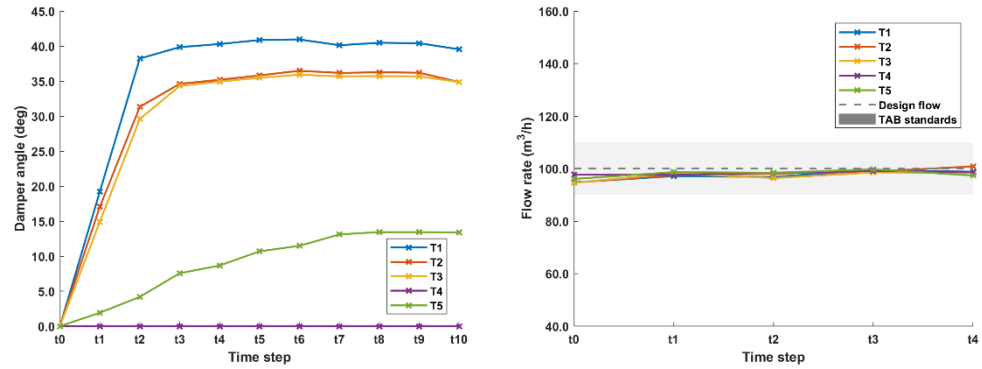

(c) Regulation of terminal damper angles (d) Final adjustment in the balancing process

Figure 5.10: Experimental validation of the base case

To further validate the GOAB method, experiments were conducted under different design flow requirements. In the first case, the design flow for T2 is changed to 50 m^3/h and the results are shown in Figure 5.11 and Table 5.8. In the second case, all terminal design flow is assigned to a different flow target, $\mathbf{q}^*$ = [120, 100, 80, 60, 130](m^3/h). The results are presented in Figure 5.12 and Table 5.9. For clarity, Figure 5.12(d) only displays the design flow for T2, and the corresponding ±10% interval is rendered red.

It can be found that the system can achieve air balance under varied flow targets. Since the algorithm focuses on proportioning the flow rather than the absolute quantities, all flow ratios gradually approach the same value. In the end, all terminal flows reach the design values within tolerance and the maximum relative error is below 4.3%.

Table 5.8: Experimental validation with single change of flow rate set point

Terminal	$q_\circ$ (m^3/h)	q_b (m^3/h)	q_f (m^3/h)	q^* (m^3/h)	ε (%)
1	129.8	108.1	99.2	100.0	0.8%
2	110.4	52.0	47.9	50.0	4.3%
3	121.9	111.5	104.6	100.0	4.6%
4	76.8	105.3	98.3	100.0	1.7%
5	80.1	107.1	95.1	100.0	4.9%

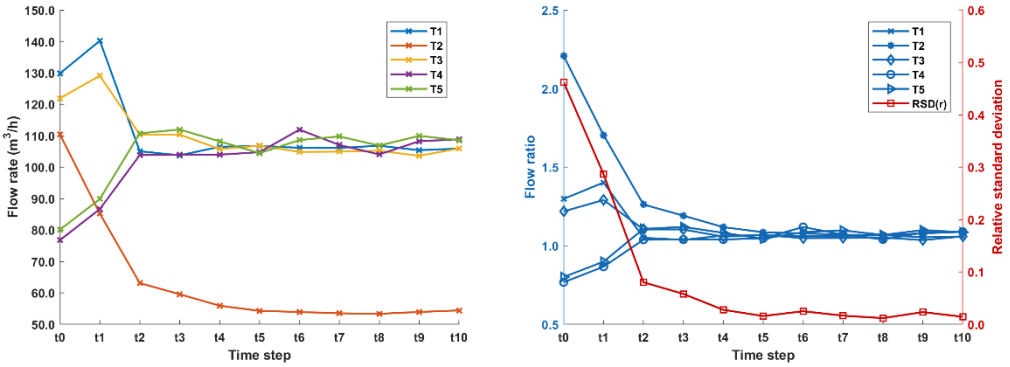

(a) Dynamic curves of terminal flow rates (b) Dynamic curves of terminal flow ratios

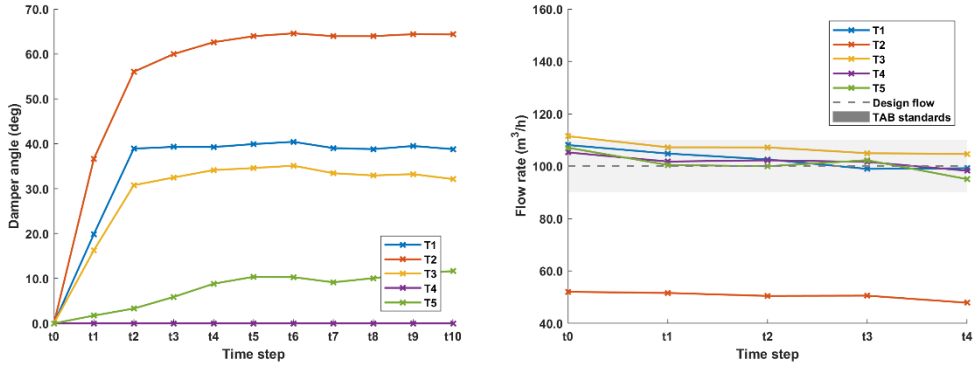

(c) Regulation of terminal damper angles (d) Final adjustment in the balancing process

Figure 5.11: Experimental validation with single change of flow rate set point

Table 5.9: Experimental validation with all flow rate set points changed

Terminal	$q_\circ$ (m³/h)	q_b (m³/h)	q_f (m³/h)	q^* (m³/h)	ε (%)
1	134.2	113.7	122.8	120.0	2.3%
2	112.5	97.2	100.7	100.0	0.7%
3	123.3	74.3	76.6	80.0	4.3%
4	76.8	57.2	61.3	60.0	2.2%
5	82.7	124.6	132.7	130.0	2.1%

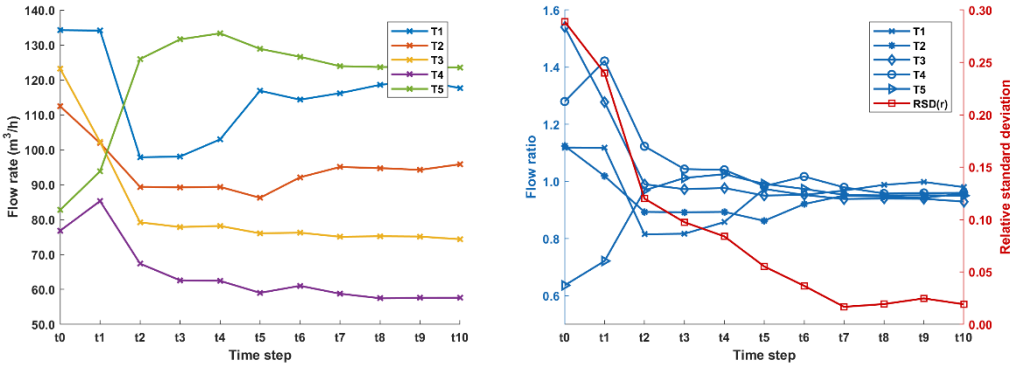

(a) Dynamic curves of terminal flow rates (b) Dynamic curves of terminal flow ratios

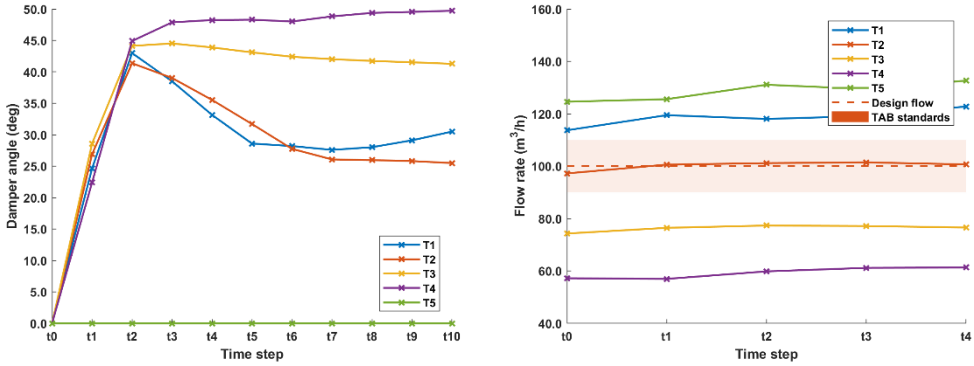

(c) Regulation of terminal damper angles (d) Final adjustment in the balancing process

Figure 5.12: Experimental validation with all flow rate set points changed

5.5 Conclusion

This chapter proposes a gradient-based adaptive air balancing method, named GOAB method to support balancing-in-service. By defining an objective function that quantifies the discrepancy between the normalized flow rate and the set point, the GOAB method calculates the increment of damper angles based on stochastic gradient descent. An online adaptive mechanism for the Jacobian estimation is applied to capture the change of Jacobian matrix during the adjustment. The overall flow resistance of terminal dampers is minimized utilizing the null space of the gradient vector, which reduces the overall energy loss. The proposed GOAB method is validated numerically and experimentally.

Simulations are conducted in MATLAB to investigate the effect of the initial condition $\boldsymbol{\theta}_{\circ}$, the refinement coefficient λ and the step size α. It has been revealed that the GOAB is independent of initial conditions. The introduction of λ guarantees at least one damper to be fully open and effectively avoids conflicts to the damper angle constraints, which leads to faster convergence towards balance. The parameter α controls the speed of convergence rate and stability of the algorithm. A conservative α

will slow down the convergence, whereas an aggressive α could lead to oscillations. The experiments demonstrate that the proposed GOAB method is effective under various design flow requirements. The relative error can be controlled within 4.3% in all test cases.

The proposed GOAB method provides the possibility to achieve accurate air supply under dynamic working conditions, which indicates a large energy saving potential. This method requires little prior knowledge of the system topology and duct parameters and therefore applies to a wide range of duct systems. Moreover, this method significantly reduces time and labour cost compared with traditional methods, endowing it great potential in industrial applications.

Chapter 6. Conclusion and future work

6.1 Conclusion

The air distribution systems rarely perform as anticipated in design due to unpredictable modelling error, inevitable adjustments and lacking regular maintenance. Air balancing is a valid means to achieve the desired air distribution so that the system can perform in conformity with design requirements. With proper air balancing approach, the system can greatly benefit from the improved thermal comfort, indoor air quality and reduced energy consumption and operating cost. It is therefore of vital importance to investigate air balancing and make improvements on the performance of the process. The present thesis has addressed the need with the following contributions:

Chapter 1 is the introductory chapter, giving some background knowledge related to this work. It begins with the overview of HVAC systems including the common types and topology of the system, major duct components and basic knowledge of TAB and air balancing process. Then the challenges faced by air balancing and the motivation of this thesis are clarified. At last, the Chapter summarizes the major contributions and outlines the structure of this thesis.

Chapter 2 is the literature review. This chapter focuses on the flow measurement techniques and air balancing methods, which corresponds to the two main challenges in air balancing. First, 7 common techniques for air flow measurement are introduced, followed by a detailed review of studies on Pitot tube. Then, the existing air balancing methods are introduced in historical context to show the development of this field. For each method, the strengths and weaknesses are evaluated and compared. By reviewing the related literature, this chapter provides an overview of the current state-of-the-art of this topic and identifies the existing limitations and deficiencies in air balancing.

Chapter 3 proposes a revised flow estimation formula for the APT inside the AFCS to improve the accuracy of measurement. This chapter first studies the effect of the downstream damper on the flow measurement by APT. Experiments are conducted to obtain the characteristic curve of the APT under different damper positions. The ANOVA test reveals a statistically significant correlation between p^* and θ, which indicates that the downstream damper could affect the amplification of the APT. The conclusion is consistent with the previous findings by Klaczek. Based on the

experimental data, a flow estimation formula for the APT is proposed to compensate for the systematic error caused by the damper. The proposed formula is later validated under different Reynolds numbers varying from 6.38×10^3 to 19.1×10^3, and the RMSE is below 0.02. To evaluate the performance of the proposed formula, the accuracy of flow measurement is compared before correction and after correction. By applying the proposed method, the flow measurement errors of APT are controlled within 0.6% for all tested cases, and the highest accuracy (0.02%) is achieved when Re = 9.57×10^3. In summary, the proposed method significantly reduces the systematic error caused by the control damper in AFCS and improves the accuracy of flow measurement to a large extent. Besides, the AFCS is equipped with wireless techniques, which enables communication among individual terminals. The AFCS with improved APT flow estimation formula serves as a foundation for the following two chapters.

Chapters 4 and 5 focuses on the studies of air balancing methods. Chapter 4 proposes an online air balancing method, named DCC-AB method. The DCC-AB method applies the consensus algorithm to solve the air balancing problems by treating the duct network as a multi-agent dynamical system. The DCC-AB method eliminates the need for centralized supervisory control and requires only a sparse communication architecture to cooperatively achieve the objective. Besides, this method is a model-free method that requires no prior knowledge on the system topology and duct parameters, making it easy to use in practical application. Based on the consensus theory, the DCC-AB method introduces an additional term that forces the critical damper to gradually open during the balancing process, which ensures that at least one damper is fully open at the balanced state. Then a series of simulation are conducted to investigate the individual model parameters on the performance of the method. The studies show that the parameter β governs the relative importance of the flow imbalance and the energy consumption in damper. By tuning this parameter, the DCC-AB method could achieve air balance with a minimum overall energy consumption. As for the parameter T_s, a conservative T_s will cause an increase in convergence time, whereas an aggressive T_s may lead to oscillation. With a proper selection of T_s, the convergence can be speeded up without compromising the stability. The method is then validated on a trunk-and-branch duct system of 5 terminals. The experimental results are consistent with the simulation studies. The results also demonstrate that the proposed DCC-AB method applies over a large range of design flow requirements. In all test cases, the maximum

APE is controlled within 6% and the best one achieves 2.3%. Besides, the fan power consumed by damper can be reduced by about 78% with the proposed method. In summary, the DCC-AB method guarantees an asymptotic convergence towards the balanced state within several steps, which significantly saves time and labour cost. Most importantly, the method can be performed during normal operation of the ventilation system without service interruptions.

Chapter 5 proposes another online air balancing method, named GOAB method. The GOAB method is based on the stochastic gradient descent algorithm. The objective function of the GOAB method quantifies the discrepancy between the actual flow rate and the set point in a normalized form. By calculating the gradient of the objective function, the damper adjustment rules are derived. Based on the null space of the gradient vector, the optimum direction of damper angle increment is selected, which forces the critical damper to be fully open. To start with, the method first conducts several runs of measurements to obtain an initial Jacobian matrix. Then an adaptive mechanism is applied to capture the change of Jacobian during the balancing process. A series of simulation are conducted to investigate how model parameters affect the performance of the method. The simulation reveals that the introduction of λ effectively avoids conflicts to the damper angle constraints and guarantees at least one damper to be fully open, which leads to faster convergence towards balance and lower energy consumption. The parameter α controls the speed of convergence rate and stability of the algorithm. A conservative α will slow down the convergence, whereas an aggressive α could lead to oscillations. The simulation also shows that the GOAB method is independent of initial conditions. The method is later validated on the same experimental platform as in Chapter 4. The experimental results demonstrate that the proposed GOAB method is effective under various design flow requirements. The relative error can be controlled within 4.3% in all test cases. Besides, this method requires little prior knowledge of the system topology and duct parameters and therefore applies to a wide range of duct systems.

To conclude, this thesis focuses on overcoming the current challenges posted by air balancing. Improvements are made on both the flow measurement and the balancing methods. A flow estimation formula is proposed to improve the accuracy of flow measurement in AFCS, and two novel online air balancing methods are proposed to make the balancing process more effective and efficient.

6.2 Future work

Despite certain achievements in this thesis, there is still much effort to be made towards an accurate, efficient, simple and low-cost air balancing process. Further research on this subject is highly valuable and urgently demanded. A list of foreseeable works in the near future is given as follows:

The proposed APT flow estimation formula is based on the experimental data obtained in the DN100 pipe. Although the formula is validated under different Reynolds numbers. The effect of the pipe diameter on the form of the formula is unknown. It is believed that the pipe diameter will only change the identified model parameters, whereas the form of the formula will remain the same. Validation of the proposed formula under different pipe diameters is necessary to make the formula more universal since the actual AFCS can be manufactured in various sizes.

Due to the space constraints during installation, the fittings can be placed very tightly in ducts. Although the proposed APT flow estimation formula compensates for the error caused by the downstream damper embedded inside the AFCS. The accuracy of the APT can still be affected by the upstream duct geometries of the AFCS. Based on the literature review, the upstream disturbances affect the amplification more dramatically than the downstream disturbances. What's more, the influence of the disturbances is possibly governed by the nearest one. Inspired by these findings, it is interesting to investigate the feasibility of the following solution: the current configuration of AFCS can be changed by placing the damper in front of the APT. The corresponding flow estimation formula for correction can be proposed following the same procedures. In this way, the AFCS can be more reliable for tight duct systems since the dominated disturbance is the upstream damper and this disturbance can be compensated by the proposed correction formula.

As for the air balancing methods, two methods are proposed in this thesis and both methods achieve high balancing accuracy. However, comparisons between the two proposed methods are not present. A reasonable cost and benefit analysis should be given to evaluate the air balancing methods more thoroughly. Possible evaluation criteria can be: 1.) the balancing accuracy; 2.) the duration of the balancing process; 3.) the cost in acquiring data or duct parameters; 4.) the time used for tuning model parameters and etc.

For the DCC-AB method, the effect of the communication graph on the performance of the method can be investigated. It is known that the eigenvalues of the communication graph determine some of the properties of the convergence process like the convergence rate, stability and etc. Hence, to further improve the performance of the method, investigation into the communication graph can be conducted to speed up the convergence. Besides, the robustness of the DCC-AB method subjected to communication failures can be examined to evaluate the reliability of the method.

For the GOAB method, the initial Jacobian matrix is obtained based on several runs of measurements. These measurements are performed in a relatively large range of damper angles and the obtained initial Jacobian can be inaccurate. Although it is updated based on the newly obtained data during balancing, the initial Jacobian may still affect the convergence process. It is possible that the stochastic gradient descent algorithm can be trapped in a local minimum far away from the global one. Further improvements can be made on the initialization of the Jacobian matrix.

The proposed air balancing methods have been validated in the laboratory. For future application in industry, validation under large-scale duct systems is necessary. In addition, currently both methods require parameter tuning. To further reduce the dependency on technicians and human involvement, self-tuning methods are in demand for more intelligent and efficient air balancing process.

References

[1] H. Mirinejad, S.H. Sadati, M. Ghasemian and H. Torab, Control Techniques in Heating, Ventilating and Air Conditioning (HVAC) Systems 1. (2008).

[2] R. Yang and L. Wang, Optimal control strategy for HVAC system in building energy management, Transmission and Distribution Conference and Exposition (T&D), 2012 IEEE PES, IEEE, 2012, pp. 1-8.

[3] B. Yu, Z. Hu, M. Liu, H. Yang, Q. Kong and Y. Liu, Review of research on air-conditioning systems and indoor air quality control for human health, International Journal of Refrigeration. 32(1) (2009), pp. 3-20.

[4] Z. Wang and J.S. Zhang, Characterization and performance evaluation of a full-scale activated carbon-based dynamic botanical air filtration system for improving indoor air quality, Building and Environment. 46(3) (2011), pp. 758-768.

[5] E. Mathews, C. Botha, D. Arndt and A. Malan, HVAC control strategies to enhance comfort and minimise energy usage, Energy and Buildings. 33(8) (2001), pp. 853-863.

[6] C.S. Canbay, A. Hepbasli and G. Gokcen, Evaluating performance indices of a shopping centre and implementing HVAC control principles to minimize energy usage, Energy and Buildings. 36(6) (2004), pp. 587-598.

[7] E. Atam and L. Helsen, Control-oriented thermal modeling of multizone buildings: methods and issues: intelligent control of a building system, IEEE Control Systems Magazine. 36(3) (2016), pp. 86-111.

[8] L. Pérez-Lombard, J. Ortiz and C. Pout, A review on buildings energy consumption information, Energy and Buildings. 40(3) (2008), pp. 394-398.

[9] A. Afram and F. Janabi-Sharifi, Theory and applications of HVAC control systems–A review of model predictive control (MPC), Building and Environment. 72 (2014), pp. 343-355.

[10] K. Chua, S. Chou, W. Yang and J. Yan, Achieving better energy-efficient air conditioning–a review of technologies and strategies, Applied Energy. 104 (2013), pp. 87-104.

[11] W.J. Fisk, D. Black and G. Brunner, Changing ventilation rates in US offices: Implications for health, work performance, energy, and associated economics, Building and Environment. 47 (2012), pp. 368-372.

[12] M.J. Crocker, J.P. Arenas and R.E. Dyamannavar, Identification of noise sources on a residential split-system air-conditioner using sound intensity measurements, Applied Acoustics. 65(5) (2004), pp. 545-558.

[13] J. Sundell, H. Levin, W.W. Nazaroff, W.S. Cain, W.J. Fisk, D.T. Grimsrud, F. Gyntelberg, Y. Li and A. Persily, A. Pickering, Ventilation rates and health:

multidisciplinary review of the scientific literature, Indoor Air. 21(3) (2011), pp. 191-204.

[14] P. Wargocki and D.P. Wyon, The effects of moderately raised classroom temperatures and classroom ventilation rate on the performance of schoolwork by children (RP-1257), HVAC&R Research. 13(2) (2007), pp. 193-220.

[15] Z. Bakó-Biró, D.J. Clements-Croome, N. Kochhar, H.B. Awbi and M.J. Williams, Ventilation rates in schools and pupils' performance, Building and Environment. 48 (2012), pp. 215-223.

[16] P. Wargocki, D.P. Wyon, Y.K. Baik, G. Clausen and P.O. Fanger, Perceived air quality, sick building syndrome (SBS) symptoms and productivity in an office with two different pollution loads, Indoor Air. 9(3) (1999), pp. 165-179.

[17] ASHRAE, 2015 ASHRAE Handbook—Heating, Ventilating, and Air-Conditioning Applications, American Society of Heating, Refrigerating and Air-Conditioning Engineers. (2015).

[18] L.C. Ng, A.K. Persily and S.J. Emmerich, IAQ and energy impacts of ventilation strategies and building envelope airtightness in a big box retail building, Building and Environment. 92 (2015), pp. 627-634.

[19] M.A. Aktacir, O. Büyükalaca and T. Yılmaz, Life-cycle cost analysis for constant-air-volume and variable-air-volume air-conditioning systems, Applied Energy. 83(6) (2006), pp. 606-627.

[20] D.W. Bearg, Indoor air quality and HVAC systems, CRC Press 1993, pp. 18-22.

[21] T.A. Reddy, J.F. Kreider, P.S. Curtiss and A. Rabl, Heating and Cooling of Buildings: Principles and Practice of Energy Efficient Design, CRC Press 2016, pp. 587-589.

[22] G.S. Okochi and Y. Yao, A review of recent developments and technological advancements of variable-air-volume (VAV) air-conditioning systems, Renewable and Sustainable Energy Reviews. 59 (2016), pp. 784-817.

[23] AHRAE. 2008 (ASHRAE Handbook-Heating, Ventilating, and Air-conditioning Sytems and Equipment (IP Edition), Altanta, Aerican Society of Heating, Refrigerating and Air-conditioning Engineers, Inc.), pp. 4.11.

[24] Y. Ma, A. Tukur and P. Kelly Kissock, Energy-efficient static pressure reset in VAV systems, ASHRAE Transactions. 121 (2015), pp. 102-109.

[25] R. Montgomery and R. McDowall, Fundamentals of HVAC control systems, Elsevier 2008, pp. 235-237.

[26] S.C. Sugarman, HVAC fundamentals, Crc Press 2005, pp.289-290.

[27] A. Robinson, High Performance Buildings: A Guide for Owners & Managers. (2014).

[28] Y. Yao, Z. Lian, W. Liu, Z. Hou and M. Wu, Evaluation program for the energy-saving of variable-air-volume systems, Energy and Buildings. 39(5) (2007), pp. 558-568.

[29] W. Kim, S.W. Jeon and Y. Kim, Model-based multi-objective optimal control of a VRF (variable refrigerant flow) combined system with DOAS (dedicated outdoor air system) using genetic algorithm under heating conditions, Energy. 107 (2016), pp. 196-204.

[30] H. Lim and J. W. Jeong, Energy saving potential of thermoelectric radiant cooling panels with a dedicated outdoor air system, Energy and Buildings. 169 (2018), pp. 353-365.

[31] J. W. Jeong, S.A. Mumma and W.P. Bahnfleth, Energy conservation benefits of a dedicated outdoor air system with parallel sensible cooling by ceiling radiant panels, ASHRAE Transactions. 109 (2003), pp. 627.

[32] S. Deng, J. Lau and J. W. Jeong, Do All DOAS configurations provide the same benefits?, ASHRAE Journal. 56(7) (2014), pp. 52.

[33] D. Int-Hout and L. Wilbar, Variable volume DOAS fan-powered terminal unit, ASHRAE Journal. 56(8) (2014), pp.70-73.

[34] M.D. Larranaga, M.G. Beruvides, H. Holder, E. Karunasena and D.C. Straus, DOAS & humidity control, ASHRAE Journal. 50(5) (2008), pp. 34-40.

[35] R.k. Yingling, D.F. Luebs and R.J. Johnson, Residential Duct Systems: Selection and Design of Ducted HVAC Systems, , pp. 33-39.

[36] B. Stein, Building technology: mechanical and electrical systems, John Wiley & Sons 1996, pp. 274.

[37] E. Silberstein, Heat Pumps, Cengage Learning. (2015), pp. 412-415.

[38] J.E. Brumbugh, HVAC Fundamentals, Vol. 2. Heating System Components, Gas and Oil Burners, and Automatic Controls. Indianapolis, IN: AUDEL, Wiley Publishing, Inc, 2004, pp. 296-297.

[39] Improving Fan System Performance: A Sourcebook for Industry, Lawrence Berkeley National Laboratory and Resource Dynamics Corporation, Washington, 2003, pp. 3-4.

[40] M. Brink, FCS Engineering Fabrication & Sheet Metalwork L4, Pearson South Africa 2009, pp. 59-60.

[41] S.A. Mumma, T.A. Mahank and Y.P. Ke, Analytical determination of duct fitting loss-coefficients, Applied Energy. 61(4) (1998), pp. 229-247.

[42] M. Abdulkadir, D. Zhao, S. Sharaf, L. Abdulkareem, I.S. Lowndes and B.J. Azzopardi, Interrogating the effect of 90° bends on air–silicone oil flows using advanced instrumentation, Chemical Engineering Science. 66(11) (2011), pp. 2453-2467.

[43] S. Sami and J. Cui, Numerical Study of Pressure Losses in Close-Coupled Fittings, HVAC&R Research. 10(4) (2004), pp. 539-552.

[44] N.K. Mylaram and S. Idem, Pressure Loss Coefficient Measurements of Two Close-Coupled HVAC Elbows, Hvac & R Research. 11(1) (2005), pp. 133-146.

[45] D. Brkić, Review of explicit approximations to the Colebrook relation for flow friction, Journal of Petroleum Science & Engineering. 77(1) (2011), pp. 34-48.

[46] ASHRAE, 2001 ASHRAE Handbook - Fundamentals, American Society of Heating, Refrigerating and Air Conditioning Engineers, Atlanta. (2001).

[47] N. Li, G. Calis and B. Becerik-Gerber, Measuring and monitoring occupancy with an RFID based system for demand-driven HVAC operations, Automation in Construction. 24 (2012), pp. 89-99.

[48] Y. Agarwal, B. Balaji, S. Dutta, R.K. Gupta and T. Weng, Duty-cycling buildings aggressively: The next frontier in HVAC control, Information Processing in Sensor Networks (IPSN), 2011 10th International Conference on, IEEE, 2011, pp. 246-257.

[49] W. Wang, J. Chen, T. Hong and N. Zhu, Occupancy prediction through Markov based feedback recurrent neural network (M-FRNN) algorithm with WiFi probe technology, Building and Environment. 138 (2018), pp. 160-170.

[50] L. Wang, S. Greenberg, J. Fiegel, A. Rubalcava, S. Earni, X. Pang, R. Yin and S. Woodworth, J. Hernandez-Maldonado, Monitoring-based HVAC commissioning of an existing office building for energy efficiency, Applied Energy. 102 (2013), pp. 1382-1390.

[51] F. Xiao and S. Wang, Progress and methodologies of lifecycle commissioning of HVAC systems to enhance building sustainability, Renewable and sustainable Energy Reviews. 13(5) (2009), pp. 1144-1149.

[52] G. Guyot, M.H. Sherman and I.S. Walker, Smart ventilation energy and indoor air quality performance in residential buildings: A review, Energy and Buildings. 165 (2018), pp. 416-430.

[53] NEBB, Procedural Standard for Testing Adjusting and Balancing of Environmental Systems, Gaithersburg, National Environmental Balancing Bureau. (2015).

[54] E.M. Saber, R. Iyengar, M. Mast, F. Meggers, K.W. Tham and H. Leibundgut, Thermal comfort and IAQ analysis of a decentralized DOAS system coupled with radiant cooling for the tropics, Building and Environment. 82 (2014), pp. 361-370.

[55] Z. Ai and C. Mak, Pressure losses across multiple fittings in ventilation ducts, The Scientific World Journal. (2013), pp. 1-11.

[56] S. Bhattacharjee, Fan affinity laws from a collision model, European Journal of Physics. 33(6) (2012), pp. 1579-1568.

[57] J.F. Richardson, J.H. Harker and J.R. Backhurst, Coulson and Richardson's Chemical Engineering. 1(1999) 232–273.

[58] S. Boetcher and E. Sparrow, Limitations of the standard Bernoulli equation method for evaluating Pitot/impact tube data, International Journal of Heat and Mass Transfer. 50(3-4) (2007), pp. 782-788.

[59] G. Gan and S.B. Riffat, Pressure loss characteristics of orifice and perforated plates, Experimental Thermal and Fluid Science. 14(2) (1997), pp. 160-165.

[60] S. Malavasi, G. Messa, U. Fratino and A. Pagano, On the pressure losses through perforated plates, Flow Measurement and Instrumentation. 28 (2012), pp. 57-66.

[61] W. Jitschin, M. Ronzheimer and S. Khodabakhshi, Gas flow measurement by means of orifices and Venturi tubes, Vacuum. 53(1-2) (1999), pp. 181-185.

[62] J.-D. Vagt, Hot-wire probes in low speed flow, Progress in Aerospace Sciences. 18 (1979), pp. 271-323.

[63] A.B. Bauer, Direct measurement of velocity by hot-wire anemometry, AIAA Journal. 3(6) (1965), pp. 1189-1191.

[64] F. Mailly, A. Giani, R. Bonnot, P. Temple-Boyer, F. Pascal-Delannoy, A. Foucaran and A. Boyer, Anemometer with hot platinum thin film, Sensors and Actuators A: Physical. 94(1-2) (2001), pp. 32-38.

[65] A.M. Al-Garni, Low speed calibration of hot-wire anemometers, Flow Measurement and Instrumentation. 18(2) (2007), pp. 95-98.

[66] T. Gieseke and Y. Guezennec, An experimental approach to the calibration and use of triple hot-wire probes, Experiments in Fluids. 14(5) (1993), pp. 305-315.

[67] J.F. Le Page, C. Chevarin, A. Kondjoyan, J.D. Daudin and P.S. Mirade, Development of an approximate empirical-CFD model estimating coupled heat and water transfers of stacked food products placed in airflow, Journal of Food Engineering. 92(2) (2009), pp. 208-216.

[68] E. Ower and R.C.Pankhurst, The Measurement of Air Flow, Elsevier. 5ed. (2014).

[69] J. Wyngaard, Cup, propeller, vane, and sonic anemometers in turbulence research, Annual Review of Fluid Mechanics. 13(1) (1981), pp. 399-423.

[70] P. Mirade and J. Daudin, A new experimental method for measuring and visualising air flow in large food plants, Journal of Food Engineering. 36(1) (1998), pp. 31-49.

[71] A. Venugopal, A. Agrawal and S. Prabhu, Review on vortex flowmeter—Designer perspective, Sensors and Actuators A: Physical. 170(1-2) (2011), pp. 8-23.

[72] V. Hans and H. Windorfer, Comparison of pressure and ultrasound measurements in vortex flow meters, Measurement. 33(2) (2003), pp. 121-133.

[73] G.L. Pankanin, The vortex flowmeter: various methods of investigating phenomena, Measurement Science and Technology. 16(3) (2005).

[74] L. Lynnworth and Y. Liu, Ultrasonic flowmeters: Half-century progress report, 1955–2005, Ultrasonics. 44 (2006), pp. e1371-e1378.

[75] M. Dell'Isola, M. Cannizzo and M. Diritti, Measurement of high-pressure natural gas flow using ultrasonic flowmeters, Measurement. 20(2) (1997), pp. 75-89.

[76] W.J. Fisk, W. Delp, R. Diamond, D. Dickerhoff, R. Levinson, M. Modera, M. Nematollahi and D. Wang, Duct systems in large commercial buildings: physical characterization, air leakage, and heat conduction gains, Energy and Buildings. 32(1) (2000), pp. 109-119.

[77] S. Cui, M. Cohen, P. Stabat and D. Marchio, CO2 tracer gas concentration decay method for measuring air change rate, Building and Environment. 84 (2015), pp. 162-169.

[78] J. McWilliams and M.H. Sherman, Review of literature related to residential ventilation requirements, Lawrence Berkely National Laboratory, Report LBNL-57236.

[79] Y. Sun and Y. Zhang, An overview of room air motion measurement: technology and application, HVAC&R Research. 13(6) (2007), pp. 929-950.

[80] X. Cao, J. Liu, N. Jiang and Q. Chen, Particle image velocimetry measurement of indoor airflow field: A review of the technologies and applications, Energy and Buildings. 69 (2014), pp. 367-380.

[81] M. Sandberg, Whole-field measuring methods in ventilated rooms, HVAC&R Research. 13(6) (2007), pp. 951-970.

[82] D. Thomas, Make the most of averaging pitot tubes, Chemical Processing. 68(7) (2005), pp. 33-35.

[83] B. Dobrowolski, M. Kabaciński and J. Pospolita, A mathematical model of the self-averaging Pitot tube: A mathematical model of a flow sensor, Flow Measurement and Instrumentation. 16(4) (2005), pp. 251-265.

[84] D. Węcel, T. Chmielniak and J. Kotowicz, Experimental and numerical investigations of the averaging Pitot tube and analysis of installation effects on the flow coefficient, Flow Measurement and Instrumentation. 19(5) (2008), pp. 301-306.

[85] M. Kabaciński and J. Pospolita, Numerical and experimental research on new cross-sections of averaging Pitot tubes, Flow Measurement and Instrumentation. 19(1) (2008), pp. 17-27.

[86] M. Kabaciński and J. Pospolita, Experimental research into a new design of flow-averaging tube, Flow Measurement and Instrumentation. 22(5) (2011), pp. 421-427.

[87] S. Sediva and M. Uher, Analysis of the effect of body shape of multiport averaging Pitot tube on permanent pressure loss using ANSYS/FLUENT, IFAC Proceedings Volumes. (2012), pp. 322-326.

[88] W. Klaczek, M. Ackerman, B. Fleck and P. Fleming, VAV Airflow Sensor Response in Relation to" Poor" Upstream Duct Geometry, ASHRAE Transactions. 112(1) (2006).

[89] S.E. Guffey and D.W. Booth, Comparison of pitot traverses taken at varying distances downstream of obstructions, American Industrial Hygiene Association Journal. 60(2) (1999), pp. 165-174.

[90] ABB, FPD350 Torbar Averaging pitot tubes, ABB Measurement & Analytics Data Sheet.

[91] E. Ower, R.C. Pankhurst, The measurement of air flow, Elsevier 2014.

[92] S. Pochwała and J. Pospolita, Analysis of Applicability of Flow Averaging Pitot Tubes in the Areas of Flow Disturbance, Metrology and Measurement Systems. 23(1) (2016), pp. 71-84.

[93] V. Krishna, C. Suresh, M. Panicker and P. Tide, Experimental analysis of multiport averaging device and effect of body shape on flow coefficient, FME Transactions. 45(1) (2017), pp. 32-37.

[94] R. Liu, J. Wen, X. Zhou and C. Klaassen, Stability and accuracy of variable air volume box control at low flows. Part 1: Laboratory test setup and variable air volume sensor test, HVAC&R Research. 20(1) (2014), pp. 3-18.

[95] R. Liu, J. Wen and M.S. Waring, Improving airflow measurement accuracy in VAV terminal units using flow conditioners, Building and Environment. 71 (2014), pp. 81-94.

[96] S. Guffey, A goal method and a target method for balancing exhaust ventilation duct systems with dampers, Journal of Occupational and Environmental Hygiene. 4(3) (2007), pp. 224-235.

[97] F. Pedranzini, L.P. Colombo and C.M. Joppolo, A non-iterative method for Testing, Adjusting and Balancing (TAB) air ducts systems: Theory, practical procedure and validation, Energy and Buildings. 65 (2013), pp. 322-330.

[98] J. Tamminen, T. Ahonen, J. Ahola and S. Hammo, Fan pressure-based testing, adjusting, and balancing of a ventilation system, Energy Efficiency. 9(2) (2016), pp. 425-433.

[99] M.L. Small, Non-Iterative Technique for Balancing an Air Distribution System, Virginia Tech, 2002, pp. 36-47.

[100] H. Chen, W. Cai and C. Chen, Model-based method for testing, adjusting and balancing of HVAC duct system, Energy and Buildings. 126 (2016), pp. 498-507.

[101] H. Chen, W. Cai and C. Chen, Fan-independent air balancing method based on computation model of air duct system, Building and Environment. 105 (2016), pp. 295-306.

[102] G. Jing, W. Cai, D. Zhai, S. Liu and C. Cui, A model-based air balancing method of a ventilation system, Energy and Buildings. 174 (2018), pp. 506-512.

[103] G. Jing, W. Cai, H. Chen, D. Zhai, C. Cui and X. Yin, An air balancing method using support vector machine for a ventilation system, Building and Environment. 143 (2018), pp. 487-495.

[104] L. Xu, J. Zheng, N. Xiao and L. Xie, Mean square consensus of multi-agent systems over fading networks with directed graphs, Automatica. 95 (2018), pp. 503-510.

[105] F.L. Lewis and K. H. Zhang, Cooperative control of multi-agent systems, Springer London Ltd. (2016), pp. 23-32.

[106] L. Zhao, Y. Jia and J. Yu, Adaptive finite-time bipartite consensus for second-order multi-agent systems with antagonistic interactions, Systems & Control Letters. 102 (2017), pp. 22-31.

[107] R. Olfati-Saber, J.A. Fax and R.M. Murray, Consensus and cooperation in networked multi-agent systems, Proceedings of the IEEE. 95(1) (2007), pp. 215-233.

[108] G.S. Seyboth, D.V. Dimarogonas and K.H. Johansson, Event-based broadcasting for multi-agent average consensus, Automatica. 49(1) (2013), pp. 245-252.

[109] M.O. Oyedeji and M.S. Mahmoud, Couple-group consensus conditions for general first-order multiagent systems with communication delays, Systems & Control Letters. 117 (2018), pp. 37-44.

[110] M. Zhu and S. Martínez, Discrete-time dynamic average consensus, Automatica. 46(2) (2010), pp. 322-329.

[111] J. Wei and A.J. van der Schaft, Load balancing of dynamical distribution networks with flow constraints and unknown in/outflows, Systems & Control Letters. 62(11) (2013), pp. 1001-1008.

[112] H. Geng, Y. Liang, Y. Liu and F.E. Alsaadi, Bias estimation for asynchronous multi-rate multi-sensor fusion with unknown inputs, Information Fusion. 39 (2018), pp. 139-153.

[113] W. Ren, R.W. Beard and E.M. Atkins, Information consensus in multivehicle cooperative control, IEEE Control Systems Magazine. 27(2) (2007), pp. 71-82.

[114] M.D. Zeiler, ADADELTA: an adaptive learning rate method, Computer Science. (2012).

[115] S. Ruder, An overview of gradient descent optimization algorithms, Computer Science. (2016).

Author's Publications

[1] **C. Cui**, X. Zhang, W. Cai and G. Jing, A gradient-based adaptive balancing method for dedicated outdoor air system, Building and Environment. 151 (2019) 15-29.

[2] **C. Cui**, X. Zhang, W. Cai and G. Jing, A novel online air balancing method for the ventilation duct system via distributed cooperative control, Building and Environment. 146 (2018) 177-189.

[3] **C. Cui**, W. Cai and H. Chen, Airflow measurements using averaging Pitot tube under restricted conditions, Building and Environment. 139 (2018) 17-26.

[4] **C. Cui**, W. Cai and H. Chen, Modelling and analysis of proportional method in duct systems under uncertainty, IEEE International Conference on Control & Automation. IEEE, 2017:921-926.

[5] G. Jing, W. Cai, X. Zhang, **C. Cui**, X. Yin and H. Xian, An energy-saving oriented air balancing strategy for multi-zone demand-controlled ventilation system, Energy. 172 (2019) 1053-1065.

[6] G. Jing, W. Cai, X. Zhang, **C. Cui**, X. Yin and H. Xian, Modeling, air balancing and optimal pressure set-point selection for the ventilation system with minimized energy consumption, Applied Energy. 236 (2019) 574-589.

[7] G. Jing, W. Cai, D. Zhai, S. Liu and **C. Cui**, A model-based air balancing method of a ventilation system, Energy and Buildings. 174 (2018) 506-512.

[8] G. Jing, W. Cai, H. Chen, D. Zhai, **C. Cui** and X. Yin, An air balancing method using support vector machine for a ventilation system, Building and Environment. 143 (2018) 487-495.